The effects of mutations in *hoxa13a, hoxa13b,* and *hoxd13a* on the zebrafish fins

Jordan Corcoran

Thesis submitted to the University of Ottawa

in partial Fulfillment of the requirements for the

Master of Science

Department of Biology

Faculty of Science

University of Ottawa

Abstract

Teleosts, or ray-finned fish, are the largest and most diverse class of vertebrates in the world. Among this diversity includes many differences in fin structure. Zebrafish typically have only soft rays in their fins, while acanthomorph fish have both soft and spiny rays in select fins. How this difference between fin elements arose remains an unanswered question in evolutionary biology, although *hox* gene expression patterns could play a prominent role in this evolutionary event. *Hox* genes encode transcription factors that are important for patterning during development. Specifically, the *hox13* genes have been shown to be essential for proper limb and fin patterning and are expressed only in soft rays and not spiny rays during acanthomorph fin development. *Hoxa13* -/-, *Hoxd13* -/- mice completely lack the autopod in their developing limbs. The function of the fish orthologs *hoxa13a, hoxa13b*, and *hoxd13a* are not as well defined in fin ray development, although clear structural changes to the fin rays such as truncations and loss of joints, bifurcations and actinotrichia can be seen in the absence of these genes. In this project, various zebrafish compound mutants for *hoxa13a*, *hoxa13b*, and *hoxd13a* are compared to gain insight into the individual roles of each *hox13* gene during fin development. From these observations, *hoxa13a* and *hoxa13b* appear to have a more prominent role in fin ray patterning, and only require one copy to produce joints, bifurcations and actinotrichia in the rays of every fin. *Hoxd13a* however requires two copies to perform a similar function. After generating and observing triple *hox13* mutant zebrafish, a comparison between these mutant rays and acanthomorph spines was performed using micro-CT scanning and *in situ* hybridization. Triple *hox13* mutant fin rays were found to have highly ossified fin rays as seen in spines, as well as proportionally increased expression of the spine marker *alx4a* during early development. All in all, the triple *hox13* mutant rays appear to be forming an intermediate structure between soft rays

and spiny rays, highlighting the potential impact of *hox13* downregulation in the evolution of acanthomorph spines.

Acknowledgements

First of all, I would like to dearly thank my supervisor Dr. Marie-Andrée Akimenko for her constant support and guidance through this project. I have been very grateful for my time in her lab and all of her knowledge she has passed on to me over these past years. Next, I would like to thank Dr. Shelley Hepworth and Dr. Marc Ekker for taking the time to be on my thesis advisory committee and provide me with constructive feedback throughout this project. Additionally, thank you to Dr. Rajakumar and Dr. Shelley Hepworth for agreeing to be my thesis examiners. I would also like to give a special thanks to Hailey Quigley for starting this project and training me on all the necessary laboratory techniques, and to Dr. Qingming Qu for creating the CRISPR-Cas9 mutants used in this study as well as for help with the CT data analysis. Finally, I would like to thank all past and current lab members of the Akimenko and Ekker labs that I have worked with for creating a positive lab environment and for constructive, collaborative feedback along the way.

Table of Contents

Table of Figures

List of Tables

List of abbreviations

AER	Apical ectodermal ridge
alx4a	*aristaless-like homeobox 4a*
And	*actinodin*
BMP	Bone morphogenetic protein
CRISPR-Cas9	clustered regularly interspaced short palindromic repeats associated protein 9
DNA	Deoxyribonucleic acid
Dsred2	red fluorescent protein isolated from *Discosma* 2
dpf	days post-fertilization
eGFP	Enhanced green fluorescent protein
evx1	*even-skipped homeobox 1*
FF	Fin fold
Fgf	*Fibroblast growth factor*
fli1a	friend leukemia integration 1a transcription factor
gli3	*Glioma-associated Oncogene 3*
grem1	gene coding for Gremlin1b protein
Hox	homeobox-containing gene
hox13	*hoxa13a, hoxa13b, and hoxd13a genes* (specific to this thesis)
hoxa13a	*homeobox a13a*
hoxa13b	*homeobox a13b*
hoxd13a	*homeobox d13a*
hpf	hours post-fertilization
ISH	*In situ* hybridization
RNA	Ribonucleic acid
RT	Room temperature
runx2a	*runt-related transcription factor 2 orthologue a*
shha	*sonic hedgehog a*
SL	Standard length
sp7	*sp7 transcription factor*
TG	Transgene

Triple *hox13* mutant	Mutant zebrafish with homozygous deletions in *hoxa13a, hoxa13b,* and *hoxd13a* (specific to this thesis)
wnt	*wingless-related integration site*
WT	wild-type
ZPA	zone of polarizing activity

Nomenclature

Zebrafish:

Gene: *hoxa13a*

Protein: Hoxa13a

Mouse:

Gene: *Hoxa13*

Protein: HOXA13

Human:

Gene: *HOXA13*

Protein: HOXA13

Chapter 1: Introduction

1.1 General introduction

Teleosts, or ray-finned fish, are the largest and most diverse class of vertebrates in the world (Ravi & Venkatesh, 2008). Among this diversity can be found many morphological differences in fin structure such as the overall shape and lobes of the fins, and the number and length of rays in each fin. A specific example is shown between two groups of teleosts known as the cypriniformes and the acanthomorphs. The fin morphology between these groups typically differs based on the types of rays present in the fins, as the fins of both groups have significant differences along the anterior-posterior axis. cypriniformes, except for the carps, have only soft rays in their fins. In contrast, acanthomorphs have soft rays at the posterior end of their fins, but also have spiny rays included at the anterior end, which are explained in section 1.3.1. The spiny-rayed acanthomorph fish evolved more recently, around 133 to 150 million years ago (Chen et al., 2014) compared to the Cypriniformes which evolved around 194 million years ago (Tao et al., 2019) however the mechanism of how these spiny rays of the acanthomorphs came to be, and why we see this difference in anterior-posterior patterning of the fins is yet to be fully understood.

To understand the differences in these fin structures, it is important to first understand the development of the fins. The cypriniform *danio rerio,* or zebrafish, is a common model to study fin development due to its large number of advantages as a model organism. First, they are very easy to house and maintain (Briggs, 2002) and do not require extensive amounts of food or care, allowing them to be raised easily in most laboratories. Zebrafish can also breed often and provide several hundred offspring per mating (Nasiadka & Clark, 2012). The generation time of zebrafish is also relatively small, as they typically reach sexual maturation at about three months of age

(Kimmel et al., 1995). In addition to their easy accommodations, the genome of the zebrafish is completely sequenced and well annotated, making it easy to manipulate and create mutant lines of zebrafish for genetic studies (Rafferty & Quinn, 2018). While there are five different fins on the zebrafish including the pectoral, pelvic, anal, dorsal, and caudal fins, most of what we know about early fin development and patterning comes from the pectoral fin due to its homology with the mammalian forelimb. As will be explained in greater detail later, the limb buds and fin folds are initiated and maintained by the same complex signalling pathways. One particular family of genes that code for transcription factors which play an essential role in fin and limb development is the *hox* gene family. Specifically, *hox9-13* are expressed colinearly in two distinct phases for early fin and limb development. Early phase *hox* expression is essential for initiation of the appendage (Zákány et al., 2004), and late phase *hox* expression plays a prominent role in the outward proliferation, and proximal-distal patterning of the developing fin or limb. These mechanisms are further outlined in section 1.2.3. In the case of mice, knockouts of *Hoxa13* and *Hoxd13* show a complete lack of the autopod in the developed forelimbs and hindlimbs (Fromental-Ramain et al., 1996). To investigate the role of the zebrafish homologs of these genes on the pectoral fin endoskeleton Nakamura et al., (2016) generated mutant fish with mosaic knockouts in *hoxa13a, hoxa13b,* and *hoxd13a*. This mutant fish was found to have an increase in the number of distal radials in the pectoral endoskeleton compared to wild-type. Furthermore, the distal radials appeared distally aligned similar to what is seen in the phalanges of the tetrapod limb. The fin rays of the *hox13* triple mutant fish generated by Nakamura et al., (2016) also appeared shortened and malformed compared to wild-type fin ray, although in depth analysis of the fin rays was not performed since the focus of this study was on the pectoral endoskeleton. Thus, a knowledge gap

has been left in the literature as to what specifically happens to the zebrafish fin rays in the absence of *hoxa13a, hoxa13b,* and *hoxd13a.*

Since the *hox13* mutants used in Nakamura et al. (2016) were unable to be obtained, the Akimenko lab generated our own *hox13* mutant fish in order to further study the impact of this mutation on the fin rays. The mutation in the *hox13* mutants from Nakamura et al. (2016), were created by inducing indels in *the hoxa13a, hoxa13b,* and *hoxd13a* coding sequencing. Since our lab wanted to ensure the deletions rendered these *hox13* genes non-functional in our mutants, we induced large deletions in *hoxa13a, hoxa13b,* and *hoxd13a* individually using CRISPR-Cas9. The sizes and locations of these deletions are each shown in figure 15. Since single homozygous deletions in *hoxa13a, hoxa13b,* or *hoxd13a* do not cause any observable defects on fin morphology, triple homozygous mutants with all three of these genes knocked out were generated through serial breeding of single homozygous mutants to observe defects in the fin rays. These triple *hox13* mutants were seen to have severe but varying defects across the different fin types which will later be explained in detail. After initial observations of these triple *hox13* mutant fish in our lab, there remained a few knowledge gaps to investigate with this project. First, definitive conclusions could not be made for the individual contributions of each of these *hox13* genes to fin ray patterning since deletions of these genes had to be observed in a combinatorial manor using the triple *hox13* deletion mutant. Furthermore, why differences in defects are observed between different fin types of the triple *hox13* mutant must still be investigated further. Finally, is there a way we can explain why we see a shift in fin ray structure in the triple *hox13* mutant as opposed to a loss of the fin rays? These are the main questions and literature knowledge gaps that I want to

address in this project, as I attempt to better characterize *hoxa13a, hoxa13b,* and *hoxd13a* function in the adult zebrafish fin rays.

With the opportunity presented by these triple *hox13* mutants, I also want to investigate some other potential defects in zebrafish morphology that could arise due to these mutations in fin endoskeleton, fin vasculature, and the urogenital pore. Beyond the structure of the pectoral fin endoskeleton, Nakamura et al., (2016) did investigate the endoskeleton of all fins in the triple *hox13* mutant, which is something that I will observe in our *hox13* triple mutants. For vasculature, knockdowns of *Hoxa13* have been found to cause defects in placental patterning, umbilical artery formation and downregulation of several pro-vascular genes in mice (Shaut et al., 2008, Stadler et al., 2001). The relationship between *hox13* and vasculature is not clear, especially in zebrafish, although the blood vessels in the triple *hox13* mutant fins will be observed to look for potential differences in blood vessel patterning as a result of the *hox13* deletions. Finally, *Hoxa13*-/+, *Hoxd13*-/- mice have reportedly shown abnormalities in the terminal parts of the urogenital tracts, including agenesis and hypoplasia of male sex glands, and mispositioning of urethral, anal, and vaginal openings (Warot et al., 1997). Considering this, it is possible that there are also defects with the terminal parts of the urogenital tract in zebrafish, which can also be investigated with the triple *hox13* mutant.

All in all, this background information and previous observations have led to two hypotheses that I will investigate in this project:

Hypothesis 1: *Hoxa13a*, *hoxa13b* and *hoxd13a* have redundant but varying roles in the fin ray formation of each fin type.

For this hypothesis, a morphological analysis of double homozygous *hox13* mutants will be performed to compare to triple *hox13* mutants and gain more insight on the individual contributions of each of these three *hox13* genes to adult fin ray phenotype. Furthermore, the fin rays of every fin type in all mutants will be compared to characterize the differences that arise between fin types as a result of the *hox13* mutations. As a small part of this morphological analysis, the fin ray vasculature of each fin, the endoskeleton of each fin, and the urogenital pore of the triple *hox13* mutant were also observed for the reasons previously described.

Hypothesis 2: *Hox13* mutant fins are forming spine-like structures as opposed to normal fin rays

Morphologically, the *hox13* triple mutant fin rays demonstrate similarities in structure to the spines commonly observed in acanthomorphs. Micro-CT analysis and gene expression of the common spine marker *alx4a* in the *hox13* mutant fins were observed to potentially support the idea of a transformation of the *hox13* rays into spine-like structures.

1.2 Early fin and limb bud development and patterning

1.2.1 Structure of the fin bud

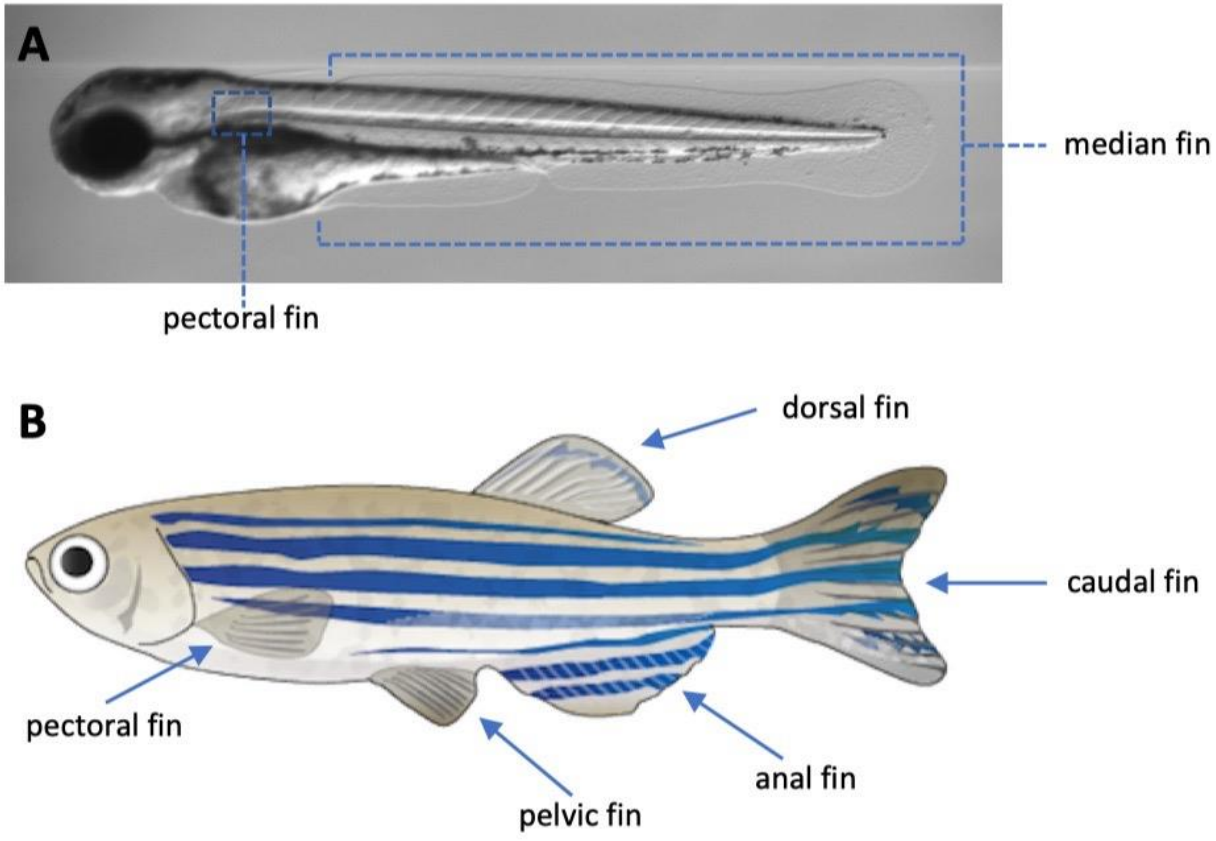

Figure 2. Fins of the zebrafish during embryonic development and adulthood. A: 3-day post fertilization (dpf) zebrafish embryo with the pectoral fin bud and median fin fold shown within the blue dotted-lines. Image captured by Robert Lalonde. B: Schematic of an adult zebrafish, showing the pectoral, pelvic, anal, dorsal, and caudal fins in adulthood. (created by Togo

Picture Gallery and obtained from Database Centre for Life Sciences (DCLS) CC BY 3.0) (https://creativecommons.org/licenses/by/3.0/deed.en)

The zebrafish has 5 different types of fins. Anteriorly, there are 2 sets of paired fins known as the pectoral and pelvic fins which develop from the pectoral and pelvic fin buds (Grandel & Schulte-Merker, 1998). Posteriorly, there are 3 median fins, the caudal, anal, and dorsal fins, which all develop from the median fin fold (Siomava et al., 2018). In order to fully understand the aim of this project, it is important to first have an understanding of fin development, and the major regulatory mechanisms involved in this process. As previously stated, the development of the pectoral fin is the most well understood due to its homology with mammalian forelimbs where limb development has been studied most extensively. The main structure of the growing pectoral fin bud includes a few key signalling centers which contribute to growth, proliferation, and patterning of the appendage. As shown in figure 2, these signalling centers include the zone of polarizing activity (ZPA) at the posterior side of the bud, and a thickened ectoderm that rims the distal part of the bud along the anterior-posterior axis known as the apical ectodermal ridge (AER). The role of these signalling centers is further described in section 1.2.3. In addition to the signalling centers, the zone of proliferation is in the distal mesenchyme, where rapidly dividing mesenchymal cells allow for growth of the bud. As the fin bud grows, it will also form a fin fold at around 36hpf (Kimmel et al., 1995), which is formed when the AER folds back onto itself. This fin fold is supported by actinotrichia fibers, that will provide support and allow for migration of mesenchymal cells into the fold as will be further explained in section 1.2.4. The adult lepidotrichia in the fin fold that will make up the exoskeleton of the adult fins in the zebrafish. The developmental mechanisms described in section 1.2.3 pertain mostly to the pectoral fin, although

some of the mechanisms discussed are also present in the dorsal and anal fins, as will be discussed in section 1.2.5.

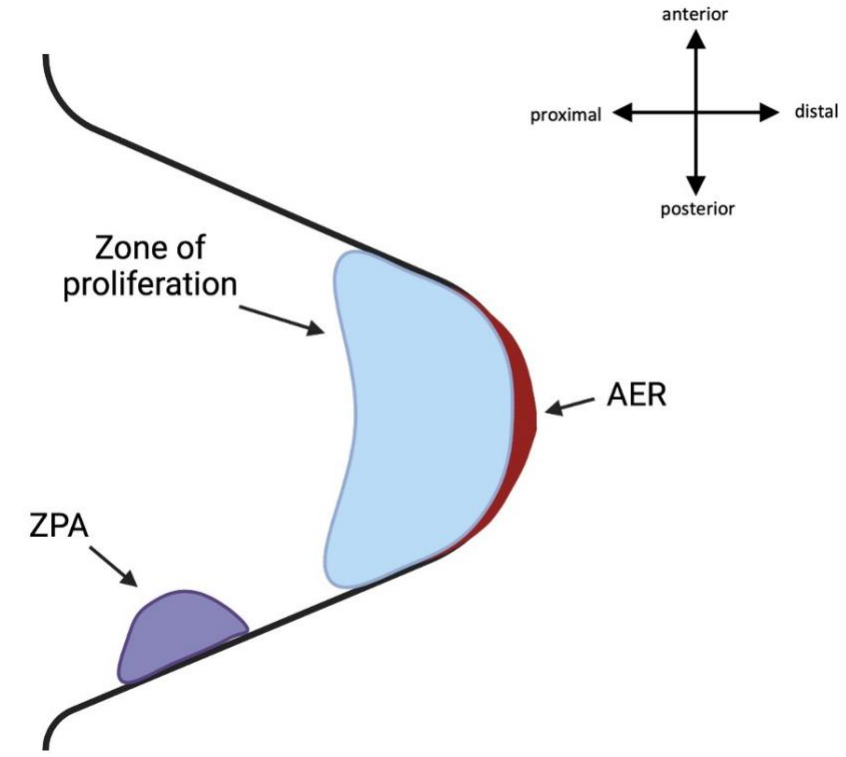

Figure 3. Schematic representation of a developing vertebrate appendage bud. The apical ectodermal ridge AER (red) is the thickened ectoderm at the distal end of the bud. The zone of polarizing activity (ZPA) is located at the posterior side of the bud, with the zone of proliferation in the distal mesenchyme. The molecular mechanisms of these components are outlined in section 1.2.3.

1.2.2 *Hox* genes are essential for body patterning

Hox genes are a family of genes that code for homeodomain transcription factors and are organized into clusters in the vertebrate genome (Lewis, 1978), and are highly conserved throughout all vertebrates (Santini et al., 2003). Mammalian species like humans and mice have four *hox* clusters (*HoxA, HoxB, HoxC,* and *HoxD*), however, zebrafish have seven clusters (*hoxAa, hoxAb, hoxBa, hoxBb, hoxCa, hoxCb,* and *hoxDa*) due to a genome duplication event in ancient ray-finned fish approximately 360 million years ago (Zardoya & Meyer, 1997). Notably, the list of zebrafish *hox* clusters excludes the *hoxDb* cluster, which has been shown to have lost all *hox* related sequences except for a single micro-RNA, *mir-10* (Woltering & Durston, 2006). As originally described in *Drosophila* by Lewis (1978), clusters of *hox* genes are colinear to their domains of action during development of the fruit fly abdomen. This collinear expression of *hox* genes initially observed in *Drosophila* was also found to be present in mice by Duboule & Dollé, (1989). Generally, collinear expression means that *hox* genes towards the 3' end of the cluster such as *hox1* will be expressed earlier and towards the anterior portion of the organism, and 5' *hox* genes such as *hox13* will be expressed later and more towards the posterior portion of the organism along the body axis during axial patterning (Duboule & Dollé, 1989). HOX transcription factors instruct cells to their morphogenic fates in each position that they are expressed in (Deschamps & Wijgerde, 1993). In the case of the limb, only the more 5' genes of the *HoxD* and *HoxA* clusters are involved, as will be explained in further detail later in the next section.

1.2.3 Molecular regulation of limb growth and patterning

The regulation mechanisms of *hox* genes about to be described during limb development were originally observed in the *HoxD* cluster, however the same mechanisms also apply to the

HoxA cluster (Woltering et al., 2014). The early phase *HoxD* expression in the mouse limb has been shown to be activated by the early limb control regulatory region (ELCR) (Zákány et al., 2004). This enhancer region found on the 3' side of the cluster causes sequential collinear expression of the *Hoxd1-13* genes in the anterior to posterior region of the early limb (Nelson et al., 1996; Tarchini & Duboule, 2006; Zákány et al., 2004). The 5' *HoxD* genes *Hoxd9-13* are expressed in the bud and will contribute to the patterning of the proximal limb or fin, as well as anterior-posterior patterning through establishing the ZPA (Zákány et al., 2004).

During the outgrowth of the limb bud, there are two separate mechanisms that occur to influence proximal-distal and anterior-posterior patterning of the developing fin. The dual gradient model is hypothesized to contribute to the proximal-distal patterning of the limb, and is supported by Cooper et al., (2011) and Roselló-Díez et al., (2011). In the dual gradient model, retinoic acid (RA) is produced from the lateral plate mesoderm, and FGF4, a signalling molecule that is part of the fibroblast growth factor family, is expressed from the AER. RA and FGF4 form opposite gradients in the developing limb bud such that RA concentration is high in the proximal part, and FGF4 concentration is high in the distal part of the limb bud. The concentration of RA and FGF4 at a given location in the bud, determines the *hox* paralog group that will be expressed in that location. The *Hox* group expressed in each location will then specify the fate of the mesenchyme (Deschamps & Wijgerde, 1993). Which *hox* genes are essential for the development of different regions along the proximal distal axis were determined from studies that observed the consequences on the limb in the absence of *Hox9-13* genes (Davis et al., 1995; Fromental-Ramain et al., 1996; Wellik & Capecchi, 2003). In the proximal part, the higher levels of RA lead to production of *HoxA/D9* and *HoxA/D10* in the forelimb, and only *HoxA/D10* in the hindlimb, which

will pattern the stylopod (humerus or femur) of the appendage (Wellik & Capecchi, 2003). In the middle part of the bud, even levels of RA and FGF4 causes the expression of *HoxA/D11*, which will pattern the zeugopod (ulna and radius or tibia and fibula) of the appendage (Davis et al., 1995). Finally in the distal part of the limb, the high FGF4 and low RA concentrations cause the expression of small amounts of *HoxA/D12*, but mainly *HoxA/D13* which will pattern the autopod (hand or foot) (Fromental-Ramain et al., 1996).

For anterior-posterior patterning of the limb, fibroblast growth factors including primarily FGF8, and FGF4 from the AER induces the formation of the ZPA in the posterior mesenchyme of the bud, which exerts its polarizing activity primarily by secretion of sonic hedgehog protein (SHH) (Riddle et al., 1993), a signalling molecule of the hedgehog family. *Shh* expression is initially activated by the early phase expression of *Hox* genes, where *Hoxd11-13* genes through binding to the enhancer region of *Shh* known as ZRS (Lettice et al., 2003). In addition to *Hoxd11-13* genes, the helix-loop-helix transcription factor HAND2 has also shown the ability to bind to the ZRS regulatory element and activate expression of *Shh* in the ZPA (Galli, et al., 2010). SHH is secreted and form a gradient starting from the ZPA at the posterior side of the limb and causes the polarization of the bud through the activation of downstream targets. 5' *HoxD* genes are activated by SHH signalling through the activation of the global control region (GCR) enhancer upstream on the 5' end of the *HoxD* cluster, which initiates the late phase *Hox* expression (expression after *Shh* activation) in the bud (Zákány et al., 2004). In addition to *5' Hox* genes, SHH signalling activates expression of *Gremlin1*, which codes for a TGFβ signalling molecule and antagonist of BMP which in turn inhibits FGF4 production from the AER (Zúeniga et al., 1999). The increased expression of *Fgf4* that results from *Gremlin1* expression then allows for sustained

maintenance of the ZPA and AER in a positive feedback loop for continued growth and proliferation (Zúeniga et al., 1999). SHH signalling is also essential for digit specification, where exposure time and concentration of SHH is crucial for each digit (Scherz et al., 2007). Digit 1 develops in the absence of SHH, digit 2 develops in low concentration and short exposure time, digit 3 develops in high concentration, low exposure time, digit 4 develops in high concentration, medium exposure time and digit 5 develops in high concentration, high exposure time (Scherz et al., 2007). Mice with homozygous deletions in *Shh* have been shown to lack all digits except for the anterior-most digit in the forelimb and hindlimb (Chiang et al., 2001), further highlighting the essentiality of *Shh* in the patterning of the digits. In the anterior part of the bud there is typically an absence of *Shh* expression. Instead, other regulatory genes that oppose SHH function are expressed in this area to and establish the identity of the anterior digits. Two of these major regulatory genes expressed in the anterior part of the bud include *Alx4*, and *Gli3*. In mice, the transcription factor *Alx4* has been shown to play a role in regulating the *Shh* domain of expression in the limb bud. Mice with homozygous mutations in *Alx4* were found to have a second ZPA on the anterior part of the limb bud in addition to the normal ZPA, inducing ectopic expression of *shh*, *Hoxd13*, and *Fgf4/8* in the limb and causing polydactyly in the mice (Qu et al., 1997). *Gli3* codes for a zinc-finger transcription factor that opposes SHH function in the anterior limb bud, as homozygous mutations in *Gli3* were found to cause a reduction in *Alx4* expression and cause polydactyly in the mutant mice (Te Welscher et al., 2002a). The polydactyly caused by the *Gli3* -/- mutation however is caused by a different mechanism, where there is no ectopic expression of *Shh*, and no ZPA established in the anterior part of the bud like in *Alx4* -/- mutants (Qu et al., 1997; Te Welscher et al., 2002b). Instead, GLI3R (the repressor isoform of GLI3) was found to likely be a repressor of SHH signaling targets. *Gli3* mutations in the absence of *Shh* were found to induce

the formation of the anterior most digits in the limb (Te Welscher, et al., 2002b), where there are typically none in *Shh* -/- mutants (Chiang et al., 2001). Additionally, it has been observed that GLI3R is a repressor of *Hand2* in the limb bud, and thus can indirectly repress *Shh*, even though there is no anterior ZPA formed in the absence of GLI3 (Te Welscher et al., 2002a). Overall, GLI3R has been better characterized as an anteriorly expressed repressor of SHH targets compared to *Alx4*. We know that ALX4 somehow plays a role in confining SHH to the posterior limb bud, although the downstream targets and mechanisms it uses to perform this function are not clear. Unlike the limb bud, the fin bud will also form a fin fold as the AER folds onto itself and elongates. This folding occurs at around 36hpf in the pectoral fin (Kimmel et al., 1995), and is supported by actinotrichia fibers during growth, as will be further explained in the next section. Within the fin fold is where the lepidotrichia will form (Géraudie, 1984).

1.2.4 The role of actinotrichia in the fin fold

An important structural component of the developing fin fold that is not present in the mammalian limb bud is actinotrichia fibers. These fibers play a role in the development of the fin folds during embryogenesis, as well as growth of the fin rays as will be described later. The role of actinotrichia in the FF has been most studied in the pectoral fin fold, which begins to form at around 36 hours post-fertilization (hpf) (Kimmel et al., 1995). Actinotrichia fibers form at the same time as the FF. These fibers are made of elastoidin, which is comprised of collagen and actinodin (Zhang et al., 2010). Actinotrichia are formed primarily by actinotrichia-forming mesenchymal cells, which are among the cells migrating into the fin fold (Zhang et al., 2010). Additionally, *and1*, a gene coding for actinodin, has also shown to be expressed in the epithelial cells (Phan et al., 2019). The actinotrichia fibers arrange into two parallel rows in the FF that provide support to the

fin fold, and act as a scaffold for mesenchymal cells to migrate into the FF (Géraudie & Meunier, 1980; Grandel & Schulte-Merker, 1998; Wood & Thorogood, 1984). Actinotrichia has also been shown to form within the median fin fold that will give rise to the median fins (Zhang et al., 2010). There are four *actinodin* genes in zebrafish *and1*, *and2*, *and3*, and *and4* (Zhang et al., 2010). Transient morpholino mediated gene knockdowns of *and1* and *and2* have been performed in our lab, which caused an absence of actinotrichia in the FF resulting in a misshaped fin fold due to the lack of support, and disrupted migration of mesenchymal cells (Zhang et al., 2010). *And1* specifically has a regulatory element known as *2Pand1*, where multiple binding domains for both HOXA13 and HOXD13 have been identified (Lalonde et al., 2016). Given the presence of HOX13 binding domains on the *and1* regulatory region, it is likely that HOX13 has a regulatory role on *and1* expression and thus the formation of actinotrichia. To what extent HOX13 transcription factors are responsible for *and1* production and how essential they are for the formation of actinotrichia as a result is not known.

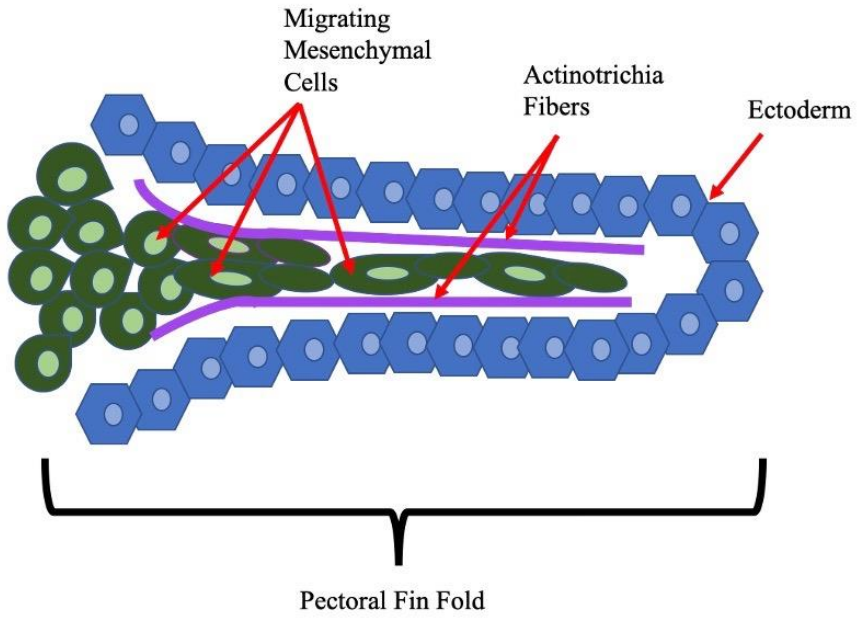

Figure 4. Actinotrichia guides mesenchymal cells and provide support in the pectoral fin fold. Schematic representation of the pectoral fin fold, mesenchymal cells (green) migrating along actinotrichia fibers (purple).

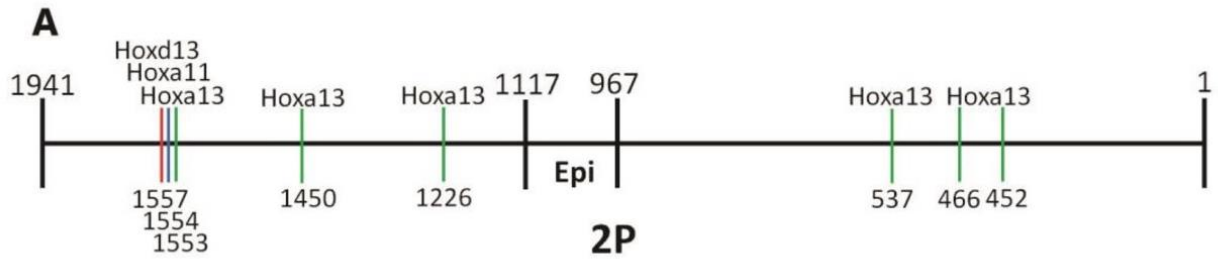

Figure 5. 2P fragment contains 6 putative Hoxa13, 1 Hoxa11, and 1 Hoxd13 consensus binding sites. (A) Schematic representation of 2P fragment showing distribution of Hoxa13, Hoxa11 and Hoxd13 putative binding sites. Hoxa13 binding sites are highlighted with a green line, Hoxa11 binding sites are highlighted with a blue line, and Hoxd13 binding sites are highlighted with a red line. Base pair locations of each site from the 3' end are mentioned below. All putative binding sites were identified via TRANSFAC transcription factor identification software. (Lalonde et al., 2016) Reproduced with permission from Copyright Clearance Center, April 22, 2023.

1.2.5 Development of the median fin fold

In contrast to the paired fins, all the median fins are formed from the median fin fold. There is less known about the development of the median fins overall, although there is evidence that many of the same mechanisms responsible for paired fin development are conserved in the dorsal and anal fins. In a study by Freitas et al., (2006), mechanisms of median fin development were observed in the catshark. The dorsal and anal fins showed similar mechanisms of development as

in the paired fin, with collinear *hoxd9-13* expression initiating the fin and forming an AER, followed by a ZPA. The main difference found between paired fin development and median fin development is that the mesenchyme appears to originate from the axial mesoderm in the medial fins as opposed to the lateral plate mesoderm in the paired fins, although the mechanisms of outward growth and proliferation as well as the mechanisms for patterning seem to be conserved in the dorsal and anal fins (Freitas et al., 2006). As previously mentioned, actinotrichia have also been shown to be produced within the median fin fold (Zhang et al., 2010).

In the median fins, less is known about the role of the *Alx4* homolog, *alx4a*, in the early development and patterning of these fins, and how well the *Alx4* regulation and mechanisms are conserved between median fin and paired appendage development. Most of what is known about the role of *alx4a* in the adult median fins comes from acanthomorph development, and a zebrafish study by Nachtrab et al., (2013) that will be described later in greater detail. Although acanthomorphs are extremely diverse as a group, *Astatotilapia burtoni (A. burtoni)* has been observed as a representative model organism to study fin spine development and morphology (Höch et al., 2021; Woltering et al., 2018). *A. burtoni* is a mouthbrooding East-African cichlid fish native to Lake Tanganyika and Lake Victoria. In contrast to the zebrafish, the fins of *A. burtoni* during development show two distinct domains in their dorsal and anal fins. This includes a spiny ray domain at the anterior side, which is a defining characteristic of acanthomorphs, and a soft ray domain at the posterior side (Höch et al., 2021). *Alx4a* expression has been observed in *A. burtoni* where it is expressed exclusively in the spiny ray domain of the dorsal and anal fins throughout development (Höch et al., 2021). Interestingly in the spiny ray domain during development, there is normally a complete lack of *hoxa13a* and *hoxa13b* expression, and only expression of *alx4a* and

alx4b (Höch et al., 2021). The soft rays on the other hand express only *hox13* and not *alx4*, such that a clear barrier between the expression domains of these genes can be observed in the dorsal and anal fin folds all throughout the appearance and growth of the soft and spiny rays (Höch et al., 2021). This observation differs from normal limb development in mice, where *Alx4* is still confined to the anterior limb bud during development, but then expression begins to fade at around the E12.5 timepoint before the digits begin to appear (Rockwell et al., 2022). During early fin bud development, *gremlin1b* is normally activated by Shha signalling from the ZPA, where it is expressed from the posterior side in a gradient pattern to establish the identity of the fin through BMP inhibition (Höch et al., 2021). The domain of *gremlin1b* expression in the developing *A. burtoni* dorsal and anal fins overlaps with the expression of *hoxa13a/b* in the soft ray domain (Höch et al., 2021). Furthermore, Höch et al., (2021) showed that modifying *gremlin1b* expression can change the location of the barrier between the spiny and soft ray domains. In this study, an expansion of the spiny ray domain and reduction of the soft ray domain can be observed when *gremlin1b* is knocked out. Based on this observation, the authors propose a pathway where *gremlin1b* is acting as an upstream activator of *hox13* (figure 6). It is unclear however in this pathway if *hox13* is directly inhibiting *alx4*, or BMP that is normally repressed by *gremlin1b* is upregulating *alx4a* in the spiny domain. In this study, two non-acanthomorph fish including the African catfish, and the *Ancistrus* catfish, were also observed. The soft ray domain in these fish extends completely throughout the entire fin, and *alx4a* is confined to only the anterior most fin ray. In the dorsal and anal fins of these fish, there appears to be an overlap between *hoxa13a/b* expression, and *alx4a* expression in the anterior part of the fins which is not the case in *A. burtoni.* In summary, it is not yet understood why acanthomorphs have this expanded, separate domain of expression for *alx4a* that denotes the spiny rays, and why this differs from what is observed in

non-acanthomorphs where *alx4a* is confined to the very anterior ray with overlapping expression of *hoxa13a/b.* Through their observations, the authors of this study hypothesize that *hoxa13a/b* could be regulating *alx4a* and confining it to the anterior spiny ray area, or that the BMP normally inhibited by *gremlin1b* expression is causing this activation of the *alx4a* and denoting the spiny ray area.

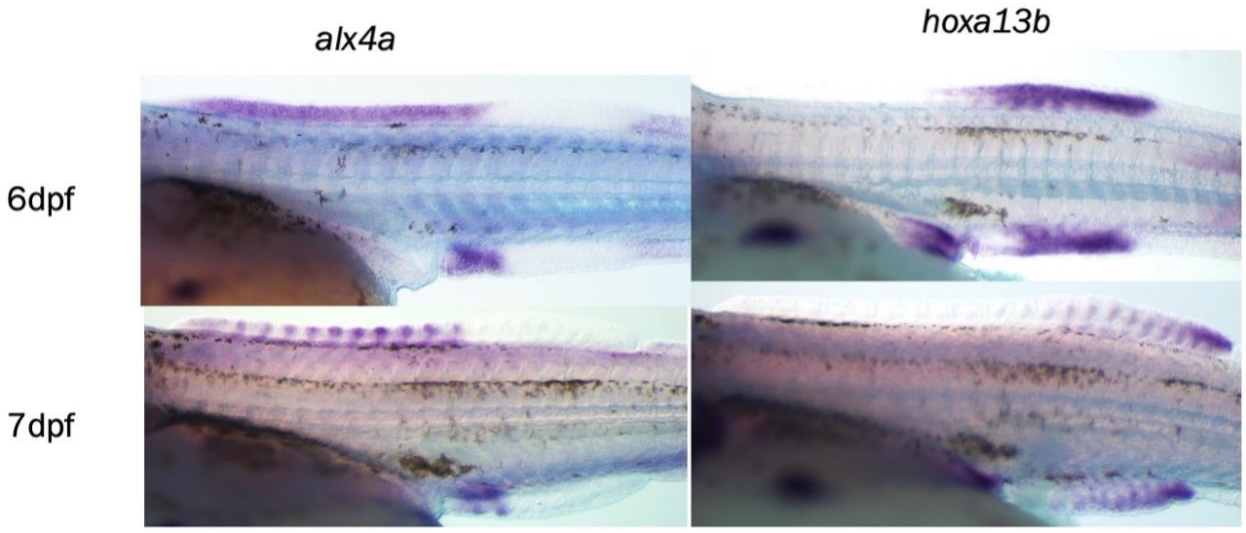

Figure 6. *alx4a* and *hoxa13b* expression patterns are exclusive to spiny ray and soft ray domains in the dorsal and anal fin folds of A. burtoni. Whole mount in situ hybridization of both *alx4a* and *hoxa13b* at 6dpf and 7dpf timepoints are presented, with the anterior spiny ray domain on the left, and the posterior soft ray domain on the right. Adapted from Höch et al., 2021 with permissions from PNAS: Open Access Articles, April 22, 2023.

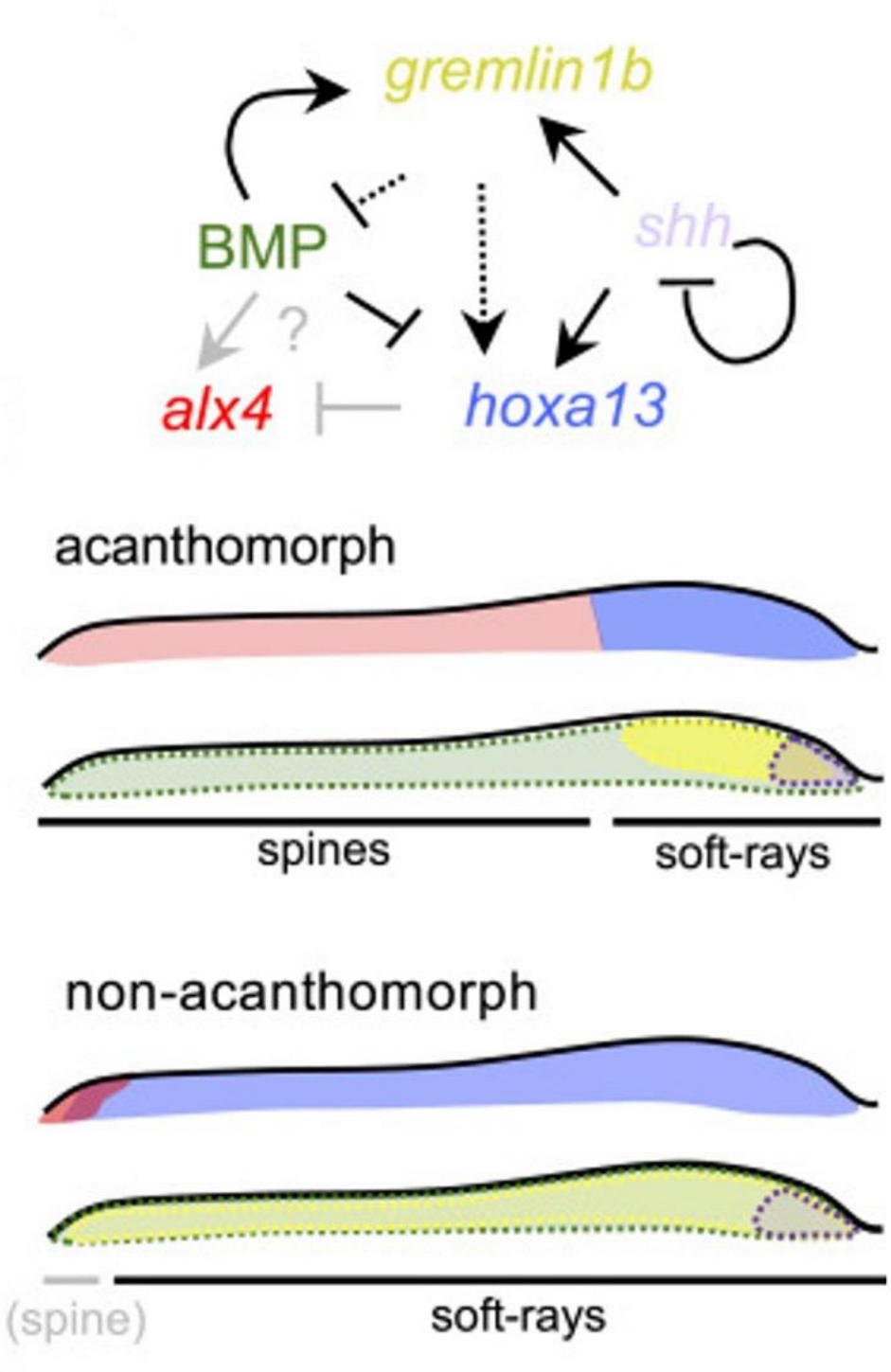

Figure 7. Model for the signaling network that establishes the soft-ray domain in acanthomorph and non acanthomorph teleosts. Pointed arrows represent activation, and lined arrows represent repression in the pathway. In acanthomorphs, the soft-ray domain is established

by expression of *gremlin1b*, which acts with SHH to activate *hoxa13* expression. The barrier between the soft ray and spiny ray expression domains is hypothesized to be controlled by the repression of *alx4* expression by *hoxa13* in the soft ray domain, and/or by the activation of alx4 by BMP in the spiny ray domain. Adapted from Höch et al., (2021) with permissions from PNAS: Open Access Articles, April 22, 2023.

1.2.6 *hox13* expression in the zebrafish fin fold

As the pectoral fin bud continues to grow, 2 separate domains develop which include the endoskeletal disc in the proximal, and the distal mesenchyme where the fin rays will emerge (Figure 7). The endoskeletal disc forms the proximal radials, and the distal radials which serve as an attachment point for the fin rays (Grandel & Schulte-Merker, 1998). The distal mesenchymal cells migrating in the fold will give rise to the lepidotrichia, which articulate to the distal radials and grow distally through the addition of bony segments. The structure of the adult fin rays and endoskeleton are explained in detail in sections 1.3.1 and 1.3.2 respectively. As previously mentioned, *Hoxa13* and *Hoxd13* in mice are expressed in and are essential for proper development of the autopod (Fromental-Ramain et al., 1996). The *hox13* zebrafish homologs *hoxa13a, hoxa13b*, and *hoxd13a* are expressed in unique overlapping patterns in the distal part of the endoskeletal disc and the distal mesenchyme of the fin fold. *Hoxd13a* expression begins at around 30hpf and is exclusive to the posterior half of the developing fin bud (Ahn & Ho, 2008). *Hoxa13b* is also expressed starting at around 30hpf and is expressed more ubiquitously throughout the fin bud (Ahn & Ho, 2008). *Hoxa13a* is expressed later at around 42hpf and is exclusive to the distal end of the proximal mesenchyme in the developing fin bud (Ahn & Ho, 2008). The overall expression of these genes after 36hpf, marking the late expression of *hox* genes in the fin bud, is primarily in the

distal mesenchyme of the bud. There is however some expression in the distal part of the endoskeletal disc as well. In a study that will further be highlighted after explanation of the adult fin structure, Nakamura et al., (2016) determined this late phase *hox13* expression to be localized to the fin rays at 90dpf using fate-mapping, highlighting the importance of these three *hox13* genes in the development of the rays. Before discussing the role of this late *hox13* expression in the mature fins, it is important to first understand in detail the morphology and structural components of adult fins.

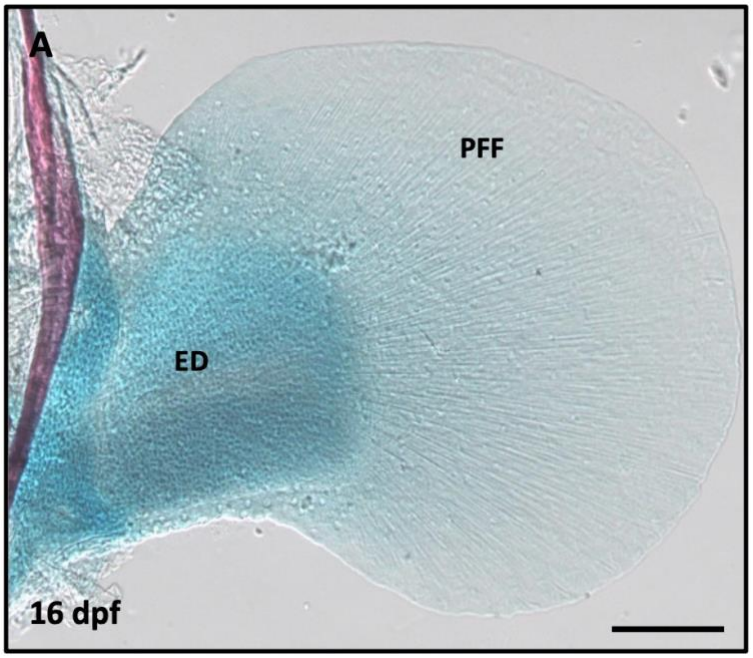

Figure 8. Structure of the 16dpf larval zebrafish pectoral fin. The endoskeletal disc can be seen on the proximal side where the proximal and distal radials will develop. The distal mesenchyme in the fin fold will give rise to the lepidotrichia. PFF = pectoral fin fold, ED = endoskeletal disc. Scale bar = 200μm. Bone and cartilage staining was performed and imaged by Rob Lalonde.

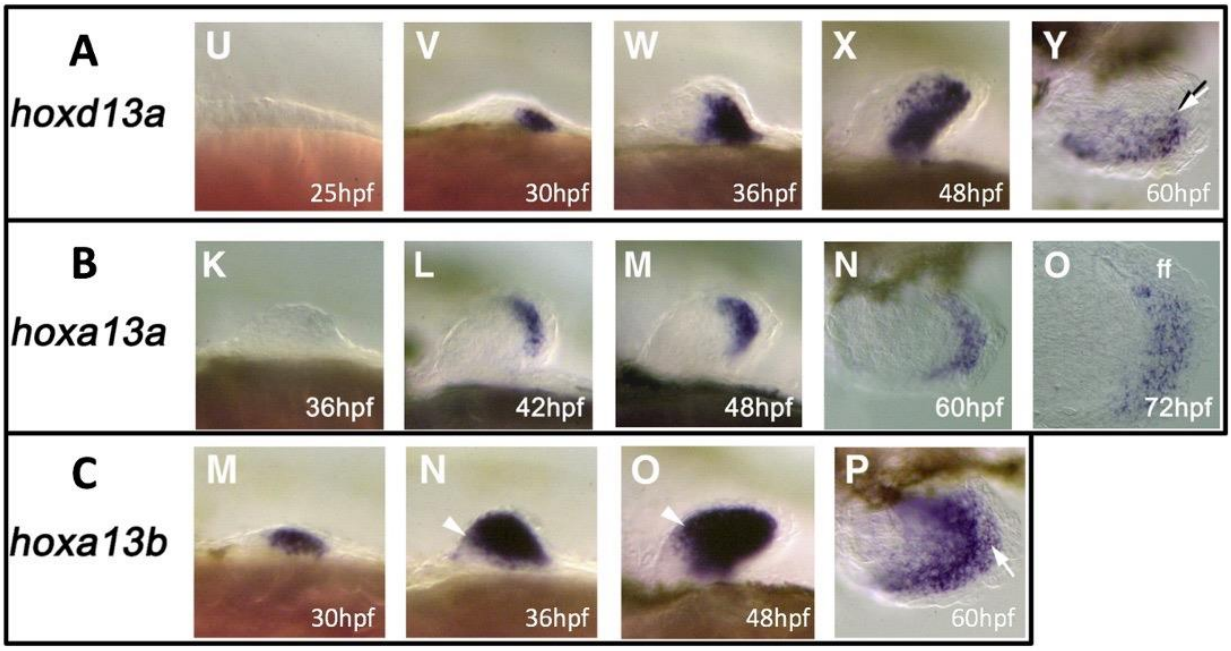

Figure 9. The expression of *hoxa13a, hoxa13b,* and *hoxd13a* in zebrafish pectoral fins during embryonic development. (A) The expression domain of *hoxd13a* at 25, 30, 36, 48, and 60 hpf is predominantly localized to the posterior region of the fin bud with some anterior expansion (B) The expression domain of *hoxa13a* at 36, 42, 48, 60, and 72 hpf is restricted to the distal region of the fin bud (C) The expression domain of *hoxa13b* at 30, 36, 48, and 60 hpf is broad throughout the fin bud. White arrowheads demonstrate the expression of each *hox13* gene in the distal mesenchyme of the fin bud. These migrating *hox13* expressing mesenchyme cells will form the fin rays later in development. Adapted from Ahn & Ho, 2008 with permissions from Copyright Clearance Center, April 22, 2023.

1.3 Adult Fin Structure

1.3.1 Exoskeleton

The visible, protruding part of each fin is the exoskeleton, and is made up of bony soft rays referred to as lepidotrichia (Akimenko et al., 2003). The endoskeleton of each fins lies proximally to the exoskeleton and attaches the lepidotrichia to the body of the fish for support (Bird & Mabee, 2003). In zebrafish, the emergence of the rays during development differs between fin type, although the rays of most fins will all typically emerge between 5.5-7.0mm standard length (SL) (Singleman & Holtzman, 2014) and 7.4-9mm SL in the case of the pectoral fin (Paulissen et al., 2022). The specific number of rays in each fin can vary, although this number is typically 16-18 rays in the caudal fin, 13-15 in the anal fin, 8-10 in the dorsal fin, 10-14 in the pectoral fin, and 7 in the pelvic fin (Bird & Mabee, 2003; Grandel & Schulte-Merker, 1998). While the number and length of rays vary, the general structure remains the same in all fins. Each soft ray is composed of two biconcave hemirays made of intramembranous bone. This bone is acellular, and is formed by intramembranous ossification, where mesenchyme cells lining the epidermal tissue differentiate into osteoblasts, and then deposit bone matrix (Akimenko et al., 2003). The mature hemirays encase connective tissue, nerves, and blood vessels in the adult rays (Géraudie & Landis, 1982). All fin rays of the zebrafish fins contain segments that are separated and maintained by fibrous joints along their proximal distal axis. All rays except for the lateral-most rays of the caudal fin, and anterior-most rays in the other fins normally bifurcate, which is when the ray splits into two sister rays towards the distal end of the fin (Azevedo et al., 2012). Bifurcations can happen multiple times in each fin ray along the proximal-distal axis. At the distal tips, each ray contains actinotrichia bundles. Evidence from our lab has observed actinotrichia forming in between the hemirays of the regenerating fin ray, where osteoblasts seem to colocalize with the fibers during

outward growth of the ray. This observation suggests that osteoblasts may be using actinotrichia fibers in the rays to migrate distally during growth, similar to how actinotrichia allow the migration of mesenchymal cells into the fin fold during early development. While the exoskeleton of the zebrafish consists only of soft rays, acanthomorph fish such as *A. burtoni* also develop spiny rays, as previously mentioned. Spiny rays develop most commonly in the dorsal and anal fins, although they do appear in the paired fins of some fish as well. During very early development, spiny rays and soft rays in *A. burtoni* anal and dorsal fins appear similar but become easily distinguishable at 10dpf as the unique characteristics of each begin to develop (Woltering et al., 2018). Of these unique differences, the first is that the spiny rays do not contain fibrous joints that can be seen in soft rays (Woltering et al., 2018). The spiny rays also do not bifurcate and are instead one long structure with no branches (Woltering et al., 2018). Instead of having actinotrichia bundles which comprise the tips of the soft rays, the spiny rays also end in a sharp point at the distal tip, which is useful as a defense mechanism against predators (Woltering et al., 2018, Price et al., 2015). Finally, the spines are more heavily ossified than the soft rays, and the hemirays of the spines are fused together at the anterior end instead of separate as in the soft rays (Weickhardt et al., 2017; Woltering et al., 2018).

Much of what is known about the growth of the adult fin rays at the molecular level comes from work done on fin regeneration, since many of the same mechanisms in regenerative fin ray growth are also thought to be involved in the normal development of the rays. The hemirays grow by successive addition of bone segments, which are separated by fibrous joints (Borday et al., 2001). Previous work in our lab have shown that there are three main stages to fin ray joint formation, which include presumptive joint cells, joint-forming cells, and mature joint cells

(McMillan et al., 2018). In the presumptive joint cell stage, cells can be seen forming a cluster where a new joint will be made (McMillan et al., 2018). Once this cluster starts to form, presumptive joint cells turn to joint-forming cells, which have been previously described by Sims et al. (2009) and form two distinct layers of cells in the forming joint. Finally, the two layers of joint forming cells separate and surround the newly formed joint as mature joint cells (McMillan et al., 2018). The exact mechanism of how joint cells are formed is not fully understood, although *evx1* and *pthlha* have been shown to be essential for joint formation (McMillan et al., 2018; Schulte et al., 2011). *Evx1* is known to act upstream of *pthlha* in joint cells, which is thought to cause an inhibition of osteoblast differentiation that results in the formation of joint cells (McMillan et al., 2018). *Hoxa13a* has also been shown to be involved in fin ray joint formation, where it is expressed strongly in presumptive joint cells before *evx1* expression (McMillan et al., 2018). From previous work done by Hailey Quigley, a former MSc student in our lab, we know that *evx1* is still expressed in the triple *hox13* mutants, suggesting that Evx1 and Hoxa13a are working in parallel instead of Hoxa13a being an upstream activator of *evx1* expression. *Hoxa13b* and *hoxd13a* however did not show expression in joint cells as was seen with *hoxa13a*, which suggested that these genes did not have a significant role in joint formation compared to *hoxa13a* (McMillan et al., 2018). In addition to just joint cells, *hoxa13a* is also shown to be expressed in the osteoblasts of regenerating fin rays (McMillan et al., 2018), further highlighting its potential role in the growth of the rays. As explained previously, the expression of some genes between the spiny ray and soft ray domains in acanthomorphs differs, where *alx4a* is expressed only in the spiny-ray domain of acanthomorph fish, and *hoxa13a/b* is only expressed in the soft ray domain (Höch et al., 2021). In adult zebrafish, *alx4a* has been shown to be expressed in the anterior rays of the fins (Nachtrab et al., 2013). *Alx4a* expression slightly differs between each fin however, where it is normally expressed in the three

anterior-most rays of the pectoral fin, the two anterior-most rays of the dorsal fin, the single anterior-most ray in the pelvic and anal fins, and the ventral-most ray of the caudal fin (Nachtrab et al., 2013). Specifically, *alx4a* is expressed in the osteoblasts and fibroblasts of these anterior fin rays (Nachtrab et al., 2013), however its exact role in these cell types remains to be fully understood. In order to see the consequences of *alx4a* overexpression in the fin, the group attempted to induce overexpression of *alx4a* in the fin using a zebrafish transgenic line Tg(*hsp70I:alx4a*) line. The results of this were relatively unsuccessful, although they were included as supplementary information. The *alx4a* fold change induced in this line was approximately 13, which was able to cause an increase in the width of the fin rays at the medial and posterior parts of the fins. This increase may not be high enough since *alx4a* expression is nearly absent in the posterior part of the fin, meaning even after the 13-fold change, expression levels are likely still very low. It could also be that there is a mechanism in place that inhibits the function of *alx4a* in the posterior rays. The other gene that was observed in this study, *hand2*, is expressed exclusively in the posterior domain of the fin during development. This gene was also overexpressed using an Tg(*hsp70I:hand2)* transgenic line. An overexpression of approximately 60-fold was induced for *hand2* to see an effect in the anterior part of the fin. Thus, the same level of overexpression for *alx4a* may be required to see significant morphological changes in the posterior fin rays.

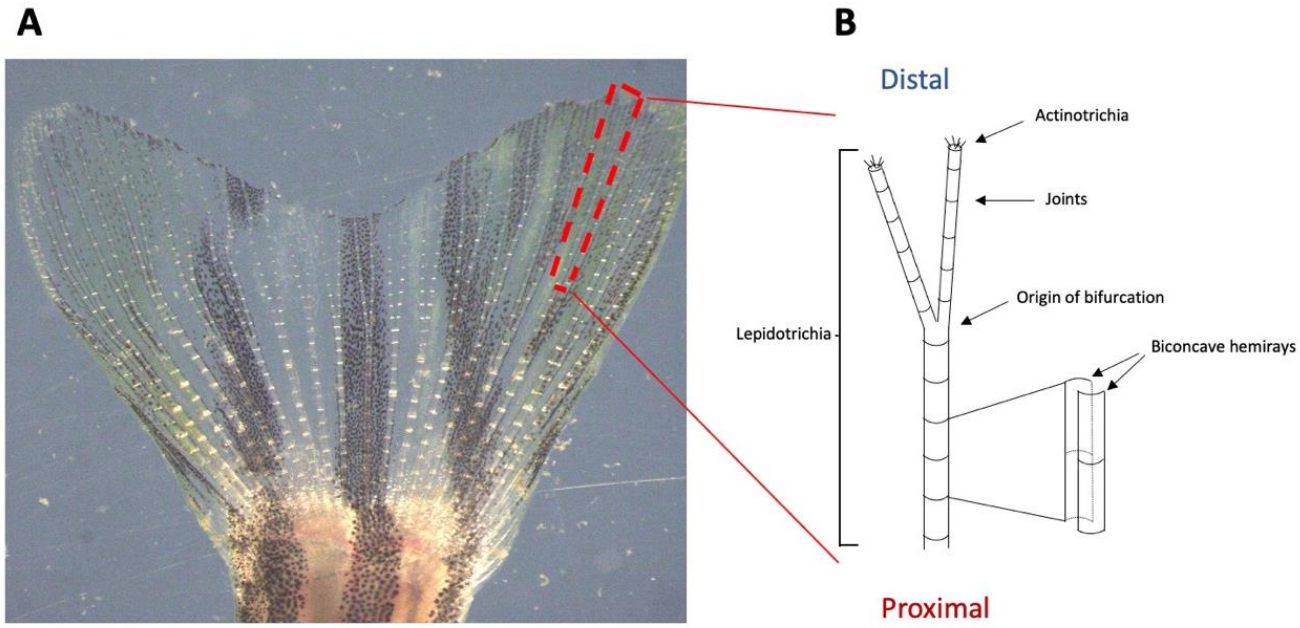

Figure 10. Main components of the zebrafish lepidotrichia. A: Brightfield image of intact zebrafish caudal fin. B: Schematic representation of a single ray with significant components labelled.

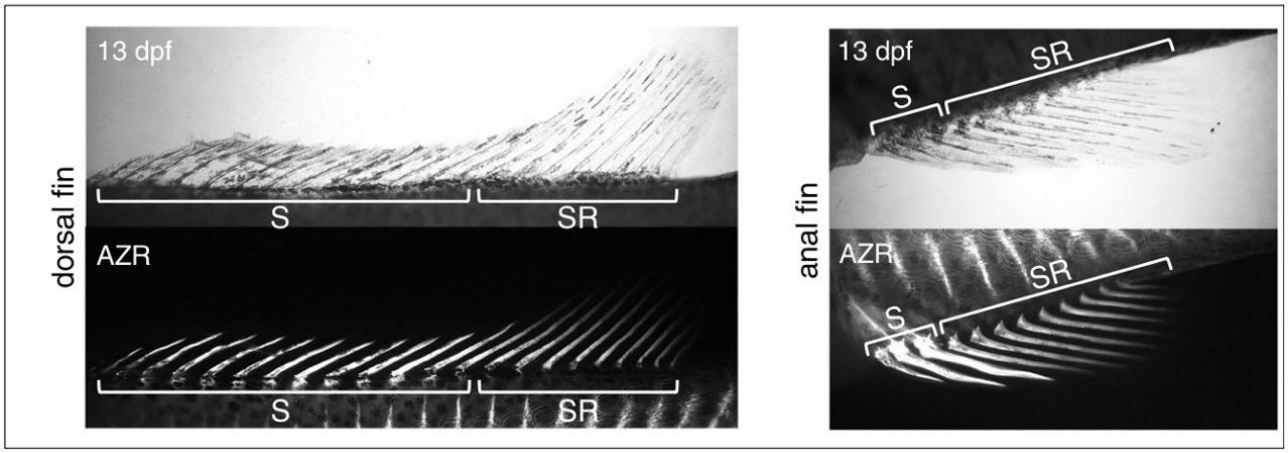

Figure 11. Visual comparison of spiny rays and soft rays in *A. burtoni* dorsal (left) and anal (right) fins. Top images show brightfield images of 13dpf dorsal and anal fins. Bottom images show fluorescent images for Alizarin red staining performed on the same specimen. S: spines, SR:

soft rays. Reproduced from Woltering et al., 2018 with permissions from PNAS: Open Access Articles, April 22, 2023.

1.3.2 Endoskeleton

Compared to the exoskeleton, which is made of dermal bone, the endoskeleton is made purely of endochondral bone, and is thus formed by endochondral ossification as opposed to intramembranous ossification. The endoskeleton of the adult pectoral fin contains 4 proximal radials, and 6-8 distal radials, which articulate to the lepidotrichia (Grandel & Schulte-Merker, 1998). The endoskeleton of the pelvic fin includes 2-3 proximal radials which articulate to the pelvic girdle on their proximal part and the lepidotrichia on their distal part (Grandel & Schulte-Merker, 1998). The paired fin endoskeleton is typically of greater interest to researchers due to its homology with mammalian limbs. The endoskeleton of the dorsal and anal fins includes 7-9, and 12-14 proximal radials, respectively, which articulate with fin rays in a 1-to-1 manner (Bird & Mabee, 2003). The distal radials of the dorsal and anal fins each articulate to a proximal radial. Each proximal radial extends proximally towards the vertebral column and anchors the fin to the intermuscular space to provide the fin with stability (Bird & Mabee, 2003). The caudal fin differs from other fins in that it develops into 2 separate lobes. The endoskeleton in the caudal fin is made from modified vertebral elements (Bird & Mabee, 2003). The largest components of the caudal fin endoskeleton are the hypurals and parahypural, which are expanded, laterally flattened hemal arches and spines that support the fin rays (Bird & Mabee, 2003). There are 3 hypurals that support the dorsal lobe (hypurals 3-5) and 2 hypurals (hypurals 1 and 2) and the parahypural that support the ventral lobe (Bird & Mabee, 2003). These elements extend from the terminal posterior vertebra known as the urostyle (Bird & Mabee, 2003). Other minor supporting elements of the caudal fin

include the hemal and neural spines, which extend from the ventral and proximal sides respectively of the second and third posterior most vertebra (Bird & Mabee, 2003).

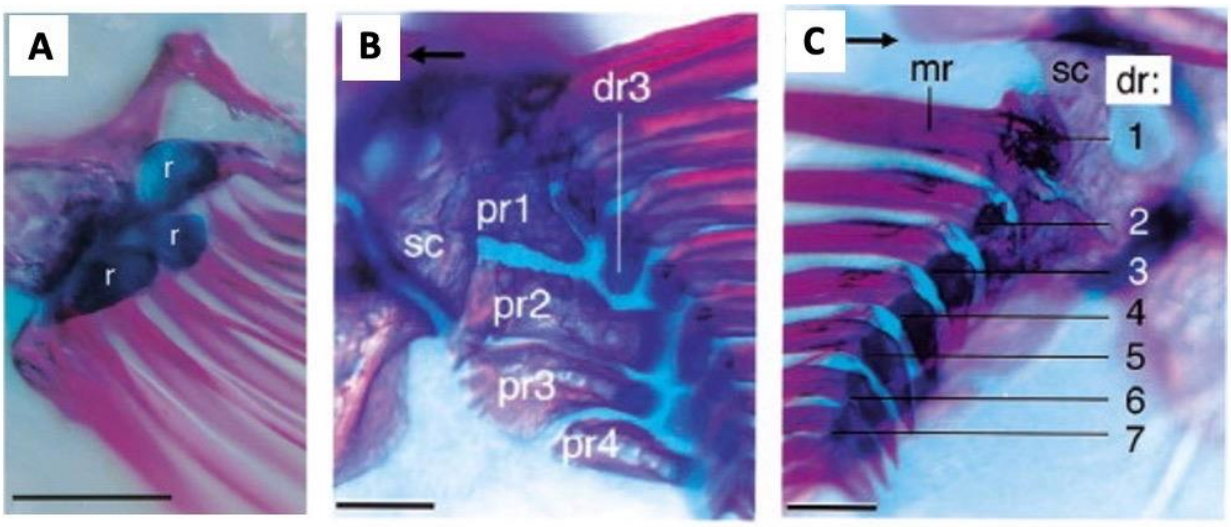

Figure 12. Anatomy of the zebrafish paired fin endoskeleton. Alizarin red and alcian blue staining of the pectoral and pelvic endoskeleton. A: Pelvic fin proximal radials (r) articulated to the pelvic girdle. B: Pectoral fin proximal radials (pr), scapula (sc), and distal radial 3 (dr3) C: Pectoral fin distal radials (dr1-7). Scale bars = 0.2mm. Adapted from (Grandel & Schulte-Merker, 1998). Adapted with permission from Copyright Clearance Center, April 22, 2023.

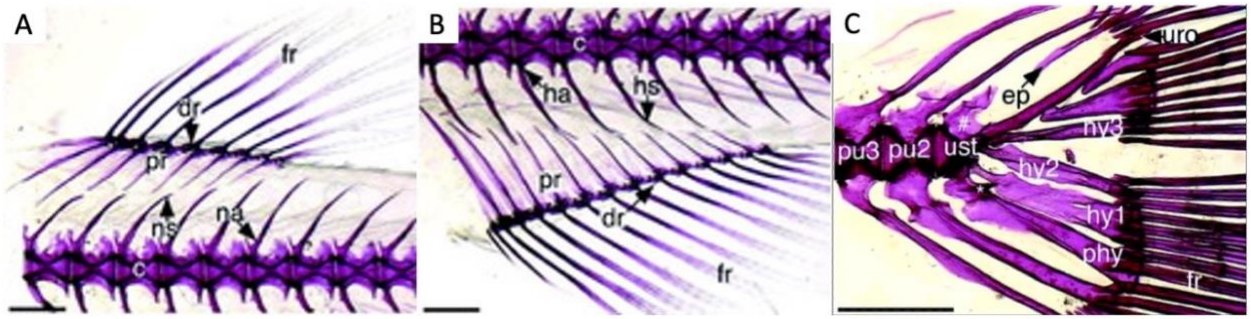

Figure 13. Anatomy of the zebrafish median fin endoskeleton. A: Bone-stained adult dorsal. Proximal radials (pr), distal radials (dr), and fin rays (fr) are dorsal to the caudal vertebrae, which include centra (c), neural arches (na) and neural spines (ns). B: Bone-stained adult anal fin. Proximal radials (pr), distal radials (dr), and fin rays (fr) are visible ventral to the caudal vertebrae, which include centra (c), hemal arches (ha) and hemal spines (hs). C: bone-stained adult caudal fin where urostyle (ust), uroneural (uro), parhypural (phy), hypural 1 (hy1), hypural 2 (hy2), hypural 3 (hy3), the epural (ep), and the centra of preural 2 (pu2) and preural 3 (pu3) are labeled. Scale bars = 0.1mm for all images. Adapted from Bird & Mabee, (2003) with permissions of Copyright Clearance Center, April 22, 2023.

1.3.3 The essentiality of *hox13* for adult fin patterning

To investigate the role of *hoxa13a, hoxa13b,* and *hoxd13a* in the adult fin, Nakamura et al. (2016) generated single knockout lines of zebrafish for each of these *hox13* genes, and double knockout lines for *hoxa13a* and *hoxa13b.* This was done by using CRISPR-Cas9 to introduce indel mutations within the coding region of each gene. Triple homozygous mosaic mutants were also generated from crossing *hoxa13a* -/- fish with *hoxa13a* -/+, *hoxa13b* -/+, *hoxd13a* -/+ fish, and injecting these embryos at the 1-cell stage with CRISPR gRNA for *hoxa13b* and *hoxd13a*. In this study however, a stable line of triple *hox13* mutants was not generated. After generating all of these mutants, CT scanning was used to analyze the radials of the pectoral fin. No changes could be observed in the single homozygous mutants. However, there was an increase in the number of distal radials in both the *hoxa13a* -/-, *hoxa13b* -/-, and triple homozygous mosaic mutants. In these mutants, 10-13 distal radials can be seen instead of only 6-8 as is normally seen in the wild-type. Furthermore, the extra distal radials in these mutants appeared to be stacked in the proximal-distal

direction, similar to what is seen in the phalanges of tetrapod limbs. Although how exactly the fin evolved to become a limb is not fully understood, it is thought to be associated with a loss of the dermal bone, and an expansion of the endochondral bone in the fish fin (Coates et al., 2008). For this reason, the expansion, increase and stacking of the distal radials along the proximal-distal axis was the main interest of the authors due to the increased resemblance to the tetrapod limb. A shortening of the fin rays was also reported in the double mutant and the mosaic mutant, although they do not further analyze the structure of the rays. The lack of explanation as to what is happening with the fin rays in these mutants has left a knowledge gap about the specific role of the *hox13* genes in the fin rays of each fin.

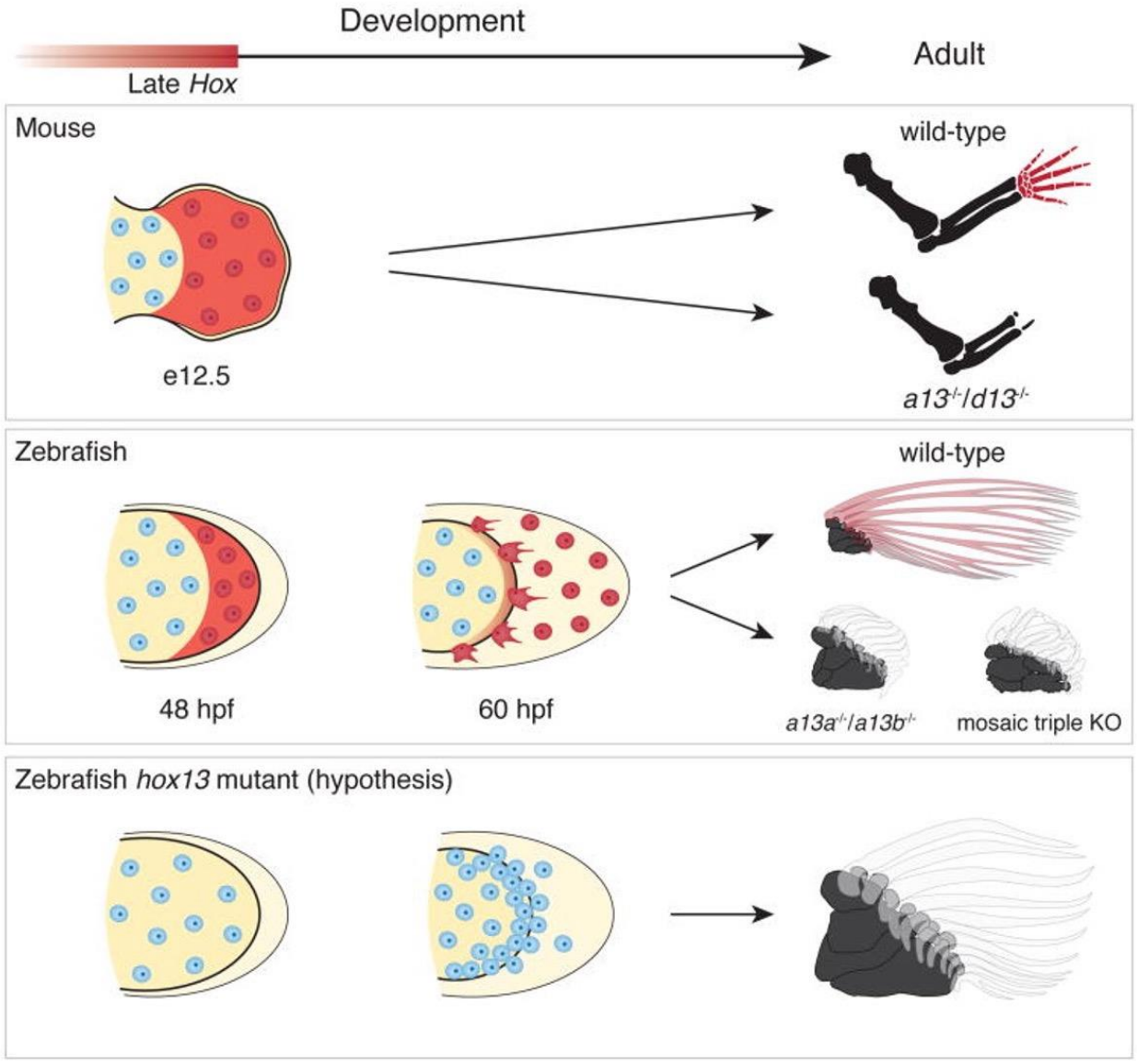

Figure 14. *Hox13* is essential for proper autopod development in mice and zebrafish. Knockouts of *Hoxa13* and *Hoxd13* in mice lead to a complete loss of the autopod (top row). Knockouts of *hoxa13a, hoxa13b,* and *hoxd13a* in zebrafish lead to defects in the pectoral fin autopod, but not a complete loss (middle and bottom rows). Red shade: late phase *hox* expression. Red cells: cells that experienced late phase *hox* expression. Nakamura et al. (2016), reproduced with permission from Copyright Clearance Center, April 22, 2023.

1.4 The potential role of *hox13* in fin ray vasculature and urogenital pore formation

Given the opportunity that will be presented by the triple *hox13* mutants, I also want to examine the role of the *hox13* genes on other aspects in the zebrafish. As previously discussed, the vasculature of the adult fin rays another element that will be observed in this project in the triple *hox13* mutants. As a result, it is important to understand the main vascular structures in the fins. The blood vessels that will vascularize the pectoral fin rays are formed by angiogenesis and emerge from the distal vascular plexus around 7.4-9mm SL (Paulissen et al., 2022). Arteries emerge and vascularize each ray after the bone of the rays begins to form (Paulissen et al., 2022). Recently, the caudal fin has also shown a similar mechanism of ray vascularization, where remodelling of an endothelial plexus occurs and arteries sprout from the plexus to vascularize the emerging rays (Bump et al., 2022). Figure 14 shows the vasculature of a fully-grown adult zebrafish ray using a transgenic line *Tg(fli1:eGFP)*^{y1} that was first described by Lawson & Weinstein (2002). In this line, eGFP is expressed in blood vessels under the control of the regulatory element of *fli1a*, an endothelial cell marker. Each adult fin ray is vascularized with one central artery inside the ray, and two paired veins that run along either side of the ray (Huang et al., 2003). In the distal half of the fin, intervessel commissures can be seen between the artery and veins of an individual ray approximately every 0.1mm along the proximal distal axis (Huang et al., 2003). Approximately every 0.5mm, branching interray vessels can be found connecting the veins of separate rays (Huang et al., 2003). Some evidence of the role of *Hoxa13* in mouse vascular development has been previously reported, where knockouts of *Hoxa13* have been found to cause defects in placental patterning, umbilical artery formation and downregulation of several pro-vascular genes in mice (Shaut et al., 2008, Stadler et al., 2001).

In addition to the blood vessels, it is possible that there are also defects in the terminal parts of the urogenital tracts in these fish from evidence seen in mice. Both *Hoxa13* and *Hoxd13* in mice are expressed in many genito-urinary structures during development such as the Wolffian ducts, the prostate, and seminal vesicles in males, and the Müllerian ducts, the cervix, and the vagina of females (Warot et al., 1997).

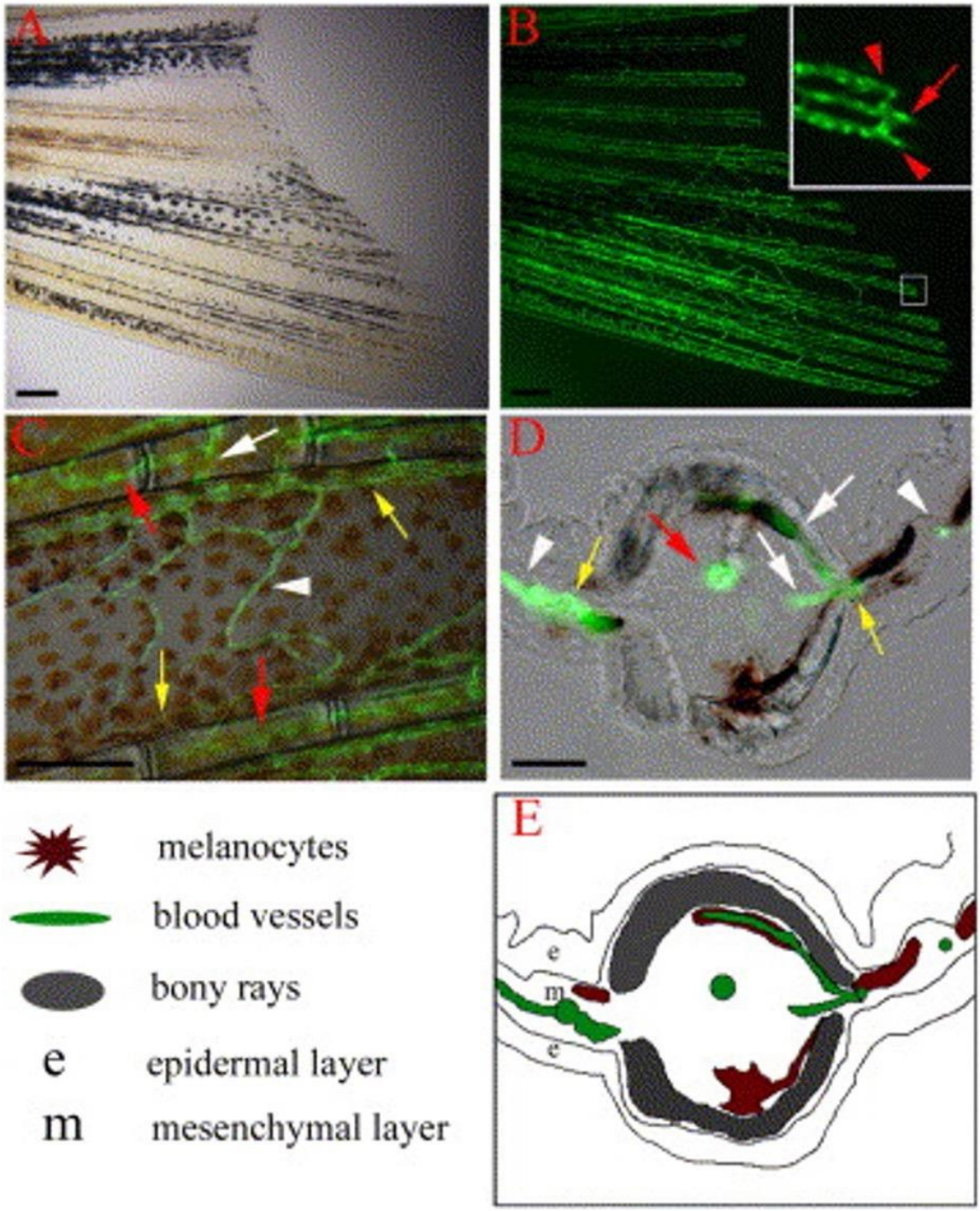

Figure 15. Vasculature of an adult zebrafish fin ray. Tg(*fli1*:EGFP)^{y1} fish expressing EGFP in blood vessel endothelial cells. (A) Bright field image of the caudal fin of an adult Tg(*fli1*:EGFP)^{y1} fish and (B) epifluorescence image of the same fin, showing the vasculature

in green. (Inset) Higher magnification of the distal end of a fin ray (boxed region) shows that each fin ray is associated with one artery (red arrow) in the center of the ray and two veins (red arrows) adjacent to the bony ray. (C) High magnification image shows the intervessel commissures within the same ray (white arrow), which connect artery to vein as well as vein to vein. The interray vessels (white arrowhead) connect vein to vein of adjacent rays. (D, E) Cross-section through a fin ray shows the artery in the center of intraray mesenchyme (red arrow), while the veins are in interray mesenchyme adjacent to the bony rays (yellow arrows). Intervessel commissures (white arrows) and interray vessels (white arrowheads) are also visible in this section. Explanatory diagram is shown in (E). Scale bars, 200 μm in (A, B, C), 20 μm in (D). (Huang et al., 2003). Reproduced with permissions from Copyright Clearance Center, April 22, 2023.

1.5 Creation of *hoxa13a -/-, hoxa13b -/-, hoxd13a -/-* mutants

In order to further study the role of *hoxa13a*, *hoxa13b,* and *hoxd13a* on the zebrafish fin rays, Dr. Qingming Qu, a former postdoctoral fellow in the laboratory, used CRISPR-Cas9 to induce deletion mutations in each of these genes. For a given gene, two guide RNAs targeting each of these genes were injected at the 1-cell stage into wild-type zebrafish embryos (accession # PRJNA11776) to create single deletion *hox* mutants. The specific deletions created are outlined in figure 15. After establishing each individual line of *hoxa13a, hoxa13b,* and *hoxd13a* mutants, no deformities could be observed in any of the fins of the single mutants. Hailey Quigley, a former MSc student in the lab, then crossed these lines together to obtain homozygous mutant lines with all three deletions, referred to as the *hox13* triple mutant. The *hox13* triple mutant displayed a very unique phenotype, that appeared to differ between different fins. The caudal fin did not appear much different from the wild type fish aside from decreases in fin ray length in the lobes, but the

dorsal, anal, pelvic, and pectoral fins all lost the ability to form joints, bifurcations, and actinotrichia. Additionally, the rays of these fins showed a large reduction in length.

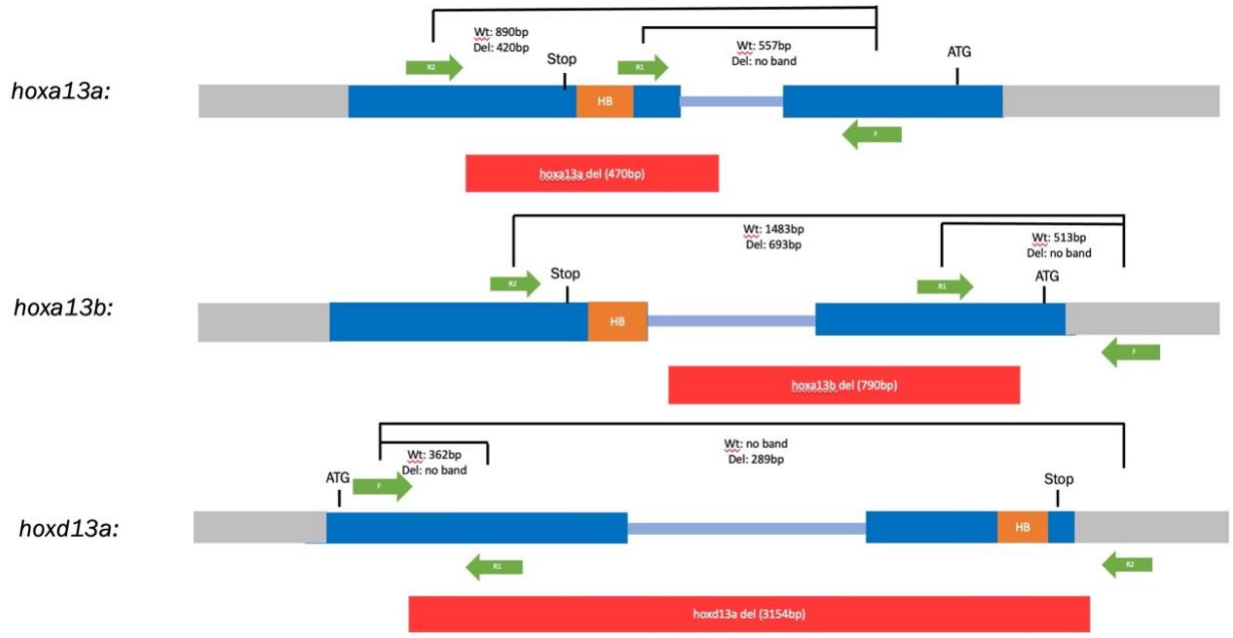

Figure 16. A schematic representation of our *hox13* deletion mutations. A representation of *hoxa13a*, *hoxa13b*, and *hoxd13a* (collectively referred to as *hox13*) are shown, with red bars representing the portion of the gene deleted in the mutants. Translation start (ATG) and stop sites are indicated on each gene. Green arrows represent primers used for genotyping, along with the expected band sizes in both wild-type and mutant fish. Homeobox domains are represented in orange as HB for each gene. Primer sequences used for genotyping each gene are outlined in Table 1.

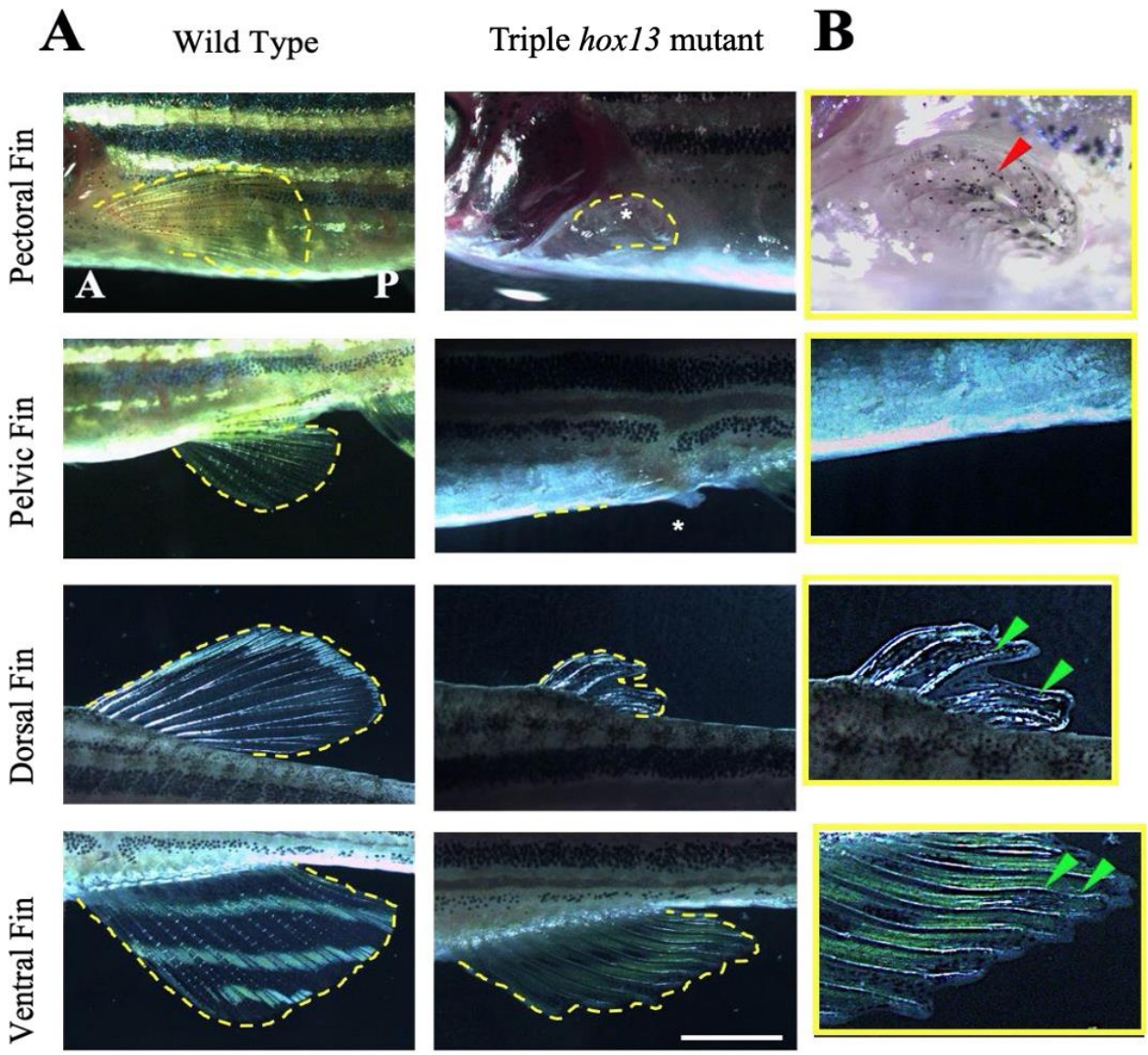

Figure 17. Triple *hoxa13a, hoxa13b, hoxd13a* deletion mutant pectoral, pelvic, ventral, and dorsal fins have a phenotype of reduced fin length and absence of joints in comparison to wild-type fins. A) Comparison of wild-type versus hox mutant pectoral, pelvic, dorsal, and anal fins. A (anterior) and P (posterior) in first panel represent orientation of fish in all panels. Scale bar = 3mm in last panel for all images in A). B) Enlarged images of triple hox13 mutant fin phenotypes: curled (indicated with red arrows) and wavy (indicated with green arrows). N= 5 fish per group. Images taken by Hailey Quigley.

1.6 Hypotheses and objectives

Hypothesis 1 and objectives

The zebrafish *hoxa13a, hoxa13b* and *hoxd13a* genes have been shown to be very important for the development and patterning of the fin rays. From single knockouts of these genes, we observe no visible repercussions on fin phenotype, indicating a likely redundancy in these genes. From the triple knockout, we see that these genes appear to have a much more significant role in the patterning of certain fins, as we see varying levels of defects in each fin type. This leads to the first hypothesis of this project, which is that ***hoxa13a, hoxa13b*** **and** ***hoxd13a*** **have partially redundant but varying roles in the fin ray formation of each fin type.**

Objective 1: Morphological analysis of double and triple homozygous *hox13* mutants.

This objective aimed to explore the individual contributions of each *hoxa13a, hoxa13b,* and *hoxd13a* to adult fin phenotype. In addition to comparing single homozygous *hox13* mutants to wild-type fish, double homozygous *hox13* mutants were also compared to the triple homozygous *hox13* mutants to observe how each gene individually is able to alter the phenotype from the triple mutants. Specifically, each adult fin of each genotype was imaged to observe the presence or absence of joints, bifurcations, and actinotrichia, as well as measure the length of fin rays. Additionally, the blood vessels in *hox13* mutant Tg(*Fli1a*:EGFP) line, and the urogenital pore of these mutants will be observed for potential defects .

Hypothesis 2 and objectives:

Following initial morphological analyses on these *hox13* mutants, the apparent similarities between the *hox13* triple mutant, and the acanthomorph spiny rays became apparent. Phenotypically, both these mutant rays and spines lack bifurcation and joints and are shorter compared to normal soft rays. This leads to the second hypothesis of this project, which is that ***hox13* mutant fins are forming spine-like structures as opposed to normal soft rays.** In order to test this hypothesis, two objectives were created to look for further similarities between the *hox13* mutant rays and acanthomorph spines:

Objective 1: Compare the thickness of the hemirays in the *hox13* triple mutant to wild-type zebrafish. In addition to the lack of joints, bifurcations, and tip actinotrichia, the acanthomorph spines are more ossified than soft rays (Weickhardt et al., 2017; Woltering et al., 2018). If the triple *hox13* mutants are indeed forming these spine-like structures, the bone of the triple *hox13* mutant hemirays should presumably be thicker and more ossified compared to the hemirays of wild-type fish. Analysis of the ray thickness was done through micro-CT scanning of the dorsal and anal fins of triple *hox13* mutants, and wild-type siblings.

Objective 2: Compare *alx4a* gene expression patterns in the developing triple *hox13* mutant, and wild-type dorsal and anal fin folds. As shown by Höch et al, (2021), *hoxa13b* is typically restricted to the soft-ray domain, and *alx4a* is typically restricted to the spiny ray domain in the acanthomorph dorsal and anal fin fold. *in situ* hybridization has been used to observe *alx4a* expression patterns in the developing dorsal and anal fins of the zebrafish triple *hox13* mutants.

Chapter 2: Materials and methods

2.1 Animal housing and breeding

2.1.1. Animal care

All zebrafish used for this project were bred and housed in the University of Ottawa aquatics facility. All fish are housed in a 28.5°C temperature-controlled room consisting of a 14-hour light/ 10-hour dark cycle. Fish were regularly fed by Animal Care and Veterinary Services (ACVS) staff at the university, and system water used in the tanks was UV sterilized. Animal care and experiments were all performed according to Canadian Council on Animal Care (CCAC) guidelines.

2.1.2 Breeding and generation of mutants

False bottom traps were used for breeding as described in Westerfield (2007). Zebrafish were fed at shorter intervals the day before the intended breeding day and were then placed into the false bottom traps with males and females separated by a plastic partition. The next morning following the lights turning on, the divider was removed, and the fish were permitted to breed. After fish were permitted to breed for a few hours, embryos were collected and stored in petri dishes filled with embryo (E3) medium (5mM NaCl, 0.33mM CaCl2, 0.33mM MgSO4, 0.17mM KCl, 6-12 µM methylene blue) in a 28.5°C incubator. After 24 hours, the embryos were exposed to 0.0003% bleach for 10 minutes, followed by a 1-minute exposure to a 0.05% $Na_2S_2O_3$ neutralizing solution and two 2-minute washes in E3 medium. Embryos were then returned to clean petri dishes in E3 medium until 5dpf. At 5dpf, E3 was changed to system water in the petri dish, and the embryos were moved into a tank containing system water to be raised to adulthood.

Double and triple homozygous *hox13* mutants were generated from heterozygous crosses. *hoxa13a* -/+, *hoxa13b* -/-, *hoxd13a* -/- mutants, *hoxa13a* -/-, *hoxa13b* -/-, *hoxd13a* -/+ mutants, and

hoxa13a -/-, *hoxa13b* -/-, *hoxd13a* +/+ mutants analyzed were all obtained from genotyping triple heterozygous crosses (*hoxa13a* -/+, *hoxa13b* -/+, *hoxd13a* -/+). *hoxa13a* -/-, *hoxa13b* -/+, *hoxd13a* -/- mutants, and triple homozygous *hox13* mutants were obtained from a combination of triple heterozygous crosses, and *hoxa13a* -/-, *hoxa13b* -/+, *hoxd13a* -/- crosses. To generate Tg(*fli1a*:eGFP); *hoxa13a* -/-, *hoxa13b* -/-, *hoxd13a* -/- mutants, Tg(*fli1a*:eGFP) fish were initially bred with triple heterozygous *hox13* mutants to obtain Tg(*fli1a*:eGFP); *hoxa13a* -/+, *hoxa13b* -/+, *hoxd13a* -/+. From triple heterozygous crosses, of these fish, the Tg(*fli1a*:eGFP); *hoxa13a* -/-, *hoxa13b* -/-, *hoxd13a* -/- were obtained through genotyping. Wild-type siblings were also obtained from triple heterozygous crosses.

2.2 DNA extraction and genotyping:

2.2.1 Adult DNA extraction:

DNA was extracted from scales taken off the side of the fish. Fish were anesthetized in tricaine at a concentration of 0.2mg/mL and placed under a dissecting microscope. Scales were taken off the body using needle-nose tweezers and placed into 50µL of 50mM NaOH in a 1.5mL microcentrifuge tube. Each sample was then boiled at 95°C for 5 minutes, vortexed, and boiled again for an additional 5 minutes. The samples were then cooled on ice for 5 minutes, and 5µL of 1M Tris-HCl (pH 8.0) was mixed into each sample before being stored at -20°C.

2.2.2 Larval DNA extraction:

This protocol was adapted from Zhang et al. (2020). Larvae were moved to a new petri dish and washed with DNA collection buffer (15mL 1M Tris-HCl pH 8, 20mL 0.4% Tricaine,

465mL water) for 2 minutes, three times. DNA collection buffer was then removed from the petri dish and replaced with DNA collection solution (25µL of 20mg/µL proteinase K in 20mL of E3). Individual larvae were then transferred to individual wells on a 96-well plate with 40µL of DNA collection solution from the petri dish. The 96-well plate with larvae was then stored on an incubated mixing plate at 37°C and mixed at 150rpm for 30 minutes. After the incubation, the solution of each well was pipetted up and down 10 times to ensure proper mixing of the collected DNA. 30µL of this mixed solution was then transferred to corresponding wells on a PCR plate, and 15µL of lysis buffer (10mM Tris-HCl pH 8, 50mM KCL, 0.3% Tween 20, 0.3% NP40, 1mM EDTA) was added to each well. 100uL of 1X recovery buffer (100X recovery stock: 0.5M NaCl, 0.68M KCl, 0.030M $CaCl_2$-$2H_2O$, 0.054M $MgSO_4$, pH 7.2) was then added to each of the wells in the 96-well plate containing larvae to ensure survival The PCR plate was then incubated in a thermal cycler at 98°C for 5 minutes to denature proteinase K and release DNA from the cells in solution. If the survival of the larvae was not necessary after genotyping, the head of the larvae can be used with the same protocol outlined in the adult DNA extraction, while the rest of the body was fixed in 4% paraformaldehyde (PFA) at 4°C overnight. After fixation, the larval bodies were washes twice in 1x PBS for 5 minutes, and then dehydrated in 100% methanol and stored at -20°C.

2.2.3 Genotyping polymerase chain reaction (PCR)

PCR reactions were mixed into 0.2mL tubes. Each individual reaction contains 0.25µM of a forward primer, 0.25µM of a reverse primer, 1X GoTaq® Green Master Mix, and ddH_2O to complete the volume to 25µL. The primers used to genotype each gene of interest are shown in the table below. The samples were run in a thermal cycler using the following program: an initial denaturation at 95°C for four minutes, followed by 30 cycles consisting of one minute denaturation

at 95°C, one minute annealing at 58°C, and two-minute elongation at 72°C, and one final elongation at 72°C for five minutes.

2.2.4 Gel electrophoresis:

To observe the size of the PCR product, product was loaded onto a 200mL, 1.5% agarose gel and run at 130V for approximately 25 minutes. For each gene being genotyped, two sets of primers are used. For each gene, there is one forward primer (F), and two reverse primers, where one reverse primer is outside of the deletion (R1), and the other is inside the deletion (R2). These primers yield varying sized product depending on the presence of wild-type and/or mutant DNA, allowing the genotype of each fish to be identified. Primer sequences and expected band lengths are shown in the table below.

Primer name	Primer Sequence	Expected Band Sizes (with corresponding F primer)
hoxa13a F	5’AGGCGAAGATTATACCAGCTCAC3’	
hoxa13a R1	5’CATCAAACAACTCATCCTTTGG3’	WT: 890bp Deletion: 420bp
hoxa13a R2	5’CCTGTCGTTCAGATAGGTTGG3’	WT: 557bp Deletion: no band
hoxa13b F	5’CCACCACTTTGTTTCAGTTCAA3’	
hoxa13b R1	5’TGATGCCCTTGTACTTGTTGAC3’	WT: 1483bp Deletion: 693bp
hoxa13b R2	5’ATATCCATAGGGCAAAGAAGCA3’	WT: 513bp Deletion: no band
hoxd13a F	5’TTTACCCATCTGCCTTCGGG3’	
hoxd13a R1	5’AGACCTCTTGCAGTCAAGGT3’	WT: no band Deletion: 362bp
hoxd13a R2	5’CTGCTGCAATTGTTTGACCAGT3’	WT: 484bp Deletion: no band

Table 1. Genotyping primers for *hox13* deletion mutants. For each given gene, one forward and two reverse primers are used in separate reactions. The expected band sizes for each reverse primer when mixed with the corresponding forward primer for that gene are presented.

2.3 Imaging adult zebrafish

2.3.1 Fin imaging

Fin imaging was done using a Leica MZFLIII dissecting microscope and images were taken on a Luminera Infinity 3 camera. Fish were anesthetized in tricaine and placed under the microscope on a petri dish containing a 2% agarose gel to be used as a background. Each fin is imaged at 1X magnification, and tips of the fins are also imaged at 8X magnification in order to observe the presence of actinotrichia in the fin. Fins are imaged with the anterior side facing towards the left side of the field of view, and the posterior side facing to the right. In the case of the pectoral fin, the fish was placed on its back in a petri dish containing 2% agarose gel with a slit for the fish to sit in. The pectoral fin was then spread over the gel to be imaged. The genotypes of interest that were imaged and used for analysis included six genotypes outlined below in table 2.

Genotype	Replicates
hoxa13a -/+, *hoxa13b* -/-, *hoxd13a* -/-	n=9
hoxa13a -/-, *hoxa13b* -/+, *hoxd13a* -/-	n=11
hoxa13a -/-, *hoxa13b* -/-, *hoxd13a* -/+,	n=8
hoxa13a -/-, *hoxa13b* -/-, *hoxd13a* +/+,	n=2
hoxa13a -/-, *hoxa13b* -/-, *hoxd13a* -/-,	n=10
wild-type siblings	n=6

Table 2. *hox13* mutant genotypes of interest. Replicates imaged and used for the morphological analysis are listed for each genotype.

2.3.2 Blood vessel and urogenital pore imaging

For imaging Tg(*fli1a*:eGFP); *hoxa13a* -/-, *hoxa13b* -/-, *hoxd13a* -/- mutants and wild-type Tg(*fli1a*:eGFP) fish, a similar process was used for brightfield images of the fin. The blood vessels of the fish were imaged on the Leica MZFLIII dissecting microscope at 4X magnification through a GFP filter. In the case of the urogenital pore, wild-type and triple *hox13* mutant fish were anaesthetized in tricaine and placed under an Axiozoom V16 dissecting microscope for imaging. Urogenital pores of each fish were imaged at 16.5x magnification.

2.4 Morphometrics and measurements

Zebrafish fin, and urogenital pore images were measured in ImageJ. Fish used for imaging and measurements were all between a standard length (SL) of 3-3.2mm. For each fin, standard fin rays were used for the measurements across all fish for all genotypes. For the caudal fin, the measured fin rays included the third ray from the dorsal side (D3), the third ray from the ventral side (V3), and the middle-most ray in the cleft of the fin (M). For the anal fin, the third ray from the anterior side (A3) and third ray from the posterior side (P3). For the dorsal fin, A2 and P3 rays were used. For the pectoral fin, A3 and P3 rays were used. For the pelvic fin, only the middle-most ray (M) was used due to the extremely small size of the mutant fins. The same fin rays used for measurements were also used to count joints. 95% confidence intervals were used to compare the length of each fin ray of interest between different genotypes of interest. For the urogenital pore, the length of the pore in each fin was measured from the body of the fish out towards the tip of the pore.

2.5 *In vitro* fertilization:

In vitro fertilization was performed on wild-type, triple *hox13* mutants, and *hoxa13a -/-, hoxa13b -/+, hoxd13a* -/- mutants. Fish are first anaesthetized in tricaine. The body of the male fish is dried completely with a Kimwipe, and the male is placed in the lid of a petri dish under a dissecting microscope. 100µL of Hank's Balanced Salt Solution (Lot # RNBK2365) is pipetted onto the male urogenital pore. The male is then pressed with a P200 pipette tip from the testes towards the urogenital pore until sperm is released. The sperm is then collected with a P200 pipette and placed into a 0.5mL tube on ice until further use. The male is then returned to the original tank for recovery. The female is then placed in the bottom of the petri dish under a dissecting microscope after being anaesthetized in tricaine. The eggs are released from the female by rubbing the belly of the fish starting from the pectoral fin and moving caudally towards the urogenital pore. Once eggs are released, the female is returned to the tank for recovery, and the sperm from the male is pipetted onto the eggs using a P200 pipette. The eggs are left for 3 minutes to fertilize, and then E3 embryo medium (0.287g NaCl, 0.0127g KCl, 0.0817g $MgSO_4$, 0.0483g $CaCl_2$, 0.00003% methylene blue in 1L of H_2O) is added to the petri dish. The fertilized embryos can then be raised to adulthood. This process was attempted three times with triple *hox13* mutants (6 males and 5 females). None of the females were ever able to release eggs, although sperm appeared to be released from one of the males twice. This sperm however was unable to fertilize eggs from *hoxa13a -/-, hoxa13b -/+, hoxd13a* -/- mutants on the first attempt, or eggs from wild-type fish on the second attempt. The process was successful with wild-type fish, and with *hoxa13a -/-, hoxa13b -/+, hoxd13a* -/- mutants.

2.6 Bone staining:

This protocol was adapted from Sakata-Haga et al. (2018). Fish was first euthanized in ice water for 10 minutes. The body of the fish was then transferred to a fixative solution consisting of final concentrations of 5% Formalin, 5% Triton X-100, and 1% KOH and incubated at 42°C for approximately 12-48 hours (until the fish is clear and there are no longer any stripes or pigment). The fixative was replaced every 24 hours if longer fixation is required. Once clear, the body was moved to enhancement solution (20% ethylene glycol, 5% Triton-X 100, 1% KOH) at 42°C for 48 hours. After enhancement, the scales were completely removed from the body, and the body is washed three times with distilled water for 10 minutes each wash. The fish was then immersed in cartilage staining solution (500µL of 0.005% alcian blue in 10mL of 70% EtOH) for 3 hours at room temperature with gentle rocking. The body was then washed twice in 1% Triton-X 100, 70% EtOH for 10 minutes each wash, and then is immersed into the bone staining solution (0.005g Alizarin red, 2mL ethylene glycol, 5mL KOH, 3mL water for 10mL) for 1 hour at room temperature with gentle rocking. The fish was then switched to pre-warmed clearing solution (20% Tween-20, 1% KOH) and incubated overnight at 42°C (the fish can be cleared longer if the body is more blue or red than desired from the staining). Once the fish was cleared to the desired point, the body was washed twice for 10 minutes in distilled water, and then immersed into enhancement solution once more at 42°C overnight. Finally, the fish was moved through a graded series of glycerol washes overnight at room temperature (50%, 70%, 90% in 2% KOH) and then stored in 100% glycerol until imaged.

2.7 Probe cloning for *In-situ* hybridization

2.7.1 RNA extraction from wild-type embryos

Total RNA was collected from 24-hour post-fertilization (hpf) embryos when *alx4a* is expressed (Dee et al., 2013). Approximately 50 embryos were pooled together in 1mL of TRIzol in a 1.5mL Eppendorf tube. The sample was homogenized by repeatedly pipetting up and down and then incubated for 5 minutes at room temperature to allow dissociation of the nucleoprotein complex. 0.2mL of chloroform was then added to the sample, and the sample was then immediately vortexed for 15 seconds. The vortexed sample was then incubated at room temperature for 3 minutes, and then was centrifuged at 12500 RPM for 10 minutes at room temperature. After centrifugation, the aqueous phase was then transferred to a clean 1.5mL microcentrifuge tube. 0.5mL of isopropanol were then added to the aqueous phase, and the sample was incubated at room temperature for 10 minutes. After the incubation, the sample was centrifuged at 12500 RPM for 20 minutes at 4°C. The supernatant was removed after the spin and the pellet is washed with 500µL of 75% EtOH. The sample was then centrifuged a final time at 10000RPM for 5 minutes at 4°C. Finally, the supernatant was removed, the pellet was resuspended in 20µL of RNAse free water, and incubated at 55-60°C for 10 minutes before being stored at -80°C.

2.7.2 Probe cloning

An *alx4a* was cloned using the same primers as Dee et al. (2013). Total RNA was isolated from 24hpf wild-type embryos. Total RNA was reversed transcribed into cDNA using a BIO-RAD iScript Reverse Transcription kit (Catalogue # 1708841). 1ng of total RNA was added to a 0.2mL tube with 4µL of iScript RT Supermix containing RNase H+ Moloney murine leukemia virus (MMLV) reverse transcriptase, RNase inhibitor, dNTPs oligo(dT), random primers, buffer,

$MgCl_2$, and stabilizers. The sample was completed to 20µL and placed in a thermal cycler, where it was run through three cycles: 5 minutes at 25°C, 20 minutes at 46°C, and 1 minute at 95°C. The cDNA product was then stored at -20°C. The cDNA product is used as a PCR template to amplify the coding region of the *alx4a* mRNA sequence (F: 5' ATG AAC GCC GAG ACG TGC 3'; R: 5' TCA TGT AGC CCA AGA GAT GGC 3'). The PCR product was run on 1% agarose gel for 25 minutes and gel extracted using a QIAquick gel extraction kit (Catalogue # 28506). The purified PCR fragment (1096bp) was then ligated into a Pdrive vector via TA cloning with a QIAGEN PCR cloning kit. 1µL of the ligated plasmid was used to transform XL-10 electrocompetent cells (40µL) using a BioRad MicroPulser electroporator. The transformed cells are grown for 1 hour in SOB medium in a shaker plate set at 37°C and 180rpm, and then plated on LB (10g/L Bacto Peptone, 5g/L Bacto yeast extract, 10g/L NaCl in ddH_2O) plates with ampicillin (100µg/mL) and kanamycin (50µg/mL) overnight in a 37°C incubator. A grown colony was then picked by stabbing with a pipette tip, and grown in 50mL of LB medium containing ampicillin (100µg/mL) and kanamycin (50µg/mL) overnight at 37°C. The plasmid was then isolated using a QIAGEN plasmid midi kit (Catalogue #12125).

2.7.3 Probe synthesis:

10µg of *alx4a*:Pdrive plasmid was linearized using *Hind*III for 2 hours in a 37°C water bath. Following the incubation, the linearized plasmid was cleaned using a QIAquick gel extraction kit. A reaction mix was then made from 1µL of linearized plasmid DNA, 2µL of Digoxygenin-labelled NTPs, 2µL of 10x transcription buffer (400mM Tris-HCl pH 7.5, 60mM $MgCl_2$, 20mM Spermidine HCL, 50mM NaCl), 0.5µL of RNAse inhibitor (40units/µL stock), 2µL of SP6 RNA polymerase, and 12.5µL of nuclease free water. This reaction mix was then incubated in a 37°C

water bath for 2 hours. The probe was then precipitated by adding 2.5µL of 4M LiCl 75µL of cold 100% EtOH and incubating at -80°C for 30 minutes. The precipitated probe was then centrifuged for 15 minutes at 4°C at top speed. The supernatant was discarded, the RNA pellet was washed with cold DEPC-70% EtOH and centrifuged again for 15 minutes at 4°C at top speed. The supernatant was discarded, and the pellet was resuspended in 25µL of nuclease free water. 1µL of the isolated probe was mixed with 4µL of 2X RNA loading buffer, and 3µL of DEPC water. The sample was heated at 70°C to denature the probe and then chilled on ice before being run on a 0.8% agarose gel for 20 minutes at 130 volts to confirm the correct size of the probe. Finally, 1µL of EDTA and 9µL of RNALater were added to the probe, and the mixture was stored at -80°C until needed. A control RNA riboprobe for *shha* was also synthesized from *shha*:pBluescript plasmid (2500bp). The same method as above was used for this probe, except the plasmid was linearized with *Eco*RI and the probe was synthesized with T7 RNA polymerase. Additionally, the *shha* riboprobe was grown in LB medium containing ampicillin (100µg/mL).

2.8 Whole mount *in situ* hybridization of zebrafish embryos and juvenile fish:

Day 1:

Fixed, dehydrated embryos or juvenile fish were first placed in small mesh baskets that can be submerged in wells of 6-well plates. The samples were rehydrated sequentially in three washes of 75% MeOH/ 25% 1X DEPC-PBS (137 mM NaCl, 10 mM phosphate, 2.7 mM KCl; pH 7.4 in DEPC treated H_2O), 50% MeOH/ 50% 1X DEPC-PBS, and 25% MeOH/ 75% 1X DEPC-PBS for 5 minutes each on a shaker plate. This was then followed by three 5-minute washes in 1X DEPC-PBST (1x PBS with 0.1% tween-20). The rehydrated embryos were then digested in 4µg/mL proteinase K (PK) according to the times listed in Thisse & Thisse, (2008), and then washes twice for 5 minutes each in DEPC-PBST. The juvenile fish were digested for 15 minutes in PK. The

embryos were then treated with 4% paraformaldehyde for 20 minutes, followed by an additional 2 washes of 5 minutes each in 1X DEPC-PBST. Embryos were then moved to an acetylation treatment, composed of 3mL of 1X DEPC-H_2O, 37.5µL of triethanolamine, and 8.1µL of acetic anhydride. Embryos/ juvenile fish were then washed twice for 10 minutes each in 1X DEPC-PBST, and then were transferred into 1.5mL tubes. Additional embryos were placed in a separate 1.5mL tube, with 960µL of 1X DEPC-PBST, 20µL of calf serum, 20µL of bovine serum albumin (BSA), and 1uL of anti-DIG AP fab fragments to preadsorb the anti-DIG antibody and reduce background. The preincubation mix was incubated for 2 hours at room temperature and was then stored at 4°C overnight until the next day. Each tube was then filled with 700µL of hybridization + mix (50% deionized formamide, 5X SSC, 0.1% Tween-20, and 0.92% citric acid, 500µg/mL yest tRNA, and 50µg/mL of heparin in DEPC-H_2O). The embryos/ juvenile fish were incubated for 2 hours at 70°C in a water bath. Before use, the *alx4a* probe and *shha* control probe was diluted in hybridization + mix in a 1 in 200 dilution from the stock. The diluted probe was then preheated at 70°C for 10 minutes to denature the probe before hybridization. The 700µL of hybridization + mix in each tube were then replaced with 200µL of probe mix, and the embryos/ juvenile fish are incubated overnight at 70°C.

Day 2:

1mL of hybridization – mix prewarmed at 70°C for 5 minutes was added to each 1.5mL tube of embryos or juvenile fish. The embryos were incubated for 10 minutes at 70°C, before being moved back to baskets. The embryos were then moved through a series of washes including 75% hybridization – mix/ 25% 2X SSC, 50% hybridization – mix/ 50% 2X SSC, 25% hybridization – mix/ 75% 2X SSC, and 100% 2X SSC for 10 minutes each at 70°C. These washes were then followed by two 30-minute washes in 0.2X SSC at 70°C. The plate was then removed from the

70°C water bath, and returned to the room temperature shaker plate, where it was moved through another series of washes including 75% 0.2X SSC / 25% PBST, 50% 0.2X SSC / 50% PBST, 25% 0.2X SSC / 75% PBST, and 100% PBST for 5 minutes each. The baskets were then moved to a blocking mixture containing 3.2mL of PBST, 400µL of calf serum, and 400µL of BSA and incubated for 1 hour at room temperature. The preadsorbed anti-DIG antibody solution was removed from 4°C and 80µL of calf serum, and 80µL of BSA are added to the mixture. The mixture was then completed to 5mL with PBST and placed in a well of a 6-well plate. The baskets were moved to this well and incubated for either 2 hours at room temperature or at 4°C overnight.

Day 3:

The embryos were moved through 6 washes in PBST for 15 minutes each. After the PBST washes, the embryos were moved through three 5-minute washes in staining buffer (100mM Tris HCl pH 9.5, 50mM $MgCl_2$, 100mM NaCl, 0.1% Tween-20). Embryos were then stained in 4mL of staining buffer containing 14µL of 5-Bromo-4-Chloro-3-Indolyl Phosphate (BCIP) and 18 µL of Nitro Blue Tetrazolium (NBT). The plate was wrapped in tin foil for staining as the reaction is light sensitive. The reaction was stained until the desired staining is achieved and is then stopped by washing three times in PBST with 1mM EDTA for 15 minutes each. Finally, embryos were stored in 100% glycerol at 4°C until imaging.

Completed *alx4a*-stained juvenile fish at 5.6mm and 6.4mm SL for wild-type and triple *hox13* mutants were imaged under an Axiozoom V16 dissecting microscope. The heads and tails were removed from the body of each completed sample and both the anal and dorsal fin folds were mounted on a slide in glycerol. The mounted fin folds were imaged at 112x magnification to

observe the *alx4a* domain of expression as well as the sizes of the fin folds in each mutant. Measurements were performed on completed *alx4a*-stained juvenile fish images in ImageJ for the 5.6mm timepoint. The widths of the *alx4a* expression domains were measured in µm for each sample (n=5 for both wild-type and triple *hox13* mutants). The widths of the entire fin folds were also measured in order to compare the proportional domain of expression in the wild-type and triple *hox13* mutant. Finally, the length of the fin fold from the base to the most distal part of the dorsal fin fold was measured in each sample at the 5.6mm timepoint as well.

2.9 CT scanning

Three samples for both the triple *hox13* mutant, and wild-type siblings were Micro-CT scanned using a SkyScan1173 Micro-CT scanner (Software v. 1.6) with the x-ray source set at a voltage of 60kV and 133uA. Voxel size was set at 7.1µm for each scan, with the object to source distance at 52.14mm, and the camera to source distance at 364mm. Scans were performed with an exposure of 1884ms and a rotation step of 0.35 degrees. Only the dorsal and anal fins were selected to be scanned to allow for higher resolution scans. These particular fins were chosen due to spines being most commonly seen in these fins in acanthomorph fish. Slices of scans were obtained upon completion and reconstructed by Dr. Qingming Qu at School of Life Sciences, Xiamen University, China using VGstudio software. Tissue surrounding the fin rays was removed, and the fins are reoriented to get cross sectional images of the hemirays perpendicular to the fin rays at specific positions along the proximal-distal axis. Hemiray thickness was compared between the wild-type and triple *hox13* mutants by measuring the width of the middle of the hemiray at a standard position in the ray. An example of this was shown in figure 17. The specific rays analyzed the dorsal fin include the A2, A4, and A6 fin rays. Measurements were performed at standard positions along

the proximal-distal axis for each ray. Due to the resolution of the scan, the distal tips of the rays became very difficult to accurately measure due to their smaller width. As a result, measurements for this analysis were mostly performed in the more proximal parts of the rays. In the A2 fin ray, 500μm, 750μm, and 1000μm from the proximal base of the ray were compared. In the A4 fin ray, 500μm, and 750μm from the proximal part of the ray were compared, and in the A6 fin ray, 500μm from the proximal part of the ray was compared. In addition to measurements, tracings of a hemirays at every position were done to give a schematic representation of the overall shape of each hemiray at each location for both genotypes.

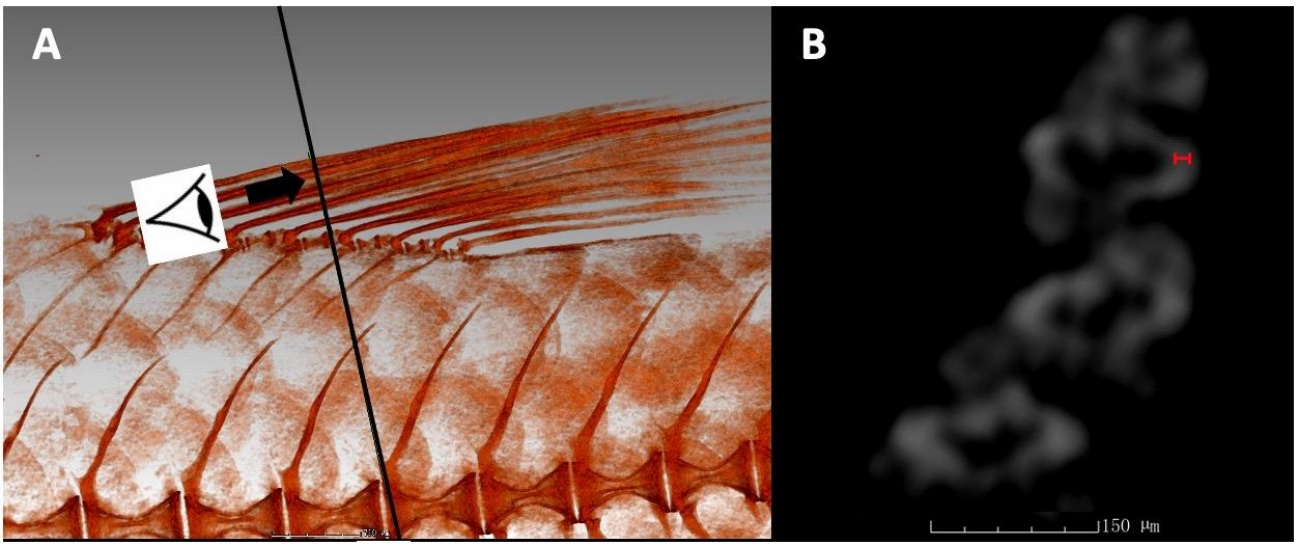

Figure 18. Sample measurement of reconstructed dorsal hemiray cross-sections. A: Wild-type siblings dorsal fin reconstruction. The black line shows the location of the cross section shown in B, where the cross section is being viewed from the proximal to distal orientation. B: Sample cross section of reconstructed dorsal fin rays at the location of the black line in A. Red lines represent an example of where the hemiray thickness was measured for a given location. Scale bars = 700μm for A and 150μm for B.

2.10 Generation of statistics:

Statistics and graphs were performed and generated using SPSS Statistics and Microsoft Excel. The normality of groups was tested using Shapiro-Wilks tests. Two-tailed Welch's T tests were used to assess significance between normally distributed groups. A Mann-Whitney U test was performed to assess significance of the non-normally distributed group (Figure 35D). To compare multiple groups in figure 22, 95% confidence intervals for each group were determined using descriptive statistics. If determined confidence intervals did not overlap between two given groups, a significance of $p<0.05$ was determined.

Chapter 3: Results

3.1 Morphological Analysis of double/ triple homozygous *hox13* mutants fin rays

3.1.1 Comparison of fin ray joints, bifurcations and actinotrichia

As was mentioned in the introduction, triple homozygous *hox13* mutants were generated through serial breeding. While only 6 of these fish were observed, defects including a loss of joints, bifurcation, and actinotrichia, as well as fin ray length reductions that varied between fins could be observed in these fish (Figure 18/19). The first step of my project was to generate additional triple *hox13* mutants in order to observe and add additional replicates to the mutants observed by Hailey Quigley. To further investigate the individual impact of each gene, *hoxa13a -/+*, *hoxa13b -/-*, *hoxd13a -/-*, *hoxa13a -/-*, *hoxa13b -/+*, *hoxd13a -/-*, and *hoxa13a -/-*, *hoxa13b -/-*, *hoxd13a -/+*, mutants were also bred and observed in order to compare to the triple *hox13* mutants. Through phenotypic observations of these mutants, the allelic contribution to joints, bifurcations, and actinotrichia were investigated. All fins of mutant fish (Figure 18/19B-F) and wild-type siblings (Figure 18/19A) were imaged for analysis of the rays. The main characteristics examined in each

fin are the length of standard fin rays as specified in chapter 2.4, the presence or absence of fin ray joints, the presence of bifurcations, and the presence of actinotrichia fibers at the tips. Images were taken of fish with the same standard length of between 3-3.2cm to ensure a similar comparison of standard fin size as the fins grow isometrically with the body (Uemoto et al., 2020).

Based on all observed mutant phenotypes, a common theme throughout this analysis was that defects tended to differ depending on the type of fin. The most consistency was observed in the caudal fin, where the fin rays of all genotypes observed contained joints, bifurcations and actinotrichia (Figure 18/19). The only exception to this, was that the lateral-most rays of the caudal fin in the *hoxa13a-/-, hoxa13b-/-, hoxd13a-/+* mutant (Figure 18/19E), and the triple homozygous mutant (Figure 18/19B) lacked actinotrichia at their tips. Aside from this, the caudal fin joint, bifurcation, and actinotrichia phenotype of all mutant caudal fins remained consistent with the wild-type sibling caudal fin. Small reductions in fin ray length could be observed in the caudal fin lobes for each mutant genotype, as will be shown in section 3.1.2.

In all other fins, dorsal, anal, pectoral, and pelvic fins, defects differ depending on the genotype of the fish. In the *hoxa13a -/+, hoxa13b -/-, hoxd13a -/-* mutants (Figure 18/19C), and *hoxa13a -/-, hoxa13b -/+, hoxd13a -/-* mutants (Figure 18/19D), joints, bifurcations and actinotrichia are present in all fin types. In contrast, in the *hoxa13a -/-, hoxa13b -/-, hoxd13a -/+* mutants (Figure 18/19E) and triple homozygous mutant (Figure 18/19B), joints, bifurcations, and actinotrichia seem to be absent from all of these fins. From these observations, *hoxa13a* and

hoxa13b seem to have much greater significance in their capacity to form joints, bifurcations and actinotrichia compared to *hoxd13a*.

From these initial observations, the mutant: *hoxa13a -/-, hoxa13b -/-, hoxd13a +/+* (Figure 18/19F) was generated to observe if having two copies of *hoxd13a* can have a significant effect on joint, bifurcation, and actinotrichia formation. In this mutant, joints and bifurcations can be seen forming in both the dorsal and anal fin rays, although the patterning of the joints in this mutant is very irregular in comparison to the wild-type fin ray joints which are evenly spaced. The paired fins of this mutant however remain with no joints and bifurcations in any of their rays. Observations from this genotype show that *hoxd13a* is still able to form joint and bifurcations in the dorsal and anal fins, although two copies of the gene are necessary for this, as opposed to only one copy of *hoxa13a* or *hoxa13b*. Furthermore, all fins except for the caudal fin of this mutant still appear to lack actinotrichia at the tips, indicating that *hoxd13a* does not have a significant role in actinotrichia formation in the dorsal, anal, and paired fins. The mutants *hoxa13a +/+, hoxa13b -/- , hoxd13a -/-* and *hoxa13a -/-, hoxa13b +/+, hoxd13a -/-* were not included in this analysis due to the fact that one copy of either *hoxa13a* or *hoxa13b* already being sufficient to form rays that resemble wild-type rays for the characteristics of interest. In all observed mutants, the only noticeable inconsistency was in the anal fin of the triple homozygous mutant (n=3/10) and the *hoxa13a -/-, hoxa13b -/-, hoxd13a -/+* (n=2/8), where irregularly spaced joints could sometimes be seen in the rays (Figure 20). All other fins in all other genotypes remained consistent across all replicates that were observed.

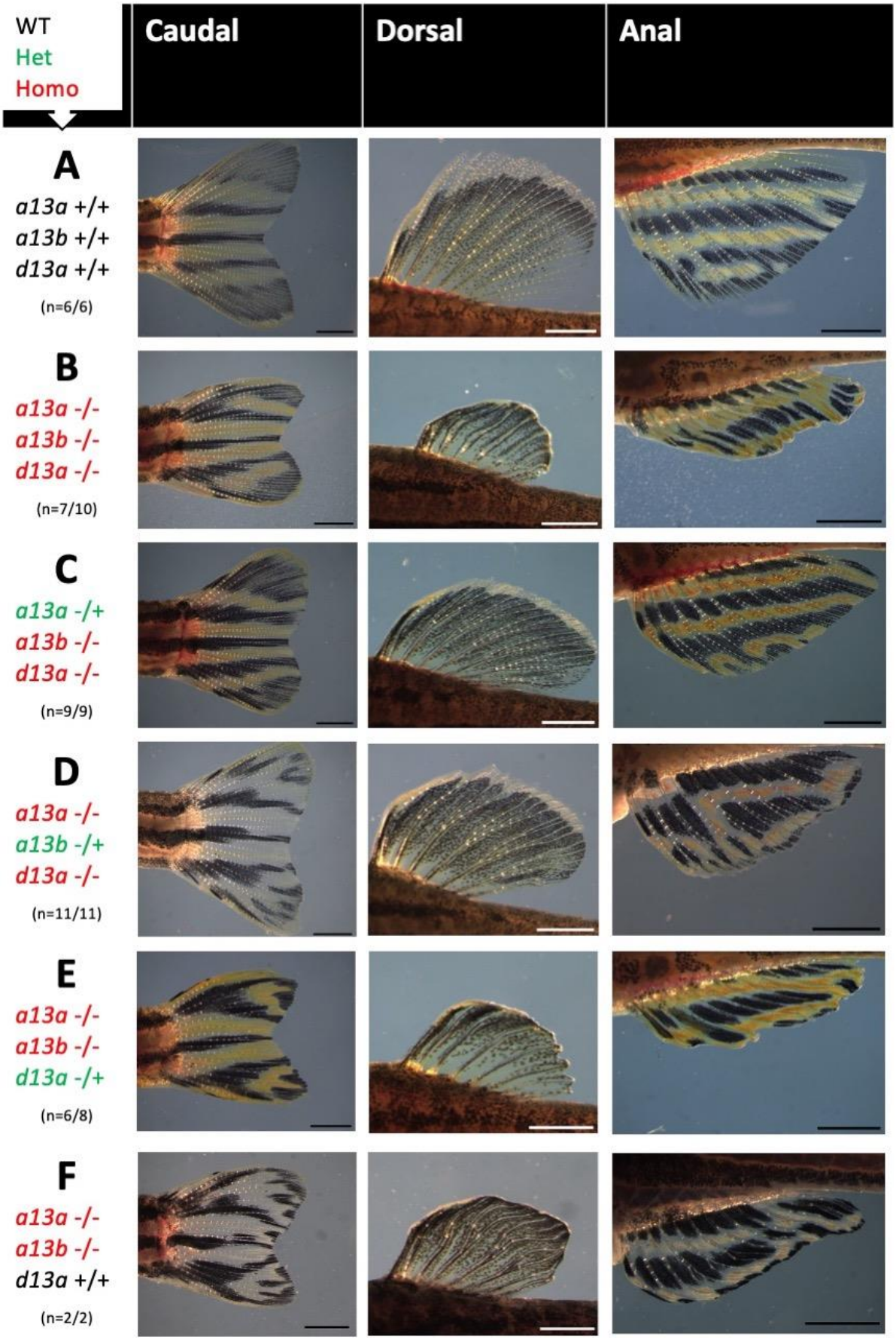
WT
Het
Homo
Caudal
Dorsal
Anal
A
a13a +/+
a13b +/+
d13a +/+
(n=6/6)
B
a13a -/-
a13b -/-
d13a -/-
(n=7/10)
C
a13a -/+
a13b -/-
d13a -/-
(n=9/9)
D
a13a -/-
a13b -/+
d13a -/-
(n=11/11)
E
a13a -/-
a13b -/-
d13a -/+
(n=6/8)
F
a13a -/-
a13b -/-
d13a +/+
(n=2/2)

Figure 19. Visual comparison of *hox13* mutant median fins (B-F) with wild type siblings (A). Genotypes are presented in the left column, with corresponding letters (A-F) for referencing. Wild-type genes are represented in black, and genes with homozygous deletions are represented in red. Replicates of how many individuals were imaged are listed below each genotype as fractions. Images are oriented with the anterior of the fin on the left, and the posterior of the fin on the right. The only inconsistency was observed in the anal fin of B and E, where 3/10 mutants in B and 2/8 mutants in E showed a small number of irregularly patterned joints in their rays. Scale bars = 2mm for caudal and anal fins, and 1.5mm for dorsal fins.

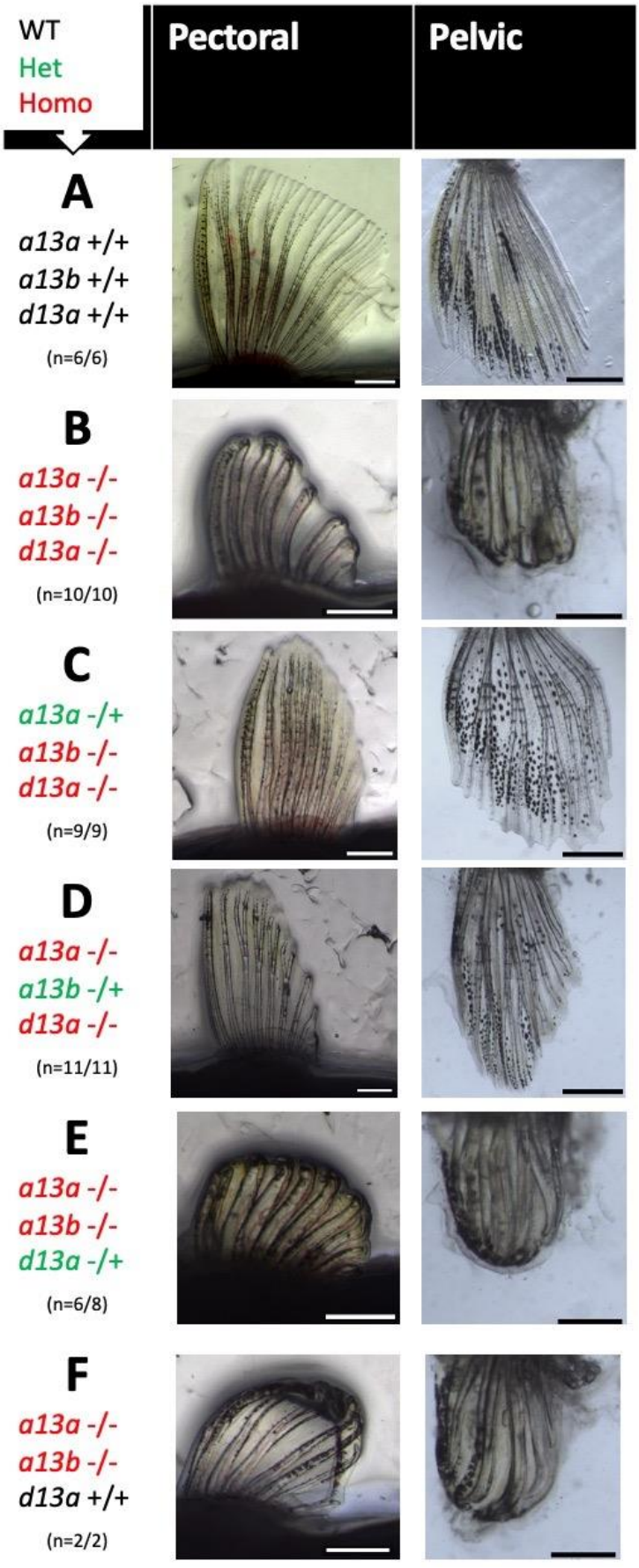
WT
Het
Homo
Pectoral
Pelvic
A
a13a +/+
a13b +/+
d13a +/+
(n=6/6)
B
a13a -/-
a13b -/-
d13a -/-
(n=10/10)
C
a13a -/+
a13b -/-
d13a -/-
(n=9/9)
D
a13a -/-
a13b -/+
d13a -/-
(n=11/11)
E
a13a -/-
a13b -/-
d13a -/+
(n=6/8)
F
a13a -/-
a13b -/-
d13a +/+
(n=2/2)

Figure 20. Visual comparison of *hox13* mutant paired fins (B-F) with wild type siblings (A). Genotypes are presented in the left column, with corresponding letters (A-F) for referencing. Wild-type genes are represented in black, and genes with homozygous deletions are represented in red. Replicates of how many individuals were imaged are listed below each genotype as fractions. Images are oriented with the anterior of the fin on the left, and the posterior of the fin on the right. Scale bars = 1mm for all pectoral fin images and 0.5mm for pelvic fin images

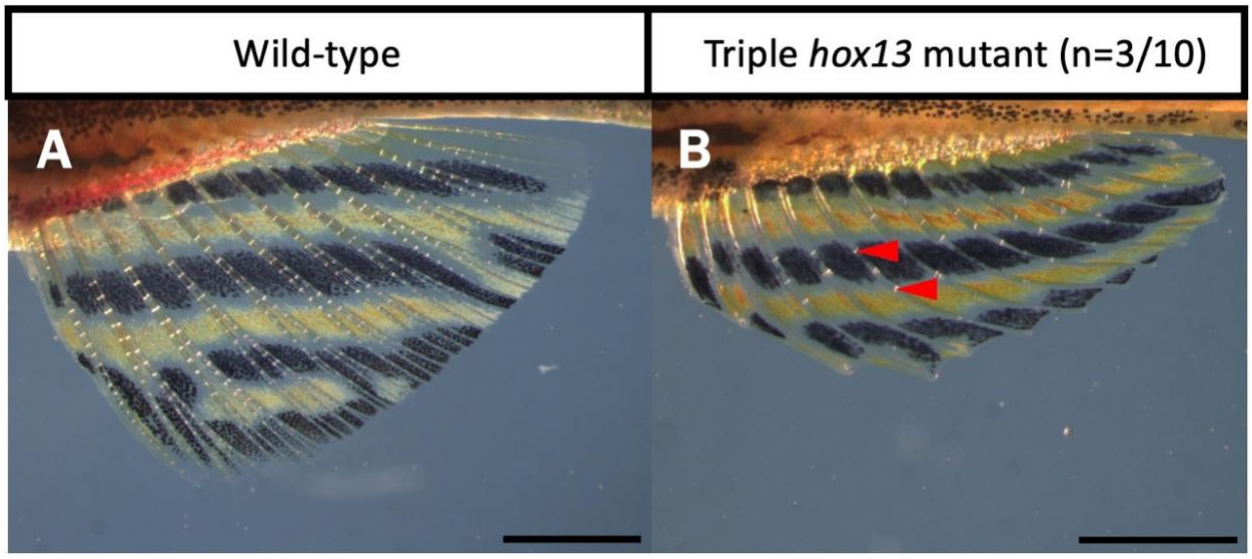

Figure 21. Minority phenotype (n=3/10) of the triple *hox13* mutant anal fin. A: Joints in the *hox13* wild-type sibling anal fin rays. B: A small quantity of joints with erratic patterning in the anal fin rays of a triple *hox13* mutant. Red arrows indicate examples of joints in this phenotype. The *hoxa13a -/-, hoxa13b -/-, hoxd13a -/+* mutants also demonstrate this phenotype in the anal fin with a minority of n=2/8. Scale bars = 2mm.

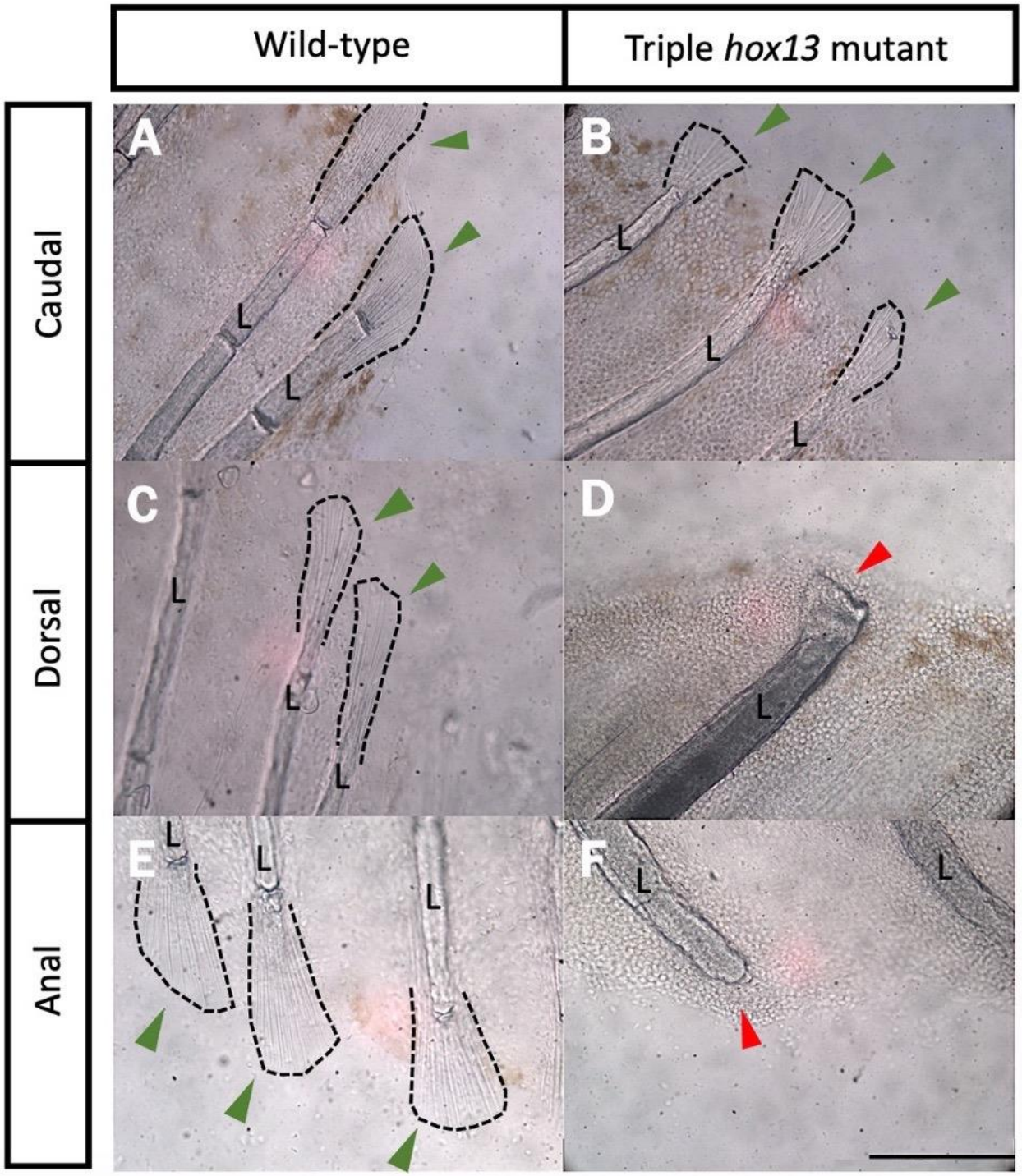

Figure 22. *Hox13* mutants have reduced actinotrichia at the tips of their fin rays. Representative images of wild-type and triple *hox13* mutant fin ray tips in the caudal, dorsal, and anal fins. Fins were treated overnight at 42°C in a solution of 5% Formalin, 5% Triton X-100, and

1% KOH. Pectoral and pelvic fins, although not shown, also show no actinotrichia at their tips. L: lepidotrichia. Actinotrichia bundles at the lepidotrichia tips are outlined in black dotted and indicated by green arrows in A, B, C, and E. Red arrows indicate lepidotrichia tips lacking actinotrichia fibers in D and F. n=6 for wild-type, and n=10 for triple *hox13* mutants. Scale bar = 200μm for all images.

3.1.2 Fin ray length comparisons

Fin ray length comparisons were performed on standard fin rays for each fin to compare between wild-type, *hox13* mutants that are double homozygous for two genes/ single heterozygous for the third gene, as well as the triple *hox13* mutants. Exact fin rays measured are outlined in section 2.4, and in figure 22. As was apparent with initial observations in joints, bifurcations, and actinotrichia, the smallest difference in fin ray length between genotypes was seen in the caudal fin. In the cleft of the caudal fin, there is no significant difference from the wild-type in any of the mutant genotypes. There are slight significant reductions in the lobes of the caudal fin for all mutant genotypes compared to WT siblings, although the length reductions are consistent and do not differ between the mutant genotypes. Additionally, both lobes of the caudal fin seem to be affected in a similar fashion.

In the anal fin, differing scales of length reductions can now be observed between different mutant genotypes. The *hox13* triple mutant, and the *hoxa13a -/-, hoxa13b -/-, hoxd13a -/+*, show significant decreases in length compared to the wild-type in both the anterior and posterior parts of the anal fin. The *hoxa13a -/+, hoxa13b -/-, hoxd13a -/-*, and the *hoxa13a -/-, hoxa13b -/+*,

hoxd13a -/-, however have only small reductions in fin ray length that are not significantly different from the wild type. For the dorsal, pectoral, and pelvic fins, significant but variable decreases in fin ray length are seen in all mutant genotypes compared to the wild-type. In the triple mutant, and the *hoxa13a -/-, hoxa13b -/-, hoxd13a -/+*, we see very significant length decreases in all parts of each fin. In the *hoxa13a -/+, hoxa13b -/-, hoxd13a -/-*, and the *hoxa13a -/-, hoxa13b -/+, hoxd13a -/-*, we still see significant decreases in every ray with the exceptions of the posterior pectoral, and medial pelvic fin rays in the *hoxa13a -/-, hoxa13b -/+, hoxd13a -/-* mutant. The decrease in these genotypes however is not as extreme as in the case of the triple *hox13* mutant and *hoxa13a -/-, hoxa13b -/-, hoxd13a -/+*. As summarized in figure 23, the caudal fin shows the lowest reduction in fin ray length, the anal and dorsal fins show medial reductions in fin ray length, and the pectoral and pelvic fins show the most severe reductions in fin ray length across *hox* mutant genotypes.

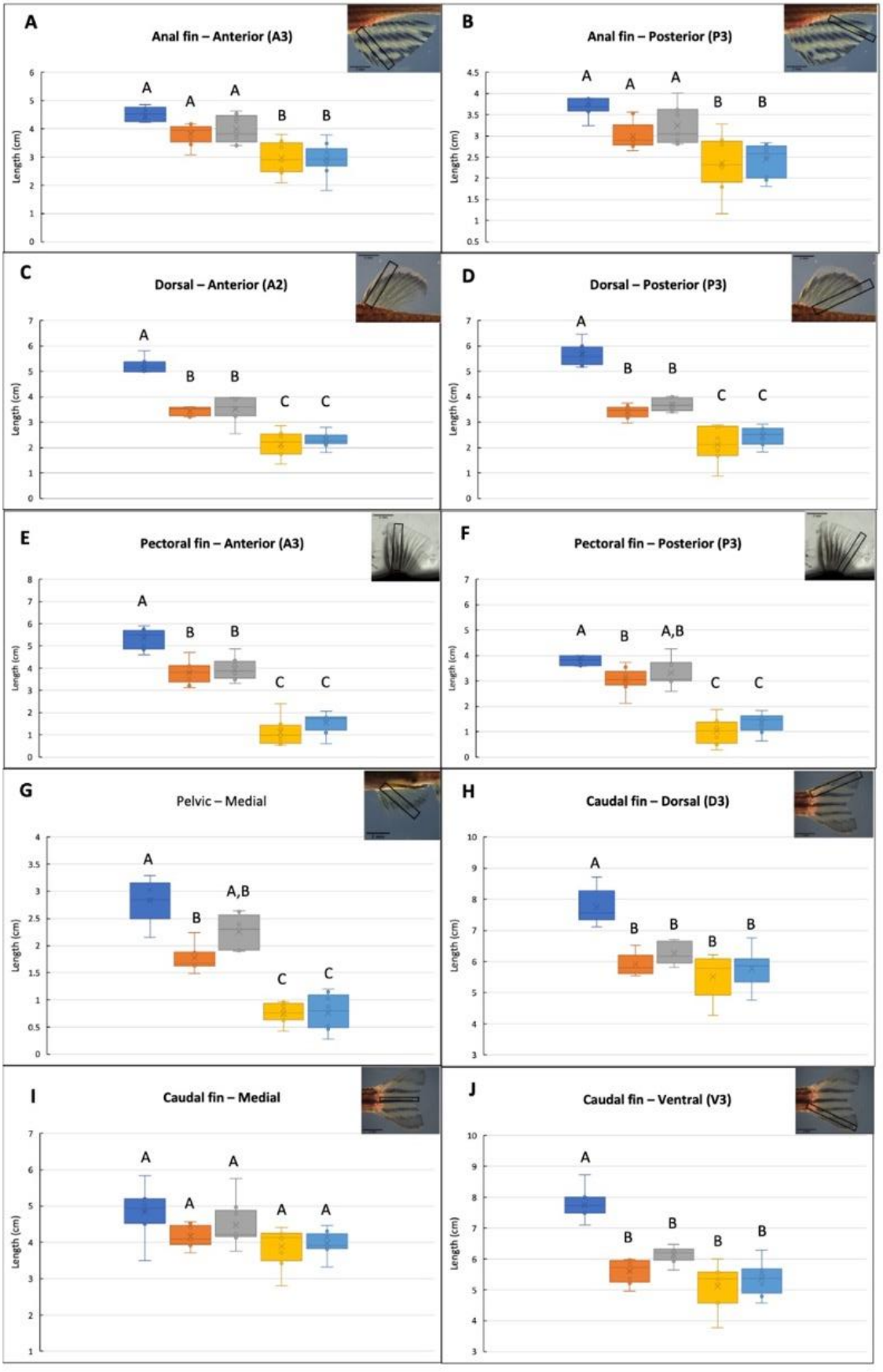
A
Anal fin – Anterior (A3)
Length (cm)
A A A B B
B
Anal fin – Posterior (P3)
Length (cm)
A A A B B
C
Dorsal – Anterior (A2)
Length (cm)
A B B C C
D
Dorsal – Posterior (P3)
Length (cm)
A B B C C
E
Pectoral fin – Anterior (A3)
Length (cm)
A B B C C
F
Pectoral fin – Posterior (P3)
Length (cm)
A B A,B C C
G
Pelvic – Medial
Length (cm)
A B A,B C C
H
Caudal fin – Dorsal (D3)
Length (cm)
A B B B B
I
Caudal fin – Medial
Length (cm)
A A A A A
J
Caudal fin – Ventral (V3)
Length (cm)
A B B B B
WT
a13a a13b d13a
a13a a13b d13a
a13a a13b d13a
a13a a13b d13a

Figure 23. Fin ray length comparisons of wild-type siblings, and double and triple homozygous *hox13* mutants. The standard fin ray of interest is indicated in the top right corner of chart, where the fin is shown with a black box around fin ray being measured. A: Third anterior fin ray of the anal fin. B: Third posterior fin ray of the anal fin. C: Second anterior fin ray of the dorsal fin. D: Third posterior fin ray of the dorsal fin. E: Third anterior fin ray of the pectoral fin. F: Third posterior fin ray of the pectoral fin. G: Medial fin ray of the pelvic fin. H: Third dorsal fin ray of the caudal fin. I: Medial fin ray of the caudal fin. J: Third ventral fin ray of the caudal fin. Box and whisker plots are presented for each genotype at each fin ray of interest. Significant groups are shown above each box on the graphs and were determined using 95% confidence intervals ($p<0.05$). Error bars represent maxima and minima for each group. In the legend, gene names in green represent heterozygous genes, and gene names in red represent homozygous deletions. Replicates are the same as those listed in figure 18 for each genotype. Scale bars in fin images = 3mm for H, I and J, and 2mm for A, B, C, D, E, F, and G.

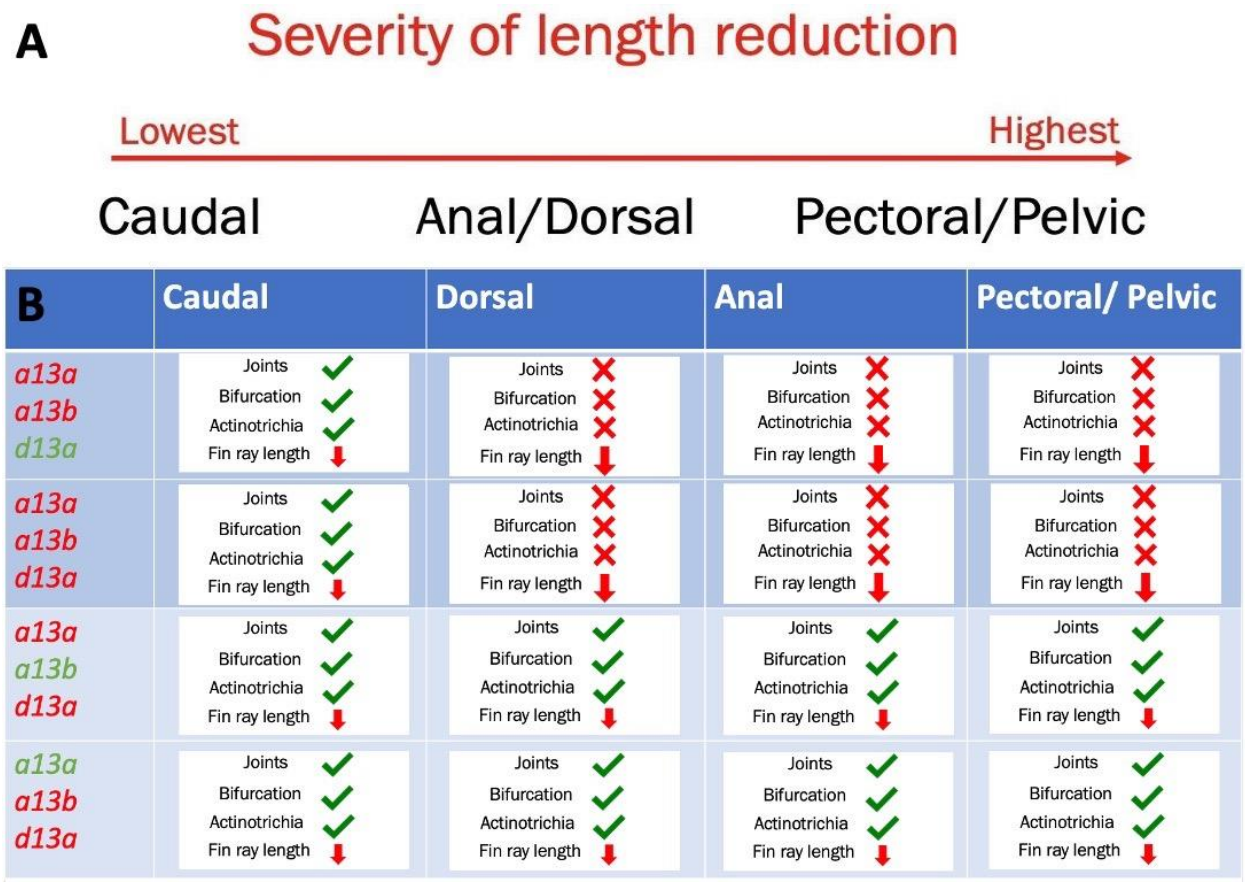

Figure 24. Summary of double and triple *hox13* mutant fin ray defects. A: Gradient of fin ray length reductions in the triple *hox13* mutant. The caudal fin demonstrates the least reduction in fin ray length as a result of *hox13* mutations with no reduction in the cleft, and small reduction in the lobes. All mutants had joints, bifurcations, and actinotrichia present in the caudal fin. The anal and dorsal fins demonstrate moderate reductions in length, with an absence of joint, bifurcation, and actinotrichia formation. The paired fins demonstrate the largest reduction in length, along with an absence of joints, bifurcation, and actinotrichia. B: Presence or absence of joints, bifurcations, actinotrichia, as well as relative fin ray length reduction in the fins of double and triple homozygous *hox13* compound mutants.

3.1.3. Triple *hox13* mutant fin ray vasculature

The vasculature of Tg(*fli1a*:eGFP); *hoxa13a* -/-, *hoxa13b* -/-, *hoxd13a* -/- mutants were imaged and compared to wild-type siblings. As previously mentioned, the main vasculature in the fin rays includes one central artery in each fin ray, and two veins that run along the sides of the ray. Intervessel commissures typically connect the veins and central artery at different points along the proximal-distal axis. Interray commissures are also typically seen connecting the veins of neighbouring rays.

In the caudal fin, the main components including the arteries, veins, intervessel commissures and interray commissures are all present (Figure 24). The anal and dorsal fin vasculature (Figure 25) shows minimal change between the wild-type and mutants. Visually, there appears to be more of a disorganization of vessels in the dorsal and anal fins of the triple *hox13* mutant, where the interray vessels appear to be longer, uneven, and randomly spaced compared to the wild-type siblings. This appearance however could possibly be attributed to the altered patterning of the *hox13* triple mutant rays and may not be a direct result of *hox13* genes regulating the formation of interray vessels. Altogether, all main components of fin ray vasculature could still be observed in each median fin, although the patterning of the smaller vessels including the intervessel commissures and the interray commissures appears to differ such that the spacing between the vessels and the length of the vessels is more inconsistent.

Larger differences can be observed in the pectoral fin of the triple *hox13* mutant (Figure 26), especially in the anterior part of the fin. The central artery of the ray is not as straight as in the

wild-type and tends to bend and curve within the ray. Veins still appear to be present in each ray, although they are small and hard to identify. Furthermore, the interray commissures as well as the intervessel commissures in the anterior part of the pectoral fin seem to be absent, as no vessels can be seen running between the first three anterior rays, or between the arteries and veins of these rays. This lack of blood vessels, and mis-patterned vessels could be an indication that the *hox13* genes have a role in the formation and patterning of vasculature in the pectoral fin rays, or it could again be a biproduct of the shortened malformed fin rays in the triple mutant fin. The smaller vessels of the pectoral fin may also be harder to observe in general due to the structure of the rays, and how close together the rays are in this fin. The pelvic fin of the triple *hox13* mutant also appears to have a disorganization of blood vessels and arteries that curl and bend as is seen in the pectoral fin. In contrast to the pectoral fin however, interray commissures can still be observed connecting the veins of all neighbouring rays in the pelvic fin. A large disorganization of intervessel commissures can again be seen in each ray, with vessels having inconsistent length and spacing. The phenotype of the paired fins is overall similar, with the except of the absence of interray vessels at the anterior side of the pectoral fin that is not seen in the pelvic fin.

In summary, a general disorganization of blood vessels in the triple *hox13* mutant fins can be seen, especially the interray and intervessel commissures where variations in the spacing between vessels, and the length of vessels seem to be inconsistent in the mutants. The paired fins have the most severe defects in vessel patterning, where arteries within the rays appear bent, and interray and intervessel commissures sprout inconsistently at varying lengths. Specifically in the pectoral fin, interray commissures are absent from the anterior fin rays.

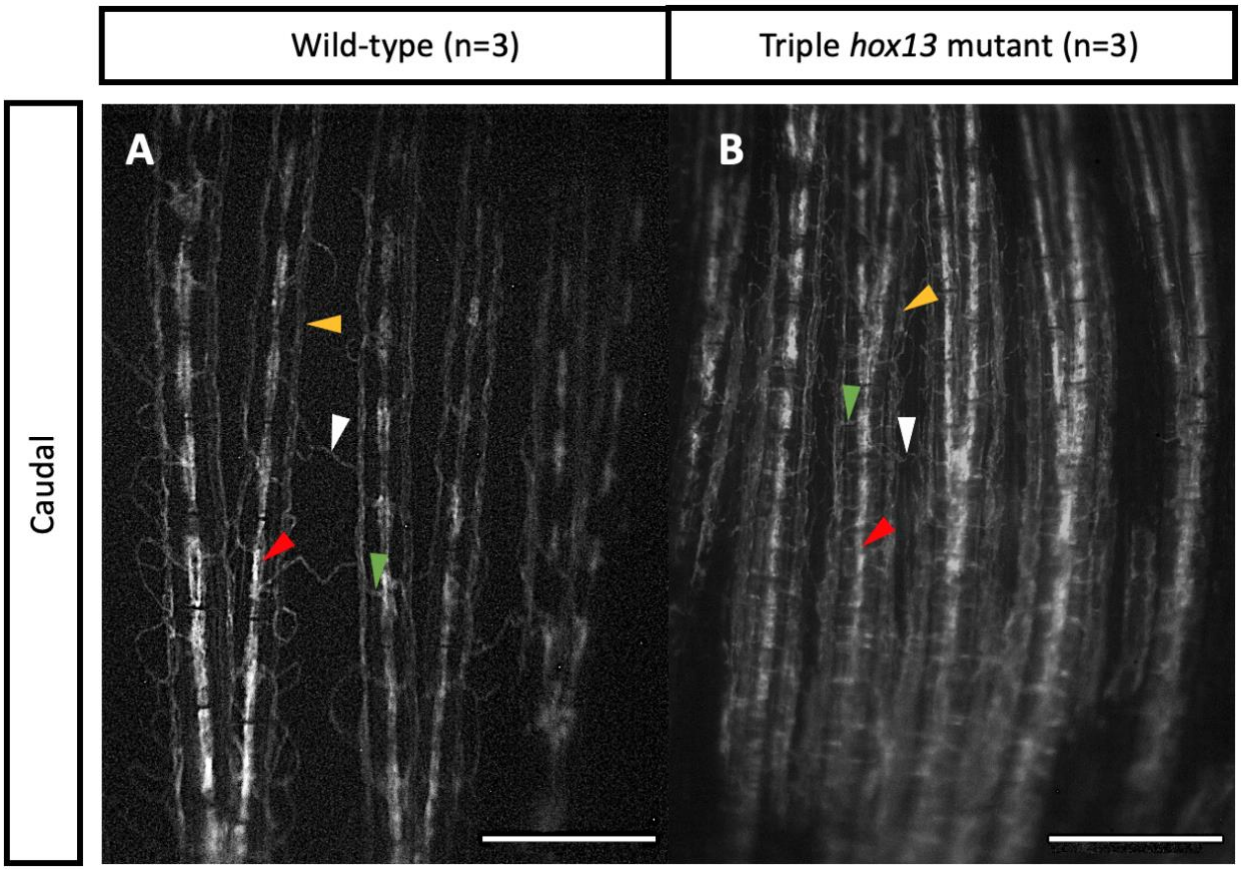

Figure 25. Caudal fin vasculature of the triple *hox13* mutant. eGFP images of wild-type (A) and triple *hox13* mutant (B) blood vessels in the caudal fin rays. Red arrows indicate central arteries inside the lepidotrichia, yellow arrows indicate veins on the lateral side of the lepidotrichia, green arrows indicate intervessel commissures running between arteries and veins of the same ray, and white arrows indicate interray vessels running between the veins of neighbouring rays. Scale bars = 500μm for both images.

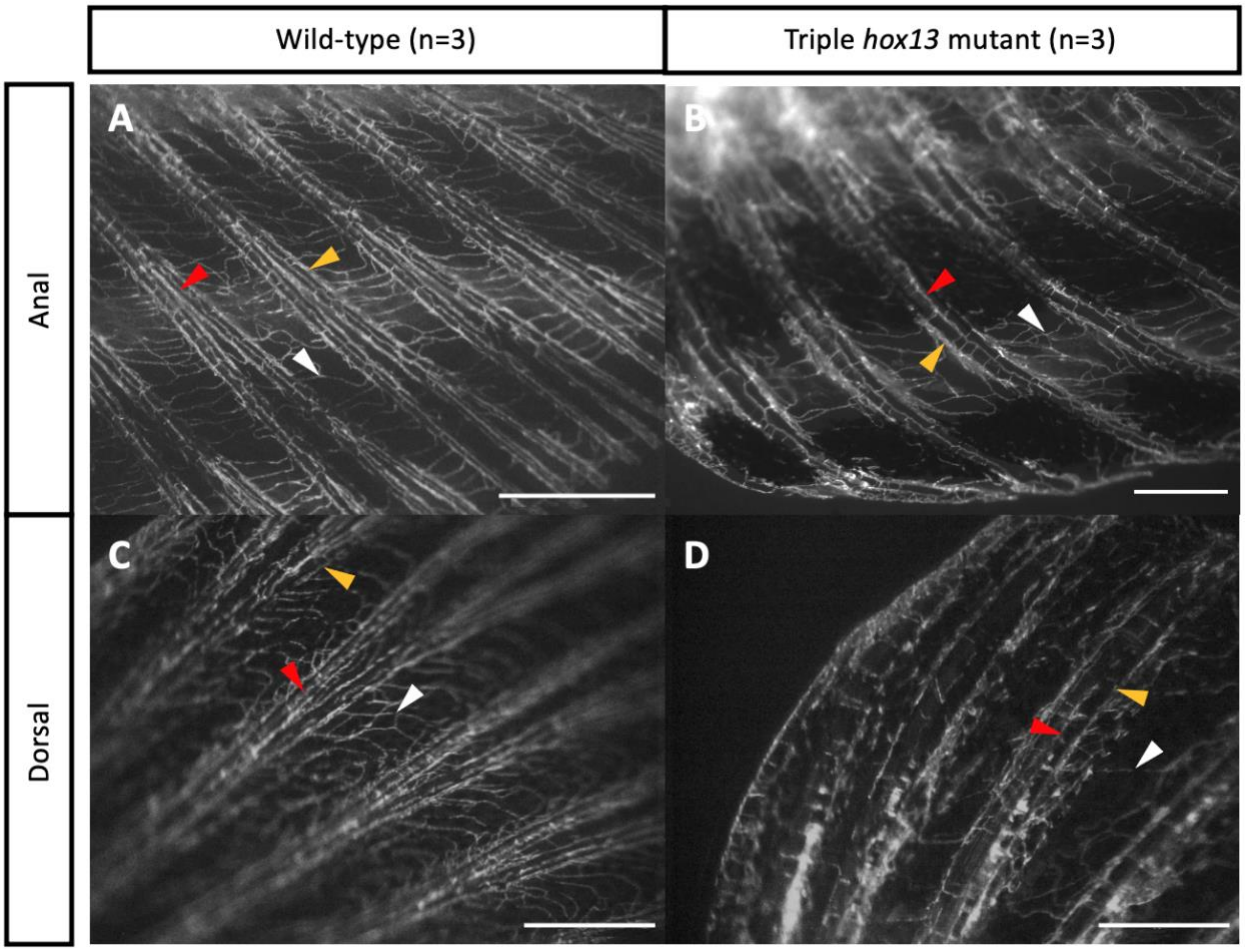

Figure 26. Dorsal and anal fin vasculature of the triple *hox13* mutant. eGFP images of wild-type anal (A) and dorsal (C), as well as triple *hox13* mutant anal (B) and dorsal (D) fin blood vessels. Red arrows indicate central arteries inside the lepidotrichia, yellow arrows indicate veins on the lateral sides of the lepidotrichia, and white arrows indicate interray vessels going between the veins of neighbouring rays Scale bars = 500μm for all images.

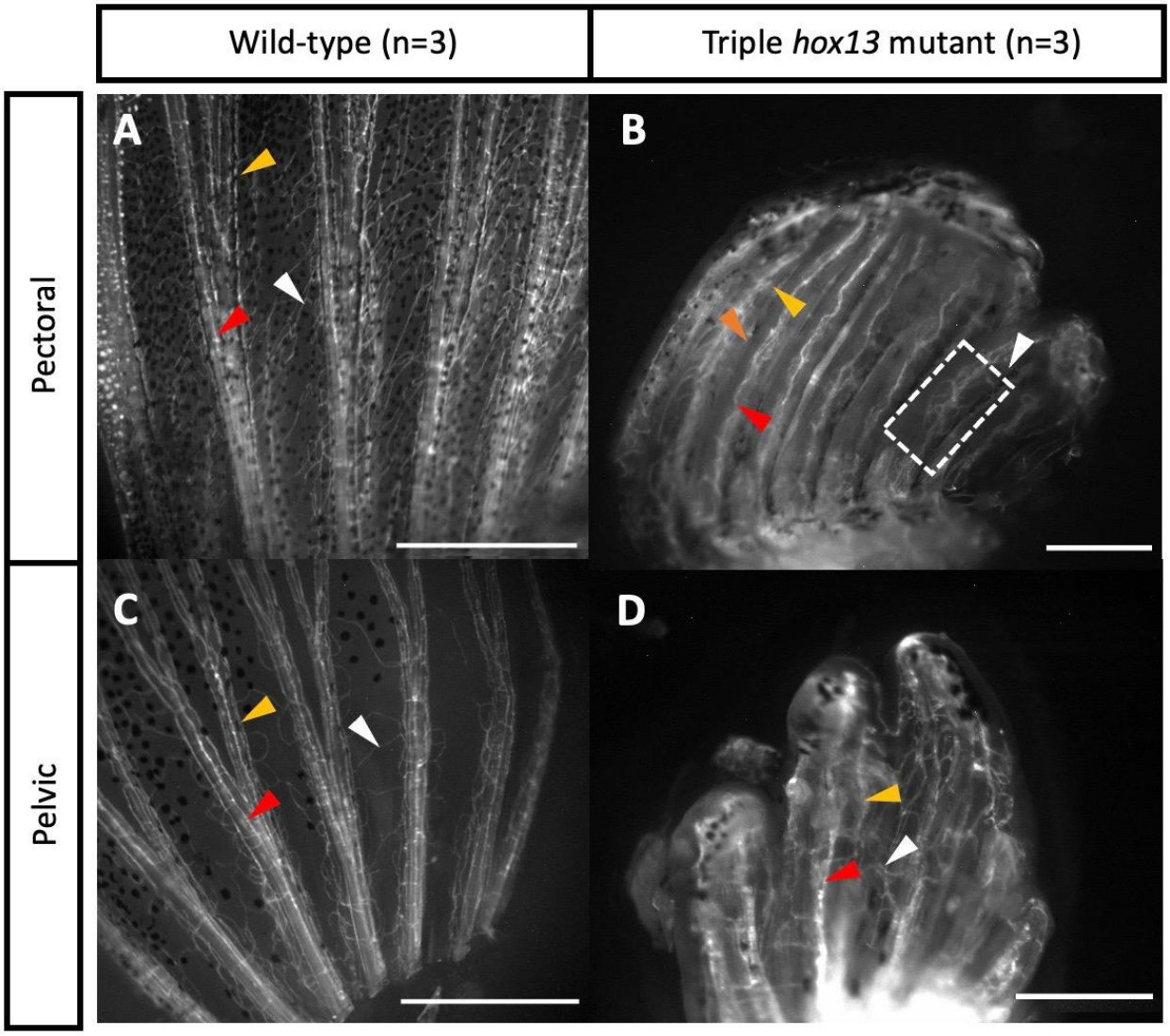

Figure 27. Paired fin vasculature of the triple *hox13* mutant. eGFP images of wild-type pectoral (A) and pelvic (C), as well as triple *hox13* mutant pectoral (B) and pelvic (D) fin blood vessels. Red arrows indicate central arteries inside the lepidotrichia, yellow arrows indicate veins on the lateral side of the lepidotrichia, and white arrows indicate interray vessels going between the veins of neighbouring rays. The orange arrow in B indicates interray space where there is an apparent absent of interray vessels in the fin. White dotted box in B shows disorganized, incomplete intervessel commissures. Scale bars = 1mm for A and C, and 500μm for B and D.

3.2 Fin endoskeleton of the *hox13* mutants

Alizarin red and Alcian blue stains were performed on adult double and triple homozygous mutant genotypes of interest. Previously, only the pectoral fin was reported to have defects in the endoskeleton as a result of the *hox* mutations by Nakamura et al (2016). In this study, *hoxa13a* -/-, *hoxa13b* -/- mutant, and mosaic triple homozygous *hox13* mutant showed an increase in the number of pectoral fin distal radials. Bone staining was performed on our triple *hox13* mutants to confirm this finding and observe if there are potentially greater defects in the fully triple homozygous mutant compared to the mosaic mutant of Nakamura et al, and to observe the endoskeleton of the other fins.

The pectoral endoskeleton of our triple *hox13* mutant showed resemblance with the mutants described in Nakamura et al (2016) (Figure 27). The triple *hox13* mutant showed an increase in the number of distal radials compared to the wild-type, where 11 distal radials could be observed in the mutants compared to the normal amount (7) in the wild-type. Stacking of the radials at the posterior side however was not clearly observed as was reported in the Nakamura et al (2016) mosaic mutant, although there did appear to be stacking of distal radial 9 that is positioned distally to distal radial 7. In the other fins, obvious defects were not present in the endoskeleton. In the pelvic fin, the same number of distal radials were observed in the wild-type and in the triple *hox13* mutant. No malformation in the radials or in the pelvic girdle could be observed in the pelvic fin of these mutants. Defects could not be identified in the caudal fin endoskeleton of the triple *hox13* mutants, as they showed the same number of hypurals as was observed in the wild-type. The overall size and shape of the endoskeletal elements also seem to be

comparable in both genotypes. Finally, the dorsal and anal fin endoskeletons also appeared to be normal in the triple *hox13* mutant, with no increases in the number of pectoral radials or large modifications to these structures. Overall, the *hox13* genes are essential for proper pectoral endoskeleton development, as mutations in these genes do cause an increase in the number of pectoral distal radials, however they do not seem to play an important role in the endoskeletal development of the other fins.

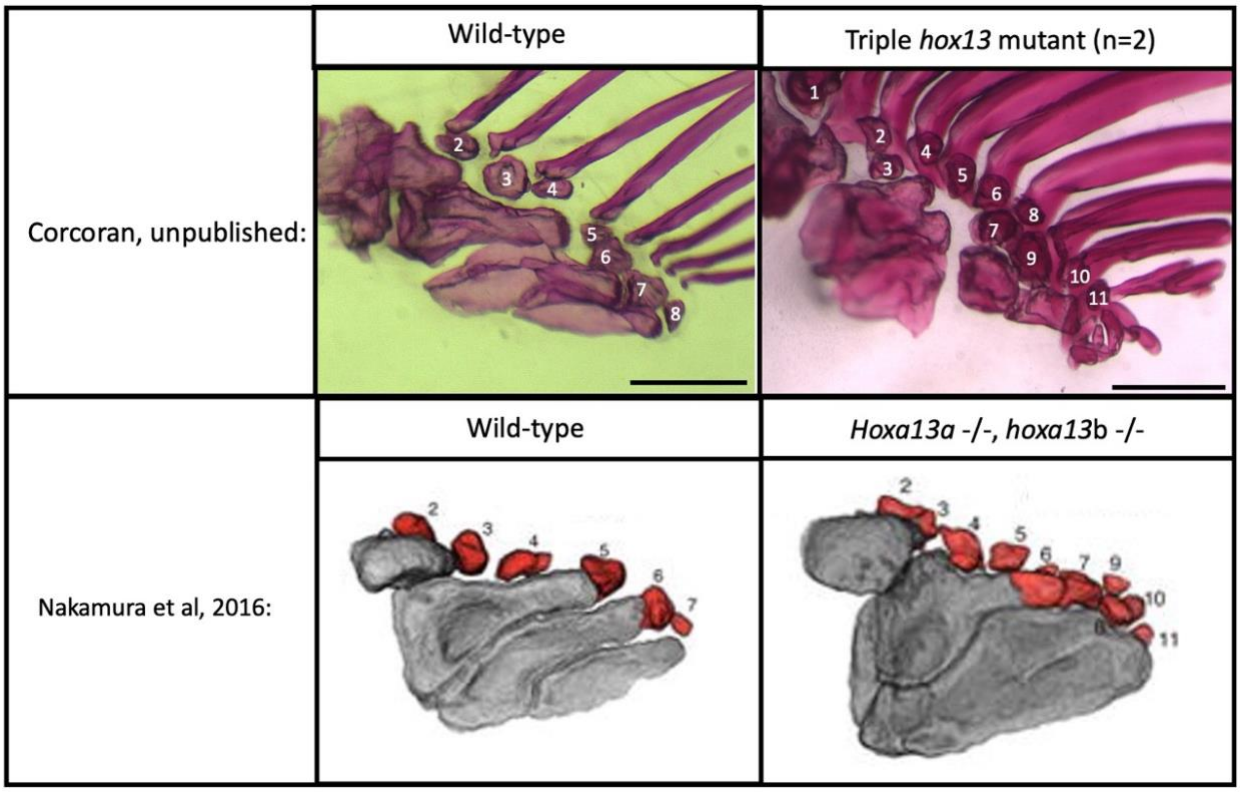

Figure 28. Pectoral endoskeleton comparison of triple *hox13* mutant and double homozygous hox13 mutant from Nakamura et al (2016). A/B: Counted distal radials are numbered for both A: wild-type (n=4/4) and B: triple *hox13* mutant (n=4/4. Scale bars = 1mm), C/D: CT scan reconstructions of wild-type (C) and *hoxa13a -/-, hoxa13b -/-* mutant (D). Individual distal radials are numbered. Adapted from Nakamura et al (2016) with permissions from Copyright Clearance Center, April 22, 2023.

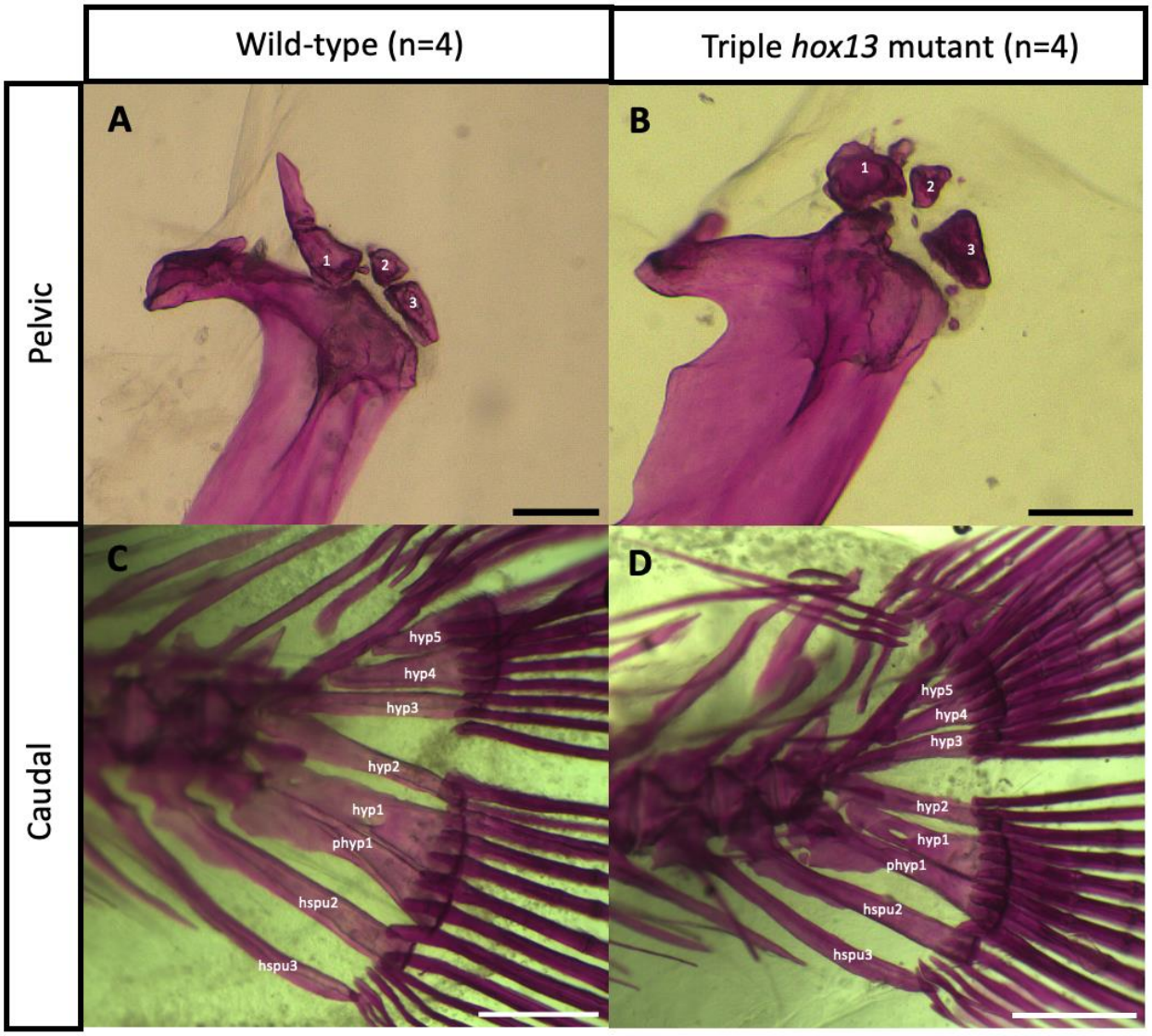

Figure 29. The pelvic and caudal endoskeletons show no defects in the triple *hox13* mutant. Alizarin red staining of the pelvic (A/B) and caudal (C/D) endoskeleton of triple *hox13* mutants and wild-type adult zebrafish. A/B: pelvic distal radials are numbered 1-3. C/D: hypurals, parahypural, and hemal spines (hyp = hypural, phyp = parahypural, hs = hemal spine, pu = preural) are labelled for each image. Scale bars = 1mm for A and B, and 2mm for C and D.

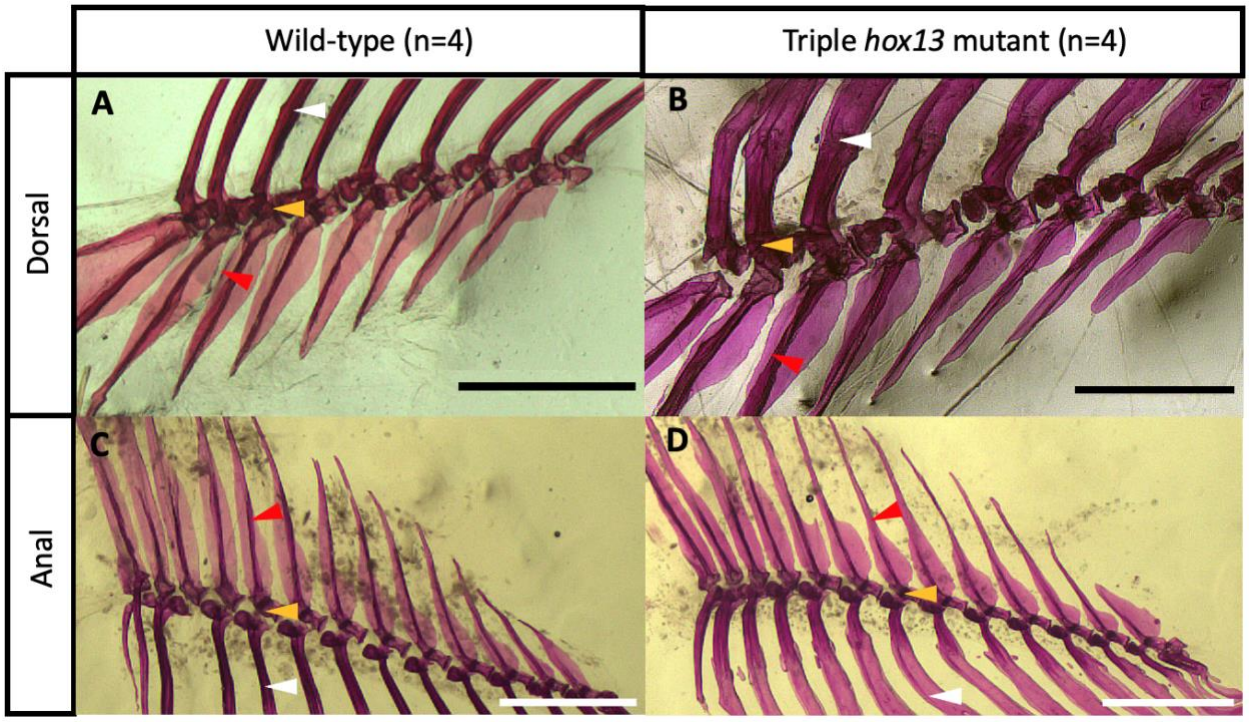

Figure 30. The dorsal and anal endoskeletons show no defects in triple *hox13* mutants. Alizarin red staining of dorsal (A/B) and anal (C/D) fin endoskeletons of triple *hox13* mutants and wild-type adult zebrafish. Red arrows indicate proximal radials, yellow arrows indicate distal radials, and white arrows indicate lepidotrichia. Scale bars = 1.5mm for all images.

3.3. Urogenital pore defects in the triple *hox13* mutant

As previously mentioned, all mutant fish must be obtained from heterozygous crosses as the triple *hox13* mutants are unable to breed. From previous dissections of our *hox13* triple mutant zebrafish, it is found that are still able to form testes (Quigley, unpublished). The inability to breed in these fish was at first presumed to be due to the fact that the pectoral fin is very small in these mutants. The pectoral fin in zebrafish is necessary for the male, as it is used to apply pressure to the belly of the female in order to stimulate the release of eggs during breeding

(Zempo et al., 2021). The female triple *hox13* mutants however are unable to breed even with wild-type males. Because of this, *in-vitro* fertilization was attempted on these fish. In the case of the male triple *hox13* mutant, three attempts were made to harvest sperm from the six adults. Out of all attempts, only one out of six males was able to release small quantities of sperm twice. This harvested sperm however was not able to successfully fertilize *hoxa13a -/-, hoxa13b -/+, hoxd13a -/-* eggs the first time it was harvested, or wild-type eggs the second time it was harvested. Considering this, it is possible that the mixture from the triple *hox13* mutant did not contain quality, viable sperm. To check this, the sperm could be analyzed using a sperm quality analyzer (SQA-IIC), which can analyze sperm samples for motility and quality of sperm (Tayama et al., 2006). In the case of the female triple *hox13* mutants, eggs were not able to be released after any of the three attempts with five fish. Upon further observation of the females, there appeared to be a malformation of the urogenital pore in the adult triple *hox13* mutant females which could be making it more difficult for eggs to be released. Indeed, the opening of the female urogenital pore appears to be very small and underdeveloped in 1-year old triple *hox13* mutant (Figure 30). Upon dissection, the female triple *hox13* mutants have still been found to produce eggs. These eggs were collected although they were unable to be fertilized by wild-type sperm when it was applied to the eggs. The male urogenital pore (not shown) is generally much smaller compared to the female pore, and so defects could not be observed in the pore of the triple *hox13* mutant male due to the size. Measurements on the average length of the urogenital pore on four wild-type and four triple *hox13* mutant females was also performed as shown in figure 30. This comparison demonstrated a significant decrease in the length of the triple *hox13* mutant urogenital pore ($p=2.092x10^{-5}$).

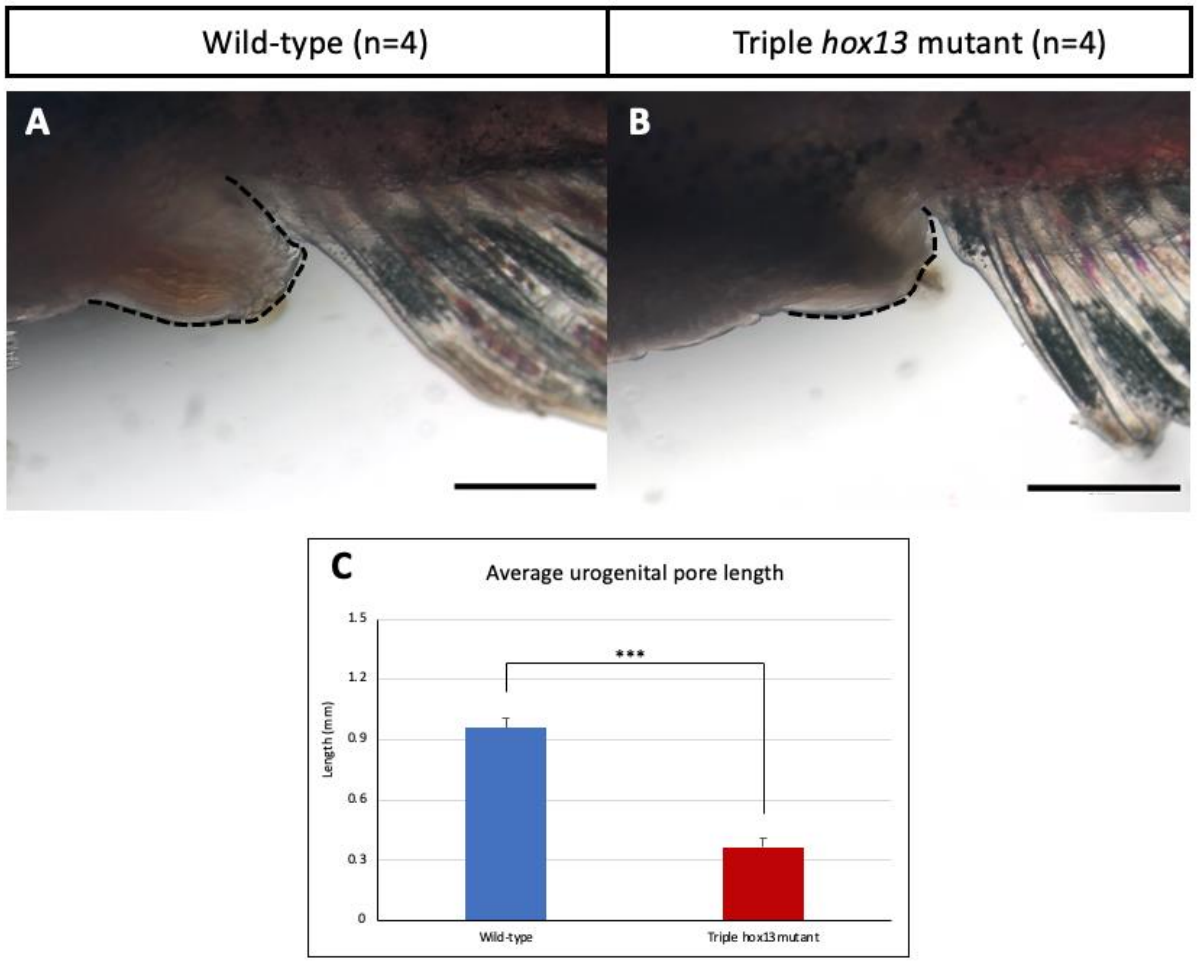

Figure 31. Triple *hox13* mutant female urogenital pore compared to wild-type. A, B: Lateral views of the wild-type and triple *hox13* mutant urogenital pores are presented, with the anterior of the fish towards the left. C: Length comparison of the urogenital pore in each genotype. Fish used for this comparison were 14 months of age with SLs between 3.4 and 3.7cm. Black dotted lines outline the urogenital pore in each image. Red dotted lines indicate the distance measured in C. Red arrows indicate the opening of the pore. Means + SE are presented. Unpaired t-tests were performed to determine statistical significance, which is shown as * ($p<0.05$), ** ($p<0.01$), or *** ($p<0.001$). Scale bars = 1mm.

Hypothesis 2:

3.4 Phenotypic similarities between zebrafish triple *hox13* mutant rays and acanthomorph spines

As previously mentioned, zebrafish are not acanthomorphs, and so their fins do not typically contain spiny rays. Phenotypically however, the triple *hox13* mutant fins observed in this project except for the caudal fin appeared to form rays that more closely resembled spine-like rays as opposed to normal soft rays. Like the spiny rays, the triple *hox13* mutant rays do not bifurcate, they do not contain joints, they are relatively short in length, and they appear to be wider and thicker compared to soft rays. Alizarin red staining on adult wild-type and triple *hox13* mutant zebrafish was performed. The dorsal fin rays were imaged and compared to *A. burtoni* fins in Figure 31. From this comparison, the *hox13* mutant rays appear similar in structure to the spines of the *A. burtoni* dorsal fin, with a lack of joints, bifurcations, and tip actinotrichia, as well as shorter length. From the initial observations of this "spine-like" phenotype, further investigation was conducted into determining how close the relationship is between true acanthomorph spines and *hox13* mutant rays. These experiments included micro-CT scanning of the triple *hox13* mutant rays to observe hemiray thickness, and *alx4a* gene expression analysis.

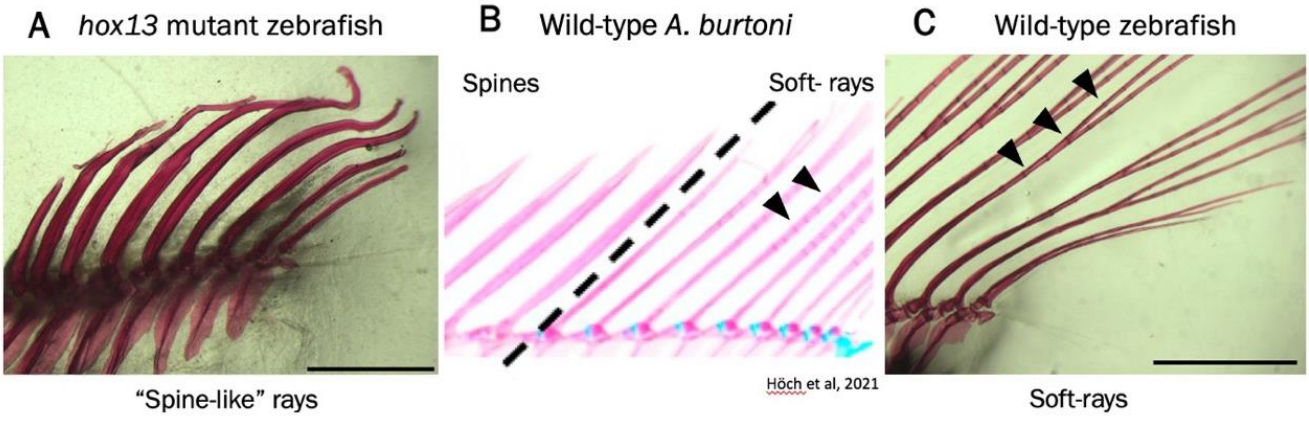

Figure 32. Triple *hox13* mutant fin rays resemble acanthomorph spines. A: Dissected bone-stained dorsal fin of a triple *hox13* mutant. B: Wild-type *A. burtoni* dorsal fin spines and soft rays, adapted from Höch et al, 2021. C: Dissected bone-stained wild-type zebrafish dorsal fin. Black arrows indicate joints in the soft rays of B and C. Scale bars = 2mm.

3.5 Micro-CT analysis of the dorsal rays of the triple *hox13* mutant

Since spines most commonly appear in the dorsal and anal fins of acanthomorph fish, Micro-CT scanning was performed on wild-type and triple *hox13* mutant dorsal fins to observe the thickness of the mutant hemirays in these fins. Scans were reconstructed and reoriented by Dr. Qingming Qu, Xiamen University, to get cross sections of specific fin rays in both the wild-type and mutants at standard levels along the proximal-distal axis of the ray. A full reconstruction of a wild-type scan is shown in Figure 32 as an example.

The overall shape of the hemirays remains similar in the triple *hox13* mutant compared to the wild-type, where they are curved inwards with no fusion at the anterior side. Between the wild-type and the triple *hox13* mutants, the hemirays at all analyzed positions appeared to be thicker in the triple *hox13* mutant. Measurements of the hemiray width at each location are shown in figure 34. The most statistically significant changes were seen in the A2 fin ray at the 500μm ($p<0.0001$) and 750μm position ($p<0.0005$), suggesting the changes between the wild-type and mutants may be most profound in the anterior, proximal part of the fin. The fold change between the wild-type and mutant hemiray thickness however seems to be very similar at all positions, where the triple *hox13* mutant hemirays tend to be about 2.5-fold thicker compared to their wild-type counterparts.

The *hox13* mutant hemirays also tend to show slightly more variation on average compared to the wild-type hemirays which are overall quite consistent at each position.

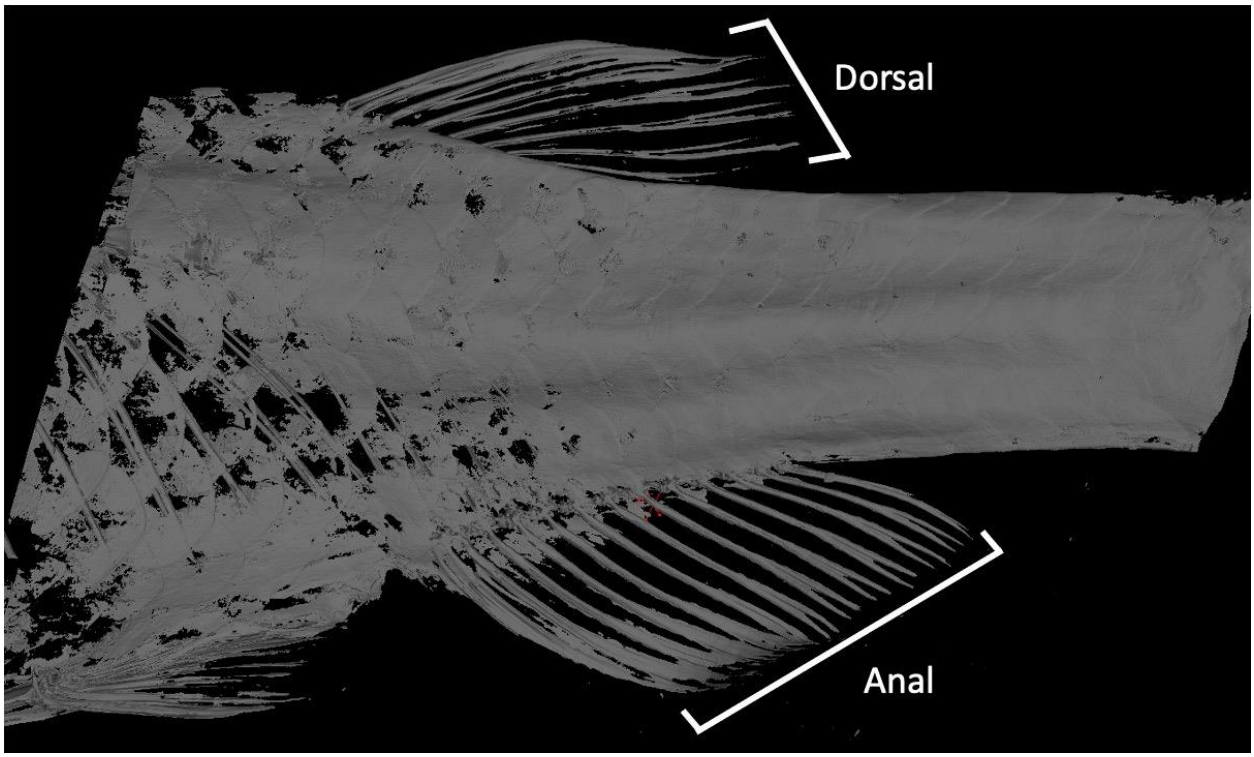

Figure 33. Complete CT-scan reconstruction of wild-type sibling dorsal and anal fins. 3D model reconstructions were made from slices in VGstudio, where tissue surrounding the lepidotrichia could be removed from the model. All scanned fish were within 3 and 3.2 cm SL. Anal and dorsal fins are shown within white brackets. Scan reconstructions were performed by Dr. Qingming Qu, Xiamen University.

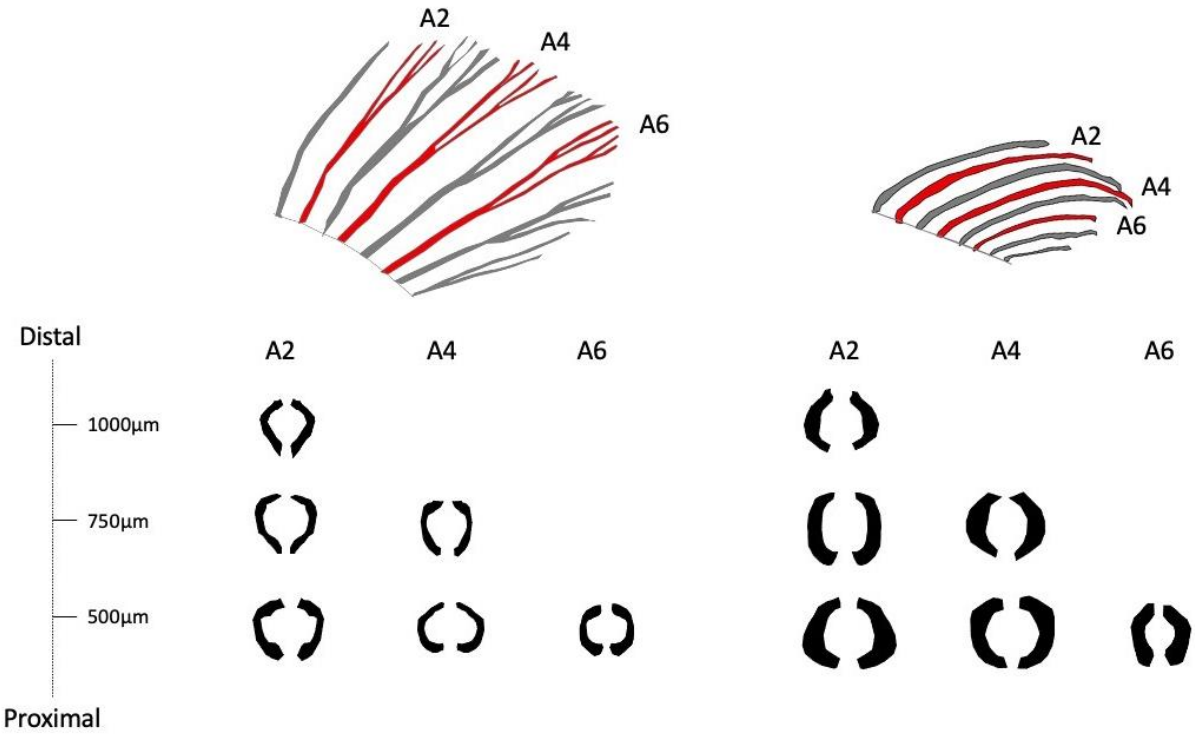

Figure 34. Schematic representation of the wild-type (left) and triple *hox13* mutant (right) dorsal fin hemirays. Whole-fin images of the wild-type and triple *hox13* mutant dorsal fins were traced, and fin rays of interest are highlighted in red. Fin rays are named according to their position in the fin from the anterior margin (ex: A2 = second ray from the anterior side). The shape of the hemirays of each genotype was traced at specific levels along the proximal-distal axis of the ray, shown on the left. SL=3.2cm for both fish measured.

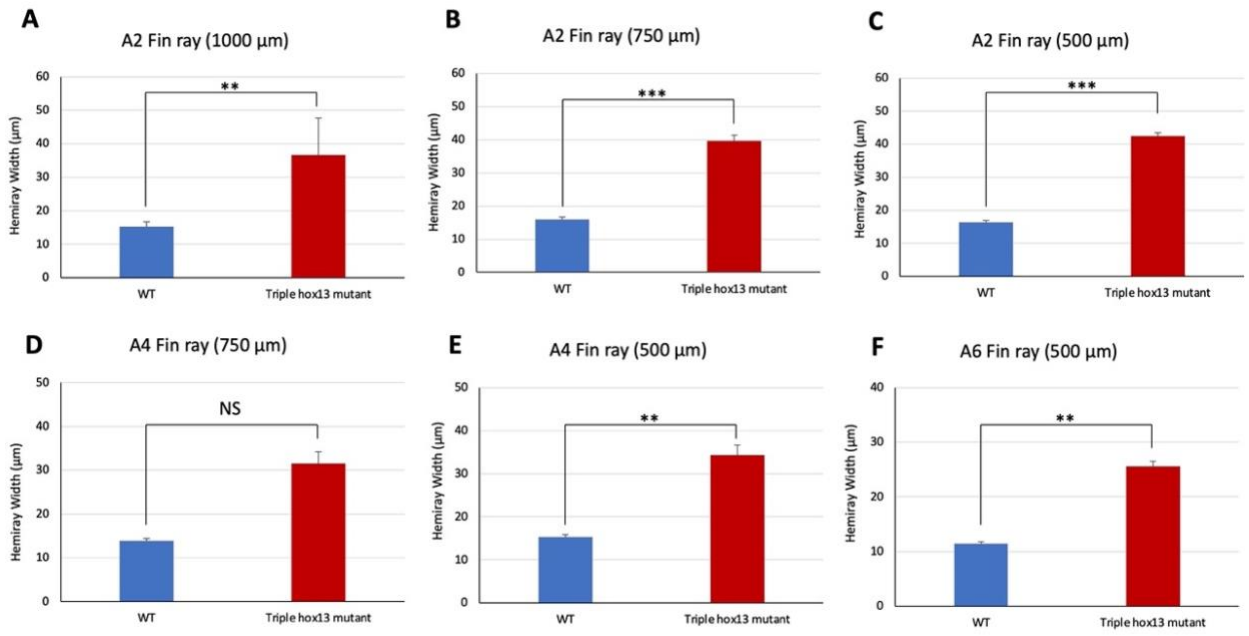

Figure 35. Triple *hox13* mutant dorsal hemirays are thicker compared to wild-type dorsal hemirays. Bar graphs of dorsal hemiray widths in µm of wild-type and triple *hox13* mutants are present at specific levels along the proximal distal axis. The fin ray of interest and distance from the proximal base of the ray in µm is listed above each corresponding graph. Measurements were averaged from n=3 replicates for each group at each location. Means + SE are presented. Unpaired t-tests were performed to test for statistically significant changes, which are indicated as * ($p<0.05$), ** ($p<0.01$), or *** ($p<0.001$). A Mann-Whitney U test was performed for D since data was not normally distributed.

3.6 *Alx4a* gene expression in the triple *hox13* mutant dorsal and anal fins

3.6.1 Developmentally similar timepoints between zebrafish and *A. burtoni*

The second prediction of what might be observed in the triple *hox13* mutant is that there will be an expanded domain of expression for *alx4a*, a gene which as previously mentioned, is known to be expressed exclusively in spiny rays in acanthomorphs (Höch et al., 2021) and restricted to the anterior margin of zebrafish fins (Nachtrab et al., 2013). In order to observe this potential change, developmental timepoints in zebrafish that seemed comparable to the developmental timepoints in *A. burtoni* observed in Höch et al., (2021) were selected to observe *alx4a* expression in wild-type and triple *hox13* mutant zebrafish.

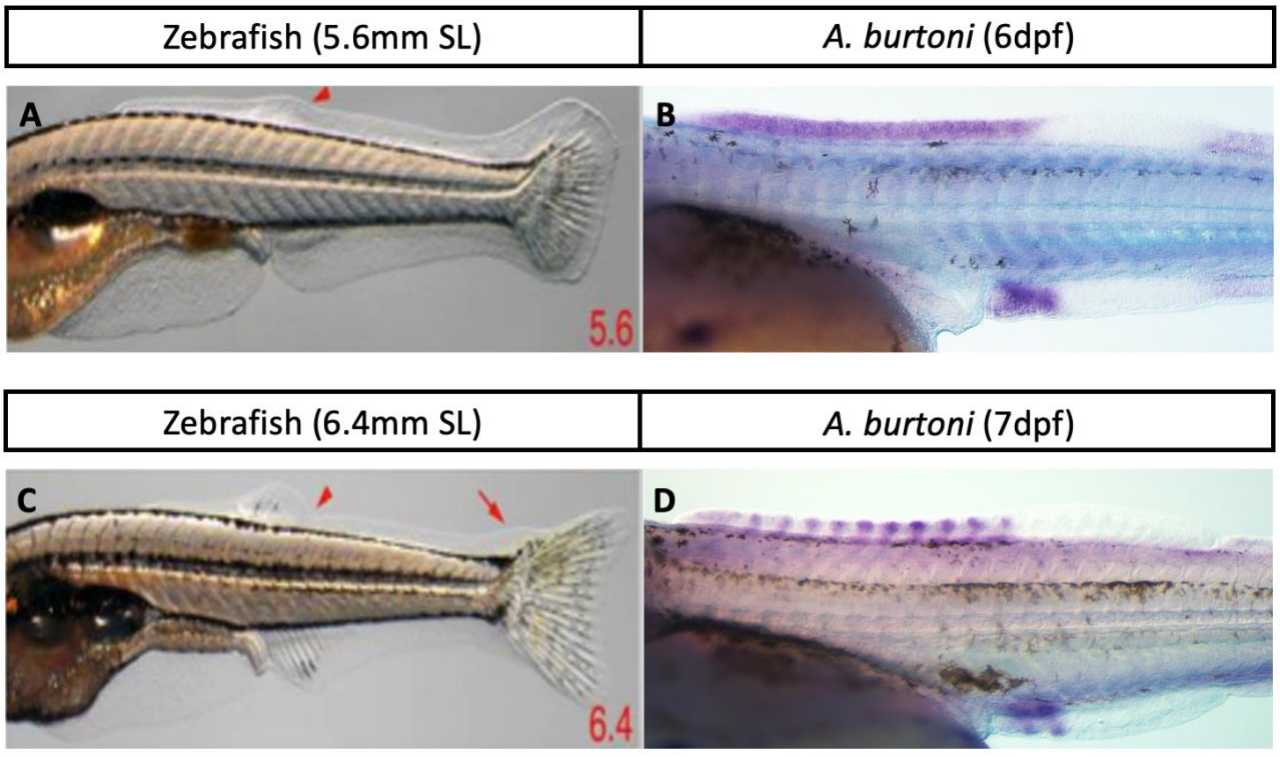

Figure 36. Dorsal and anal fin primordia of the zebrafish are visible at 5.6mm SL. A: Developing juvenile zebrafish at 5.6mm SL where anal and dorsal fin primordia become visible. B: 6dpf *A. burtoni* whole mount in situ hybridization showing *alx4a* expression in the dorsal and anal fin primordia C: 6.4mm SL juvenile zebrafish with the fin rays visible in the dorsal and anal fins. D: 7dpf *A. burtoni* whole mount in situ hybridization showing *alx4a* expression in the developing dorsal and anal fin rays. Images A and C were taken by Marissa Northorp. Images B and D were adapted from Höch et al., 2021 with permissions from PNAS: Open Access Articles, April 22, 2023.

As shown in figure 35, both dorsal and anal fin primordia emerged at 5.6mm SL, which appears to developmentally resemble the 6dpf timepoint in *A. Burtoni* reported by Höch et al. (2021). At both timepoints, the fin primordia can be observed, but the rays have not yet formed Although *alx4a* expression in zebrafish at this specific timepoint has not been described, it should be expressed in the anterior portion of the dorsal and anal fin primordia as it is in other non-acanthomorphs (Höch et al., 2021). Thus, *alx4a* expression was observed at this 5.6mm timepoint, and the expression patterns were compared between wild-type and triple *hox13* mutant zebrafish.

3.6.2 *Alx4a* expression in the dorsal and anal fin primordia at 5.6mm SL

Whole-mount *in situ* hybridization on 5.6mm wild-type zebrafish has confirmed the domain of expression of *alx4a* in non-acanthomorph dorsal and anal fin primordia. The primordium of the fin includes the condensed part of the mesenchyme proximal to the median fin fold where the dorsal or anal fin will form. *Alx4a* expression was exclusive to the anterior portion

of the developing zebrafish dorsal and anal fin primordia. After measuring the extent of the domain of expression in both the wild-type and triple *hox13* mutants (Figure 37) there did not seem to be any difference between *alx4a* expression in the anal fin primordium (p=0.261) or the dorsal fin primordium (p=0.193). Upon measurement of the fin primordium size in both wild-type and triple *hox13* mutants, the width of the mutant dorsal (p=0.00147) and anal fin primordia ($p=2.24x10^{-6}$) was found to be smaller at 5.6mm SL. In addition to the primordia, the base of the adult dorsal fin ($p=3.09x10^{-5}$) and anal fin ($p=2.39x10^{-4}$) are also not as wide as wild-type fins by comparing average measurements of n=5 replicates, supporting the significance of the smaller fin primordia in the triple *hox13* mutant. After finding that the triple *hox13* mutants had smaller fin primordia, the width of each *alx4a* expression domain was then divided by the width of each fin primordia, to compare the relative *alx4a* expression domains in each individual. Because of this decrease in the size of the fin primordia, an increase of *alx4a* in the triple *hox13* mutant was found, where *alx4a* is proportionally expressed in more space in the dorsal (p=0.0024), and anal ($p=3.64x10^{-5}$) fin primordia. While the *in situ* hybridization experiments on the wild-type and mutant fish were run in parallel and stained for the same amount of time, at this timepoint *alx4a* expression is stronger in the mutants compared to the wild-type. A definite conclusion cannot be made here about the exact expression levels since ISH is not a true quantitative experiment, although a relatively higher expression of *alx4a* would indicate that *hox13* has a repressive role on *alx4a* in the anterior part of the fin primordium.

In addition to measuring the width of each fin primordia to observe proportional *alx4a* expression domains, the length from the base to the distal-most tip of the dorsal and anal primordia was also measured to compare the triple *hox13* mutants to the wild-type (Figure 37). A significant

decrease in length can be seen in the triple *hox13* mutant in the dorsal (p=0.000681) and anal ($p=7.424x10^{-5}$) fin primordia, further highlighting the importance of *hox13* genes for the development of these fins. In summary, this data indicates that *hoxa13a, hoxa13b*, and *hoxd13a* have significant roles in the proper development of the dorsal and anal fin primordia, as significant decreases in both length and width can be seen as a result of mutations in these genes. Although the proportion of the *alx4a* expression domain is higher in the triple *hox13* mutant due to the smaller fin primordia, the *alx4a* expression domain itself is the same width in both genotypes. This indicates that *hoxa13a, hoxa13b,* and *hoxd13a* do not seem to have a role in regulating the expression domain of *alx4a* in zebrafish, however these *hox13* paralogs do seem to play a role in the regulation of *alx4a* expression level in the anterior part of the dorsal and anal fin primordia.

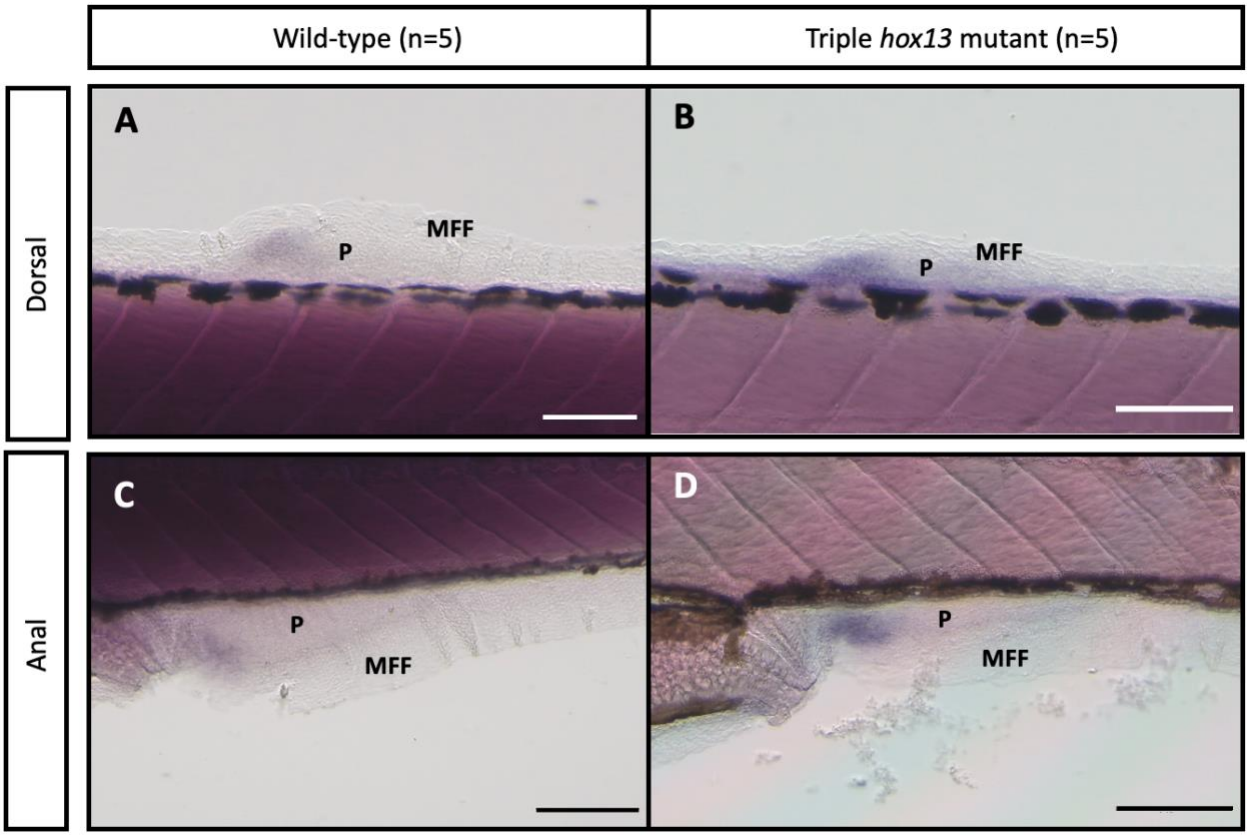

Figure 37. *alx4a* expression at 5.6mm SL in the wild-type and triple *hox13* mutant fin primordia. Whole mount in situ hybridization for *alx4a* for both dorsal and anal fin primordia are presented. N=5 replicates for both wild-type and triple *hox13* mutants. P: primordia, MFF: median fin fold. Scale bars = 100μm for A and B, and 150μm for C and D.

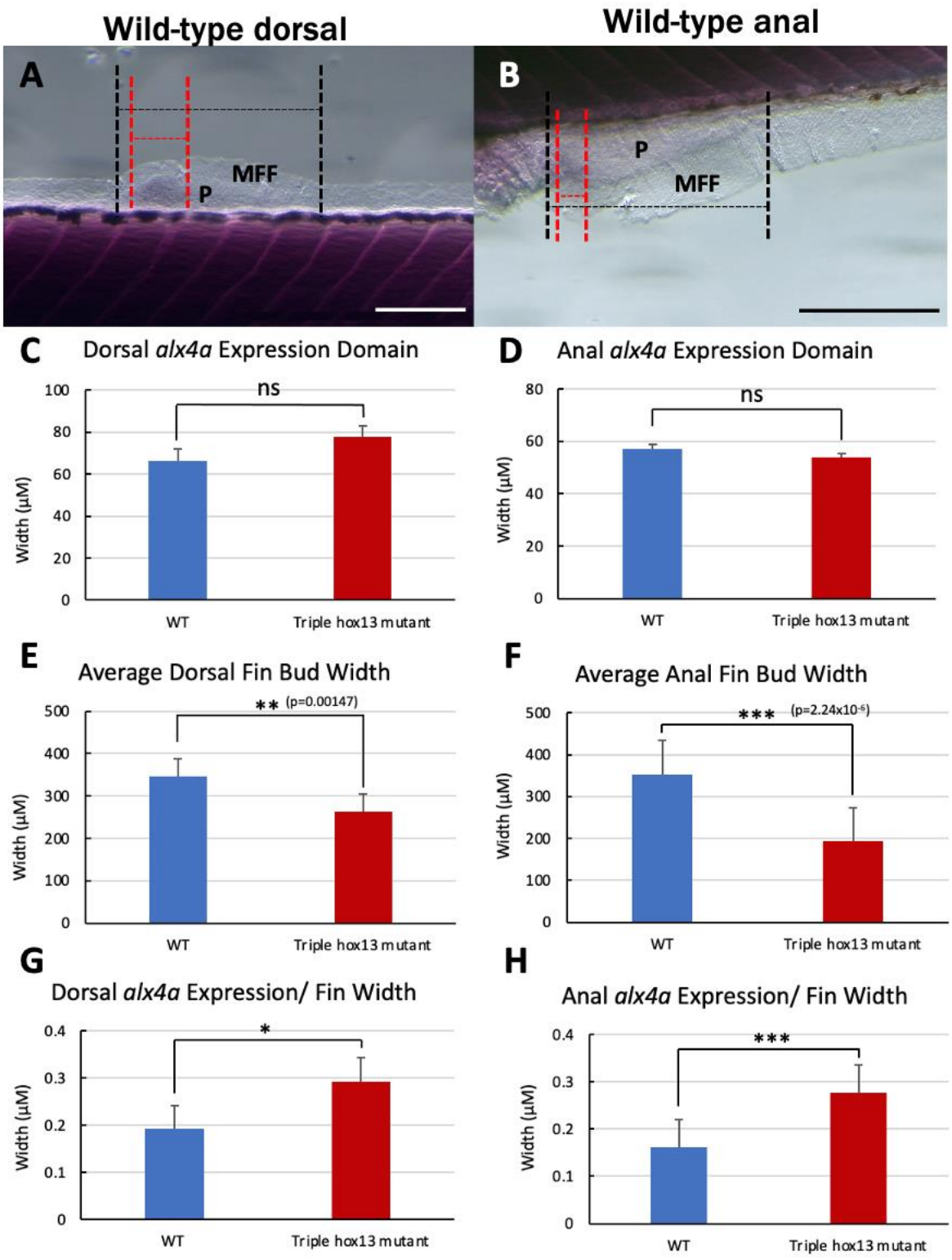
Wild-type dorsal
Wild-type anal
A
MFF
P
B
P
MFF
C
Dorsal alx4a Expression Domain
ns
Width (µM)
WT
Triple hox13 mutant
D
Anal alx4a Expression Domain
ns
Width (µM)
WT
Triple hox13 mutant
E
Average Dorsal Fin Bud Width
** (p=0.00147)
Width (µM)
WT
Triple hox13 mutant
F
Average Anal Fin Bud Width
*** (p=2.24x10-6)
Width (µM)
WT
Triple hox13 mutant
G
Dorsal alx4a Expression/ Fin Width
*
Width (µM)
WT
Triple hox13 mutant
H
Anal alx4a Expression/ Fin Width
***
Width (µM)
WT
Triple hox13 mutant

Figure 38. Triple *hox13* mutants show a proportionate increase in alx4a expression in the dorsal and anal fin primordia. A,B: *alx4a* expression in wild-type fish detected by in situ hybridization in the dorsal fin (A) and anal fin (B). Black dotted lines represent examples of measurements taken for the length of the *alx4a* expression domain that is compared in C and D. The distance between the two vertical black dotted lines that span the *alx4a* expression domain was measured. The red dotted lines represent examples of measurements taken for the fin primordium at this timepoint. The distance between these red lines was compared in E and F. The proportionate expression of *alx4a* taking in to account the size of the fin fold is shown in G and H, where the distance between the red lines is divided by the distance between the black lines. N=5 replicates were observed for both wild-type and triple *hox13* mutants. P: primordia, MFF: median fin fold. Means + SE are presented. Unpaired t-tests were performed to test for statistically significant changes, which are indicated as * ($p<0.05$), ** ($p<0.01$), or *** ($p<0.001$). Scale bars = 150μm for A, and 250μm for B.

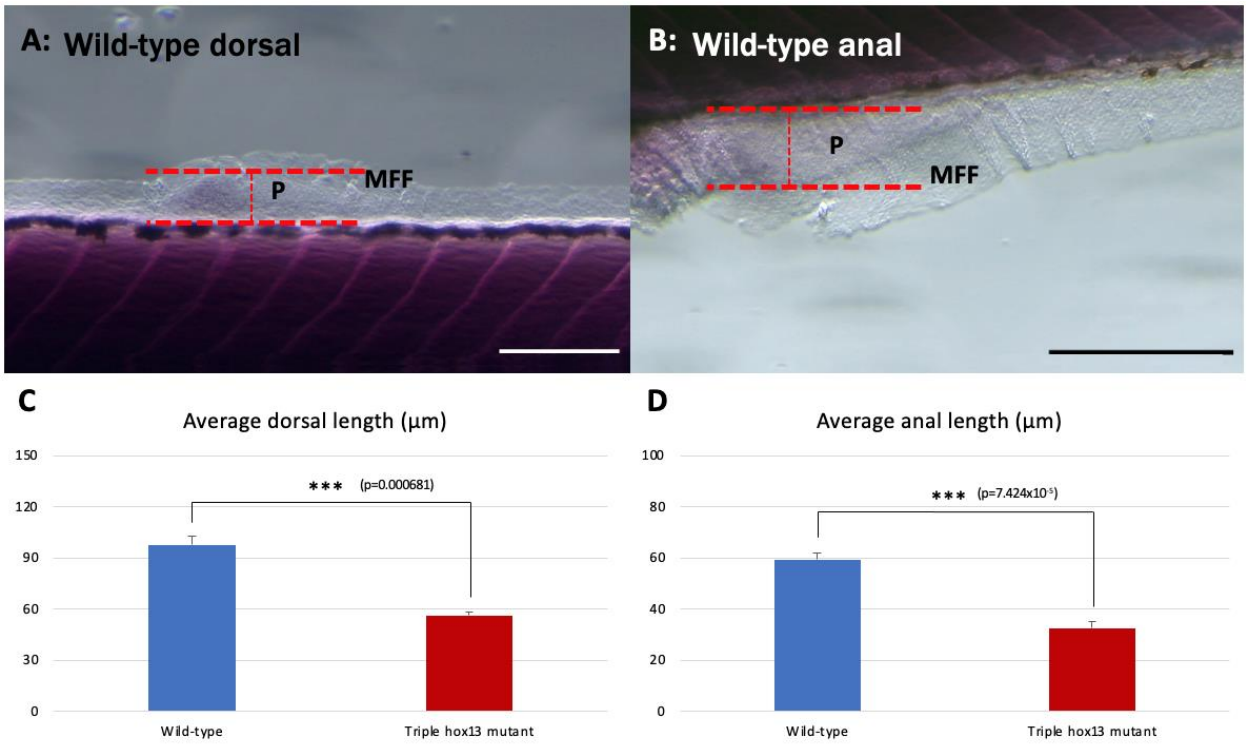

Figure 39. Dorsal and anal fin primordia length is decreased in the triple *hox13* mutant at 5.6mm SL. A: Wild-type dorsal (A) primordium and anal (B) primordium *alx4a* expression. Red lines represent the distances measured from the base to the distal-most point of the fin primordium. C, D: Average length of the dorsal (C) and anal (D) primordia lengths in the wild-type and triple hox13. N=5 replicates for each genotype. P: primordia, MFF: median fin fold. Means + SE are presented. Unpaired t-tests were performed to test for statistically significant changes, which are indicated as * ($p<0.05$), ** ($p<0.01$), or *** ($p<0.001$). Scale bars = 150µm for A, and 250µm for B.

Chapter 4: Discussion

4.1 Summary of objectives

The first overall objective of this thesis was to better characterize the individual contributions of *hoxa13a, hoxa13b,* and *hoxd13a* to zebrafish fin phenotype. This was done primarily by comparing various single heterozygous, double homozygous *hox13* mutants to the triple *hox13* mutant in order to observe phenotypic differences caused by the presence of single *hox13* genes. The second overall objective was to subsequently investigate the potential similarities between the triple *hox13* mutant rays, and the acanthomorph spiny rays. This was done primarily through CT scanning our triple *hox13* mutants, as well as *in situ* hybridization of the *alx4a* spine marker on specific developmental timepoints in the triple *hox13* mutant.

4.2 The role of *hox13* genes in joint, bifurcation, and actinotrichia formation

All genotypes in Table 2 were observed for a morphological comparison of joints, bifurcations, and actinotrichia. Since single homozygous deletions for *hoxa13a, hoxa13b,* and *hoxd13a* do not have a phenotypic difference from wild-type fish, double homozygous fish were compared to triple homozygous deletions for these genes in order to get a better understanding of the individual contributions of each of these *hox13* genes to adult fin phenotype. From this analysis, it was observed that the *hoxa13a -/+, hoxa13b -/-, hoxd13a -/-* mutant as well as the *hoxa13a -/-, hoxa13b -/+, hoxd13a -/-* mutant fins showed vast similarities to wild-type fins, with joints, bifurcations, and actinotrichia always present in every fin. In contrast, the *hoxa13a -/-, hoxa13b -/-, hoxd13a -/+* mutant showed more similarities to the triple *hox13* mutant where there is an absence of joints, bifurcations, and actinotrichia in all fins except for the caudal fin. Finally,

for the *hoxa13a -/-*, *hoxa13b -/-*, *hoxd13a +/+*, joints can consistently form in the caudal, anal, and dorsal fins, although not in the paired fins.

First, all mutant genotypes demonstrate a reduction in fin ray length in all fins. In this analysis, the pectoral and pelvic fins have the largest reductions in length, the dorsal and anal fins have medial reductions, and the caudal fin has only minor reductions in the lobes. Shortening of the fin rays was the only defect still present in *hoxa13a -/+*, *hoxa13b -/-*, *hoxd13a -/-*, and *hoxa13a -/-*, *hoxa13b -/+*, *hoxd13a -/-* mutants indicating that only one copy of either *hoxa13a* or *hoxa13b* is not able to induce the normal wild-type length in fin rays. Similar to joints, bifurcations and actinotrichia however, one copy of either of the *hoxa13a* and *hoxa13b* genes allows for longer fin rays compared to one copy of *hoxd13a*. In previous studies, *hoxa13a* and *hoxa13b* have been shown to be expressed in the blastema and the tip of the fin rays during regeneration (Géraudie & Borday Birraux, 2003; McMillan et al., 2018). Specifically, *hoxa13a* has been shown to be expressed in the osteoblasts during regeneration (McMillan et al., 2018). Furthermore, all three *hox13* genes observed in this project have been shown to be enriched in the distal portion of the caudal fin using RNA seq (Rabinowitz et al., 2017) as is further explained in the next paragraph. Since the fins of the zebrafish grow throughout the lifetime of the fish, the distal expression of these genes potentially highlights their importance for fin ray growth.

As outlined in section 1.3.1, the process of exoskeletal joint formation has been shown to involve osteoblasts forming clusters in the developing rays that will become joint forming cells to form the mature joint (McMillan et al., 2018; Sims et al., 2009). The exact mechanism of how joint

cells are formed is not fully understood, although *hoxa13a* and *evx1* both seem to work upstream of *pthlha* to allow for joint formation (McMillan et al., 2018). Both *hoxa13a* and *evx1* are expressed in the absence of one another, suggesting that they work in parallel to form joints in the fin rays (McMillan et al., 2018; Quigley, unpublished). *Hoxa13b* and *hoxd13a* however did not show clear expression in joint cells as was seen with *hoxa13a*, which suggested that these genes did not have a significant role in joint formation (McMillan et al., 2018). Based on the results of this project, evidence has shown that, in addition to *hoxa13a*, *hoxa13b* and *hoxd13a* can be responsible for fin ray joint formation in zebrafish, although with differing capacities. Only one copy of either *hoxa13a* or *hoxa13b* is necessary for joint formation in all fins. *Hoxd13a* is still capable of causing joint formation in the dorsal and anal fins, although two copies of the gene are necessary compared to only one copy in the case of *hoxa13a/b* and the joints in the fins remain irregularly spaced along the proximal-distal axis of each ray. Conversely, none of these genes are necessary for caudal fin joint formation. Unlike *evx1-/-* mutants, the triple *hox13* mutant still has joints in the fin rays of the caudal fin, suggesting that there could be higher genetic compensation in this fin compared to other fins as is further explained in section 4.3.

Fin ray bifurcation appears to follow a very similar trend with joint formation in terms of defects due to the *hox13* mutations. While the role of *hox13* on fin ray bifurcation has not been examined specifically, we know that *shha* and *bmp2b* have been shown to play a role in the bifurcation process (Quint et al., 2002; Zhang et al., 2012). Much of what we know about these genes during fin ray growth has been studied in caudal fin regeneration, where regenerating fin rays grow through partial recapitulation of developmental outgrowth pathways. During regeneration, *shha* is expressed in a subset of epidermal cells. Bifurcation of fin rays correlates

with a splitting of this *shha* expression into two domains (Quint et al., 2002). Furthermore, reducing *shha* expression using cyclopamine resulted in reduced bifurcation and proliferation in regenerating fin rays (Quint et al., 2002). Laser ablation of these *shha*-expressing cells in the regenerate also results in a delay of branching in newly formed fin rays (Zhang et al., 2012), further highlighting the potential importance of *shha* expression for fin ray bifurcation. The relationship between *shha* and *hox13* in the fin rays however has not been well described, although it is possible that *hox13* could be acting as an activator of *shha* in the adult fin rays as is seen in early limb development (Lettice et al., 2003). The expression of *shha* however would have to be observed in the regenerating triple *hox13* mutant fin rays to conclude if this is accurate. If *hox13* expression is indeed activating *shha* in the fin ray, we should expect to see lower than normal expression of *shha* in the regenerating fin rays of triple *hox13* mutant dorsal, anal, and paired fin regenerates since these fins do not normally bifurcate in the mutant.

Defects in actinotrichia again follow the same trend as joints and bifurcations, where they are absent from all fins except for the caudal fin in the triple *hox13* mutant, and the *hoxa13a* -/-, *hoxa13b* -/- *hoxd13a* -/+, mutants. The only difference is that actinotrichia are not observed in the lateral-most rays of the caudal fin in these mutants whereas they normally are in wild-type fish. Previously, Rob Lalonde used a site-directed mutagenesis approach in a *Tg(2Pand1:eGPF)* line investigate the capacity of mutated sites in the *and1* enhancer region to activate GFP expression (Lalonde et al., 2016). From this experiment, a genomic region containing binding sites for several *hox13* and *hox11* genes was found to be essential for GFP/*and1* expression in the *Tg(2Pand1:eGFP)* line (Lalonde et al., 2016). Considering the binding sites of *hox13* on *2Pand1*, it is likely that the lack of *hox13* is causing *and1* to be downregulated, preventing actinotrichia

fibers from forming properly. In addition to the *hox13* mutants, our lab also has generated a double homozygous deletion mutant for *and1* and *and2*. This mutant lacks the ability to form actinotrichia fibers, and the fin rays of this mutant display a shortened, curled phenotype similar to the triple *hox13* mutant. Unlike the triple *hox13* mutant however, joints are still present in the *and1* -/-, *and2* -/- mutant fin rays. Fin rays in the double homozygous *and1* and *and2* mutant display shortened length, as well as a wavy structure to their fin rays. From observations of this *and1 and2* double mutant, we can infer that the shortening and irregular wavy patterning of many fin rays in the triple *hox13* mutants may be due to the inability to form actinotrichia fibers in all fins except for the caudal fin.

Conclusively, it appears all three of these *hox13* genes have some redundancy with one another in their role on fin ray joint and bifurcation, although there is a varying degree to which each of these three genes affect these fin ray characteristics. In the case of *hoxa13a* and *hoxa13b*, only one copy of either gene is required to have proper fin ray joint, bifurcation, and actinotrichia formation in all fins. In contrast, only one copy of *hoxd13a* is unable to exert this same effect. When only two copies of *hoxd13a* are present, joints and bifurcations are able to form in the dorsal and anal fins in very irregular patterns, and the paired fins remain with an absence of these characteristics. Conversely, *hoxd13a* alone does not seem to have a significant effect on actinotrichia formation, as fibers were still absent from the tips of the *hoxa13a -/-*, *hoxa13b -/-*, *hoxd13a +/+* mutants. Overall, the function of *hoxa13a* and *hoxa13b* show very high similarity, although a higher gene dosage of *hoxd13a* is required to exert the same effect in the fin rays as *hoxa13a/b.* An explanation for why this is the case can be seen in the baseline expression levels of each of these three *hox13* genes. In a study by Rabinowitz et al., (2017) RNA-seq was performed

on the intact zebrafish caudal fin at different point along the proximal-distal axis. The fins of the zebrafish grow throughout their lifetime, and so presumably the targets that were enriched in the distal portion of the caudal fin compared to the more proximal portion have a larger role in fin ray growth. From datamining performed on the dataset published by this study, *hoxa13a*, *hoxa13b*, and *hoxd13a* were all found to be distally enriched in the intact caudal fin. The expression levels of them however differed greatly from gene to gene. In the distal portion of the caudal fin, *hoxa13b* showed the highest expression of the three genes with 1003.8 reads per million (RPM), *hoxa13a* showed expression of 279.9 RPM, and *hoxd13a* showed the lowest expression level by far with only 14.6 RPM. Due to this difference in baseline expression level, it could be that all three *hox13* genes of interest have very similar function, and that a difference in expression level can explain the defects that we observed in the double homozygous *hox13* mutants of this study. One copy of either *hoxa13a* or *hoxa13b* may cause longer fin ray length, and more joint, bifurcation and actinotrichia formation compared to one copy of *hoxd13a* due to the higher expression levels of *hoxa13a/b*. Since *hoxd13a* is lowly expressed, one copy of this gene alone is insufficient to meet this required threshold for joint, bifurcation, and actinotrichia formation, although two copies of this gene seem to be able to meet the expression threshold in the dorsal and anal fins for joint and bifurcation formation.

4.3 Fin-type specific defects from *hox13* mutations

A common theme observed in this project was that the caudal fin showed very little variation between all mutant genotypes. Independent of the genotype, joints, bifurcations, and actinotrichia were always present in the fins, and fin ray length reductions were minor. Exactly why this occurs is not fully understood, however it could be a result of increased genetic compensation on this fin.

From an evolutionary perspective, it is likely that the caudal fin has more compensatory mechanisms in place to conserve the structure of this fin due to its importance for swimming. The caudal fin is the primary fin that provides forward thrust to the fish when swimming to influence the swim speed of the fish (Naser & Rashid, 2020). Furthermore, amputations of the caudal fin have been shown to have significant effects on swimming speed and performance in many fish species including sockeye salmon (Webb, 1973), rainbow trout (Webb, 1977), goldish, carp, and qingbo (Fu et al., 2013). Considering this mechanistic importance, there may be more pressure to maintain a proper caudal fin since deformities or amputation in this fin may cause decreases in the fitness of the fish. Thus, more genetic compensatory mechanisms may be in place to maintain its structure. Some candidates for this compensation include *hoxc13a* and *hoxc13b*. In a study by Thummel et al., (2004), both of these genes were shown to be expressed in the caudal fin region until 72hpf. Problematically however, later timepoints were not observed in this study, so it is not known if *hoxc13* expression appears later in the other fins as well. The same group also showed that both *hoxc13* paralogs are important for caudal fin regeneration, as knockdowns of these genes after fin amputation led to significant reductions in proliferation and fin ray outgrowth (Thummel et al., 2007). Similarly, the other fins were not observed in this study, and so it is not known if *hoxc13a* or *hoxc13b* play a role in the regeneration and growth of other fins as well. In order to confirm this possibility, the expression of *hoxc13a* and *hoxc13b* should be observed throughout later developmental timepoints in zebrafish when the dorsal and anal fins begin to emerge. Additionally, *hoxc13a* and *hoxc13b* expression could also be observed during regeneration in the dorsal, anal, and paired fins, to see if these genes are strongly expressed in the regenerate in the same way that they are in the caudal fin. This would allow us to say with more confidence that the

expression of *hoxc13* is exclusive to the caudal fin and is responsible for genetic compensation in this fin.

4.4 Endoskeletal defects are exclusive to the pectoral fin in the triple *hox13* mutants

The pectoral endoskeleton of the triple *hox13* mutant has an increased number of distal radials, as was seen in the *hoxa13a* -/-, *hoxa13b* -/- mutant, and triple mosaic mutant in Nakamura et al. (2016). This study had also reported a proximal distal stacking of the radials on the posterior side of the fin. While some of this stacking seemed apparent in our triple mutant as shown by radials 7 and 9 in Figure 27 (n=2), this stacking did not seem as obvious as with the triple mosaic mutant. The triple mosaic mutant in in Nakamura et al. (2016) was observed using CT scanning (n=5), while our mutants were observed using bone staining and dissection, which could have caused distal radials to shift slightly from their original positions. As a result, CT scanning on our triple *hox13* mutant pectoral endoskeleton may be necessary to draw definite conclusions as to whether or not the distal radials are stacked in this mutant. Aside from the pectoral fin distal radials, no defects could be observed in the endoskeleton of the triple *hox13* mutant fins. The triple *hox13* mutant pelvic fin had the same number of distal radials (3) as the wild-type, and no changes in the pelvic girdle. The dorsal and anal fins of the triple *hox13* mutant also had no visible changes in the proximal or distal radials compared to the wild-type. Finally, the caudal fin elements appeared the same in both genotypes with the parahypural and all hypurals still visible in the triple *hox13* mutant. Given these observations, *hoxa13a*, *hoxa13b*, and *hoxd13a* do not seem to be essential for proper endoskeleton formation in all fins with the exception of the pectoral fin. The primary role of these *hox13* genes in the fins is thus in the patterning of the fin rays, indicating that *hox13* does not have a role in the endoskeletal patterning of the pelvic and medial fins. As previously

concluded by Nakamura et al., (2016), the stacking of the radials in the proximal-distal direction in the triple *hox13* mutant resembles closer to what is seen in mammalian phalanges. This observation led the authors to hypothesize that the loss of the *hox13* genes was causing less migration of cells into the fin fold, resulting in a larger number of endochondral bones as opposed to fin rays (Nakamura et al., 2016). Considering this hypothesis however, we should also predict to see an elaboration in the pelvic fin endoskeleton since it is homologous to the mammalian hindlimb, although there does not appear to be any difference in the pelvic fin endoskeleton for the triple *hox13* mutant.

4.5 Blood vessel patterning differs in the triple *hox13* mutant fins

Vasculature defects in the fin rays appeared to be minor overall and are mainly defined as a general disorganization of blood vessels. The most severe defect was seen in the pectoral fin, where the anterior-most rays seem to lack interray commissures. Why this is only observed in the pectoral fin however is not clear. It could be hypothesized that the hemiray bone is much thicker and closer together in the triple *hox13* mutant making it difficult for blood vessels to pass through the gap between the hemirays. To observe this, micro-CT scanning of the triple *hox13* mutant pectoral fin rays could be used to analyze the structure. Additionally, the central artery of the paired fins in each ray tends to curve compared to the wild-type arteries that are very straight. As a conclusion, the lack of *hoxa13a, hoxa13b,* and *hoxd13a* appears to cause some mispatterning of fin ray blood vessels, especially the smaller interray and intervessel commissures. It is difficult however to separate how much of the observed defects can be directly attributed to the *hox13* genes in regulating blood vessel patterning, compared to if the vascular defects are a biproduct of the patterning defects in the triple *hox13* mutant fin ray structure. Many of the observed patterning

defects could simply be due to the morphology of the fin rays being different and the spacing between the rays being variable, causing blood vessels to form longer indirect vessels between neighbouring rays. Furthermore, the hemirays of the pectoral fin could be very thick and close together, not allowing for the formation of vessels in between the opening between the hemirays. The curving of the arteries may also be attributed to the lack of straight fin rays in the triple *hox13* mutant, making the blood vessels also appear curved. To determine if this is right, the blood vessels could be observed in the *and1 -/-, and2 -/-* double mutant generated by our lab as well. These mutants demonstrate shorter, curved fin rays similar to the triple *hox13* mutant, although the fin rays of this mutant still have joints and bifurcations. If the blood vessels do not appear to be mispatterned in this mutant, the defects in the triple *hox13* mutant could more easily be attributed to the role of *hox13* in blood vessel patterning.

4.6 Triple *hox13* mutant fin rays show defects in the female urogenital pore

Physical deformities in the female triple *hox13* mutant were observed where the urogenital pore is shorter. The result of this deformity seems to make it difficult for eggs to be released from the female triple *hox13* mutant during breeding, which could be contributing to infertility in these mutants. A similar defect could not be observed in the males; however, the male urogenital pore is much smaller and harder to observe compared to the female pore in zebrafish. Defects in the terminal part of the urogenital tract from *Hoxa13* and *Hoxd13* mutations have been previously reported in mice (Warot et al., 1997; Warot et al, 2015). In *Hoxa13* -/+, *Hoxd13* -/- mice however, abnormalities in the terminal parts of the urogenital tracts have been reported, including agenesis and hypoplasia of male sex glands, and mispositioning of urethral, anal, and vaginal openings (Warot et al., 1997). Problematically, *Hoxa13* -/-, *Hoxd13* -/- mutations in mice

result in lethality between 10.5-days and 18.5-days post coitum (Fromental-Ramain et al., 1996), meaning the adult urogenital system and external genitalia are difficult to observe. The urogenital pore of the triple *hox13* mutant zebrafish does not seem to be misplaced as it is in these mouse mutants since the positioning of the urogenital pore is in the same place and not off to the side, although a sort of hypoplasia could describe what is happening in the triple *hox13* female urogenital pore. The mechanism for this change is not fully understood, although it appears to happen in the adult stage, as defects in the pore could not be observed at the 5.6mm ISH timepoints Figure 36. However, only a visual inspection was performed, so it is possible that the *hox13* genes are expressed later in the urogenital pore. To further examine this idea, *in situ* hybridization of the *hox13* genes in the urogenital pore at this and later developmental timepoints could be performed to get a better understanding of when *hox13* are expressed in the zebrafish urogenital pore. In addition to this defect, this may only be one part why the triple *hox13* mutant females are not able to breed. The dorsal fin of female zebrafish, and the pectoral fin of male zebrafish have also been shown to be important for breeding behaviour. During breeding, the male will typically hook onto the female dorsal fin with its body in order to press on the female belly with its pectoral fin and stimulate the release of eggs from the female (Zempo et al., 2021). Amputations of the dorsal fin in wild-type females caused a 32% decrease in fertilization rate (Zempo et al., 2021). The small size of the female dorsal fin in the triple *hox13* mutant may be inhibiting the male form hooking on during breeding, contributing to the inability of the *hox13* mutant female to breed. For the male, it may be the same kind of problem since the pectoral fin is essential for breeding. The pectoral fin of the male zebrafish typically contains breeding tubercles, which are small, keratinized structures that facilitate the maintenance of body contact during spawning (Wiley & Collette, 1970). The male uses these structures to stimulate the belly of the female during breeding, causing the female

to release her eggs. In the triple *hox13* mutant male, breeding tubercles are still present, although the small, curled structure of the mutant pectoral fin may impact the correct use of these breeding tubercles, rendering the male unable to stimulate the release of eggs from the female. Overall, the breeding behaviour of the triple *hox13* mutants would have to be observed more closely to conclude if the defects in the urogenital pore are leading to infertility, or if it is a combination of these deformities and altered breeding behaviour resulting from the small pectoral fin of the male, and dorsal fin of the female.

4.7 Increased hemiray thickness as a result of *hox13* mutations

As previously explained, zebrafish typically have only soft rays in all their fins. In contrast, acanthomorph fish such as *A. burtoni* have spiny rays in addition to soft rays in the anterior parts of select fins. As opposed to soft rays, the triple *hox13* mutant zebrafish develop rays that are closer in appearance to acanthomorph spiny rays. This included physical characteristics such as the lack of joints, lack of bifurcations, and reduction of ray length that were discussed in 3.1.1 and 3.1.2.

Upon analysis of the micro-CT data, it was found that there was increased thickness in the triple *hox13* mutant dorsal and anal fin rays across the anterior-posterior axis of the fin. The hemirays of the triple *hox13* mutant were on average about 2.5-fold thicker compared to the wild-type hemirays. Spines are described as being more heavily ossified as opposed to soft rays (Woltering et al., 2018), although the exact proportional increase to thickness between acanthomorph spines and soft rays is not shown in the literature. The proportional increase between the thickness of these fin elements varies due to the vast amount of variation in acanthomorph fin

structure (Price et al., 2015; Weickhardt et al., 2017). Consequently, it cannot be concluded if the exact proportion of the hemiray thickness increase in the *hox13* mutants compared to wild type rays is the same as what is seen between soft rays and spines in acanthomorphs. There is however more ossification in the triple *hox13* mutant fin rays relative to wild-type fin rays which is consistent with what is seen between spines and soft rays of acanthomorphs (Woltering et al., 2018).

From visual observations shown in objective 1, the *hox13* mutations in *hoxa13a/b,* cause an absence of actinotrichia in all fins except for the caudal fin. Mechanistically, it is possible that this lack of actinotrichia fibers is resulting in a lack of osteoblast organization in the growing fin rays of the triple *hox13* mutant, resulting in mis-patterned osteoblast layers. In the mature fin ray, each hemiray is typically lined by a single layer of osteoblasts on both the inner and outer sides of the hemiray. With the lack of actinotrichia guiding migration however, it is possible that osteoblasts may not migrate as efficiently, resulting in disorganized osteoblasts and thus the increase in ossification in the triple *hox13* mutant. To check this, the patterning of the osteoblasts could be observed in the dorsal and anal fins, and possibly the paired fins of the triple *hox13* mutant fin rays. This could be done with longitudinal sectioning of intact or fin regenerate rays in these fins. Due to the paired fins being extremely small and curved, straight longitudinal sections are very difficult to obtain and so these fins may not be feasible to use for this analysis. The dorsal and anal fins are not quite as short and curled, and so quality longitudinal sections of the rays are possible but still difficult to obtain. If sections could be obtained for these rays, an *in situ* hybridization or immunostaining on an osteoblast marker such as *sp7, zns-5* or *runx2a* could be

performed to compare the triple *hox13* mutant osteoblast pattern with the wild-type osteoblast pattern in these fins.

Although the hemirays are thicker, one of the main differences between *hox13* mutant rays and spines is that *hox13* mutant rays do not fuse at the anterior side. This difference highlights the idea that mutations to the *hox13* genes do not cause a complete transformation to spines. It seems instead that *hox13* mutant rays are forming an intermediate structure between spines and soft rays. Thus, the reduction of *hox13* expression in soft rays may be a partial contributor to the evolution of acanthomorph spines, however there seems to be an additional mechanism causing the anterior fusing that is typically seen in spines, as will be further explained later. An analysis of actinotrichia in acanthomorph spines would be essential to say that the loss of actinotrichia we see in the triple *hox13* mutant is contributing to the spine-like phenotype. As previously mentioned, it is not known if spines contain actinotrichia within their hemirays during development, although it is absent from the tips in mature spines. If it could be determined that spines lack actinotrichia entirely throughout development, this could further support the relationship between the triple *hox13* mutant rays and acanthomorph spines.

4.8 *Alx4a* expression differs in the triple *hox13* mutant dorsal and anal fin primordia

From comparisons of *alx4a* expression domains between wild-type and the triple *hox13* mutants, no expansion in the *alx4a* domain of expression could be observed in the mutants. There were however significant differences in the length and width of the triple *hox13* mutant fin primordia. As demonstrated in Nakamura et al., (2016), the pectoral fin of their triple *hox13*

mutants showed a significant decrease in length. They did not however observe the other fins, which was done in this project for the dorsal and anal fins. Unsurprisingly, the dorsal and anal fin primordia demonstrate a decrease in length, similar to what was previously shown in the pectoral fin bud. This observation further supports the importance of *hox13* for the development of the dorsal and anal fins, and the probable similarity of developmental mechanisms between the paired fins and the dorsal and anal fins as suggested by Freitas et al., (2006). The decrease in width in the dorsal and anal fin primordia caused there to be an incidental proportional increase of *alx4a* in the triple *hox13* mutant domain of expression. In addition to the primordia, the adult dorsal ($p=3.09x10^{-5}$) and anal ($p=2.39x10^{-4}$) fins were also found to be narrower at the base of each fin from comparing average measurements of n=5 replicates, showing the significance of this smaller fin primordia on the adult fins. Furthermore, the expression levels seemed to be higher in the triple *hox13* mutant. Since ISH however is not an ideal quantitative experiment, confirming these results using qRT-PCR or ddPCR may be necessary to conclude if there is indeed an overexpression of *alx4a* in the triple *hox13* mutant. Due to the smaller fin primordia, it is possible that this relative increase in *alx4a* expression is resulting in ectopic *alx4a* in more posterior rays, thus contributing to the formation of the spine-like phenotype in the anterior and medial rays of the dorsal and anal fins.

After the initial early *alx4a* expression in the fin primordia, *alx4a* is normally expressed in the two anterior-most rays of the dorsal fin, and the anterior-most ray of the anal fin during development. In order to see if there are more rays during development that are expressing *alx4a* in the triple *hox13* mutant, a later timepoint at 6.4mm SL was also attempted to be observed through *in situ* hybridization. This 6.4mm timepoint is meant to be similar to the 7dpf timepoint

in *A. Burtoni* shown by Höch et al., 2021 (Figure 32). The 6.4mm SL timepoint in zebrafish was meant to give a similar result to this expression pattern of 7dpf *A. burtoni*, where *alx4a* expression can be seen in the distal tips of the rays. Unfortunately, the only expression visible at this timepoint is a small amount still seen in the proximal portion of the fin, and none was visible at the distal tips of the rays. This lack of visible expression could be due to the bone of the zebrafish rays at 6.4mm being too thick in order for the *alx4a* probe to penetrate, as this has previously been shown to be an issue with whole mount *in situs* in adult zebrafish fin rays (Smith et al., 2008). As a result, sectioning of the tissue may be necessary to observe *alx4a* expression within the fin rays at this timepoint. Observing an earlier timepoint right as the rays are beginning to form may also work since the rays may not be formed enough to block penetration of the *alx4a* probe. It is also possible that there is simply a difference in expression patterns between zebrafish and *A. burtoni*, such that *alx4a* is more strongly expressed in the *A. burtoni* spines compared to the fin rays of zebrafish, making the expression easier to observe in *A. burtoni*.

4.9 Possible mechanisms of the partial transformation of triple *hox13* mutant rays to spines

In addition to the loss of actinotrichia, the triple *hox13* mutants could also have resulting altered expression of anterior-posterior patterning genes that is contributing to the formation of spine-like structures. As previously mentioned, the mechanism of action of *alx4a* expression in the osteoblasts of the fin rays is not fully understood, although it is normally only expressed in the osteoblast of the two anterior-most fin rays in the dorsal fin, and the single anterior-most ray of the anal fin in zebrafish (Nachtrab et al., 2013) From evidence shown by Nachtrab et al. (2013), slight overexpression of *alx4a* caused a minor non-significant decrease in *cyp24a1*, which in turn contributes to an increase in bone formation through a decrease of vitamin D degradation

(Minghetti & Norman, 1988). If *alx4a* expression does indeed cause a decrease of *cyp24a1*, an overexpression of *alx4a* would thus result in the increased bone formation shown in the micro-CT scans of the triple *hox13* mutants (Figure 33). Since the *alx4a* expression domain does not however encompass the entire fin primordia as was initially predicted, it does not explain why there is an increase in thickness in the triple *hox13* mutant rays. Consequently, an additional explanation is required. Among possibilities, a decrease in *hand2* expression within the posterior rays could be the reason that there is also an increase in ossification in this location. *hand2*, like *alx4a* has also been shown to be expressed in osteoblasts, although its expression is exclusive to the posterior rays of the fins as opposed to the anterior rays for *alx4a* (Nachtrab et al., 2013). While the regulation of *cyp24a1* expression by Alx4a is not as clear, Hand2 has been shown to have the opposite effect on *cyp24a1* expression, where it causes an increase of *cyp24a1*, more vitamin D degradation, and thus a decrease in bone formation in the rays (Nachtrab et al., 2013). Given this mechanism, it could be that the *hox13* deletions in these mutants are resulting in an anterior increase in *alx4a*, and a posterior decrease in *hand2*, causing an overall increase in ray ossification across the anterior-posterior axis of the fins. The precise mechanism of how *hox13* expression could be affecting *alx4a* and *hand2* expression levels remains to be fully understood, however altered expression of *gli3* seems a possible explanation. GLI3 has been shown to be both an activator of *Alx4* (Te Welscher et al., 2002b) and a repressor of *Hand2* (Te Welscher et al., 2002a) in the limb bud. While much less is known about the role of *gli3* in fin development, a study by Letelier et al., (2021) observed the expression of *gli3* in the medaka fin bud, as well as the consequences of *gli3* knockouts in the fins. *Gli3* is still more strongly expressed at the anterior side of the fin bud, however faint expression can also be seen in the posterior side of the fin bud as well which is not typically seen in limbs (Figure 39 C). Targets that have been shown to be regulated

downstream of *Gli3* in mice were tested in the *gli3 -/-* medaka fin bud to see possible shifts in expression patterns using *in situ* hybridization (Figure 39). *Hoxd12a* expression has been shown to be exclusive to the soft ray domain during acanthomorph fin development (Höch et al., 2021). Although significant quantitative differences could not be observed using qRT-PCR, knockouts of *gli3* appear to cause slightly stronger expression of *hand2* and *hoxd12a* in the same domain that they are normally expressed (Figure 39 B). The results shown here appear to resemble the results of the *alx4a* expression in the triple *hox13* mutant compared to the wild-type, where the domain of expression remains unchanged, but stronger expression levels are visible. This difference could potentially indicate that the knockouts in *hox13* are causing an overexpression of *gli3*, resulting in the *alx4a* overexpression observed in the anterior domain of the triple *hox13* mutant fins. Observations of *gli3* expression in zebrafish *hox13* mutants however are required to confirm this potential mechanism.

In terms of the relationship of the mutant *hox13* rays and acanthomorph spines, the *hox13* mutant rays appear to be forming intermediate structures between spines and soft rays. The physical similarities between the spines and *hox13* mutant rays include short length, lack of joints and bifurcations, and more ossified hemirays. The difference between the two structures however is that the fusing at the anterior side of the hemirays that is seen in spines and not the mutant rays, and *alx4a* is also not expressed throughout the fin of the triple *hox13* mutant the way it is in the entire spiny ray domain of acanthomorph fins. Why the rays do not form spines is not fully understood, although this indicates that there are likely genes other than *hox13* that are responsible for specifying soft rays. A possible candidate that could be contributing to the soft ray phenotype could include *hoxd12a*, which like *hox13*, is expressed exclusively in the soft rays of

acanthomorphs (Höch et al., 2021). With this speculation, more gene knockouts in addition to *hox13* such as *hoxd12a* may be required to see the complete transformation of soft rays to spines in zebrafish. It may also be useful to analyze *hoxd12a* expression in the triple *hox13* mutant as *hoxd12a* could potentially be compensating for the loss of *hox13.*

Using *in situ* hybridization, the expression of targets such as *hand2, hoxd12a*, and *gli3* could be observed at 5.6mm SL, to see if the expression of these genes is indeed altered in the developing triple *hox13* mutant dorsal and anal fin primordia. Expression of *alx4a* was not seen within the rays of the triple *hox13* mutants presumably due to the expression being within the bone of the hemirays at 6.4mm SL. As a result, sectioning of the rays may be necessary to observe *alx4a* expression in the maturing fin rays of the mutant. *Alx4a* and *hand2* could both be observed in the osteoblasts of the adult triple *hox13* mutant dorsal and anal fins using *in situ* hybridization if quality longitudinal sections can be obtained. This would allow us to see if *alx4a* is expressed in more posterior rays of the triple *hox13* mutant fins, and if *hand2* is expressed less in the posterior rays. Furthermore, a quantitative analysis could be done on the fin primordia to determine if there is a true increase of *alx4a* expression levels and other potential genes such as *hand2* and *gli3*. In the study by Bastida et al., (2020), qRT-PCR of *hand2* was performed on *gli3* -/- medaka, although significant differences in gene expression could not be observed even though there seemed to be a difference in expression on the in situ performed for *hand2* on these mutants (Figure 36). It could potentially be that the overall expression levels are very low, explaining why significant changes could not be seen. As a result, another quantitative strategy such as ddPCR could be a better method to determine significant changes of these genes in the fins due to the absolute

quantification of ddPCR and its superiority over qRT-PCR for low copy targets (Pinheiro et al., 2012).

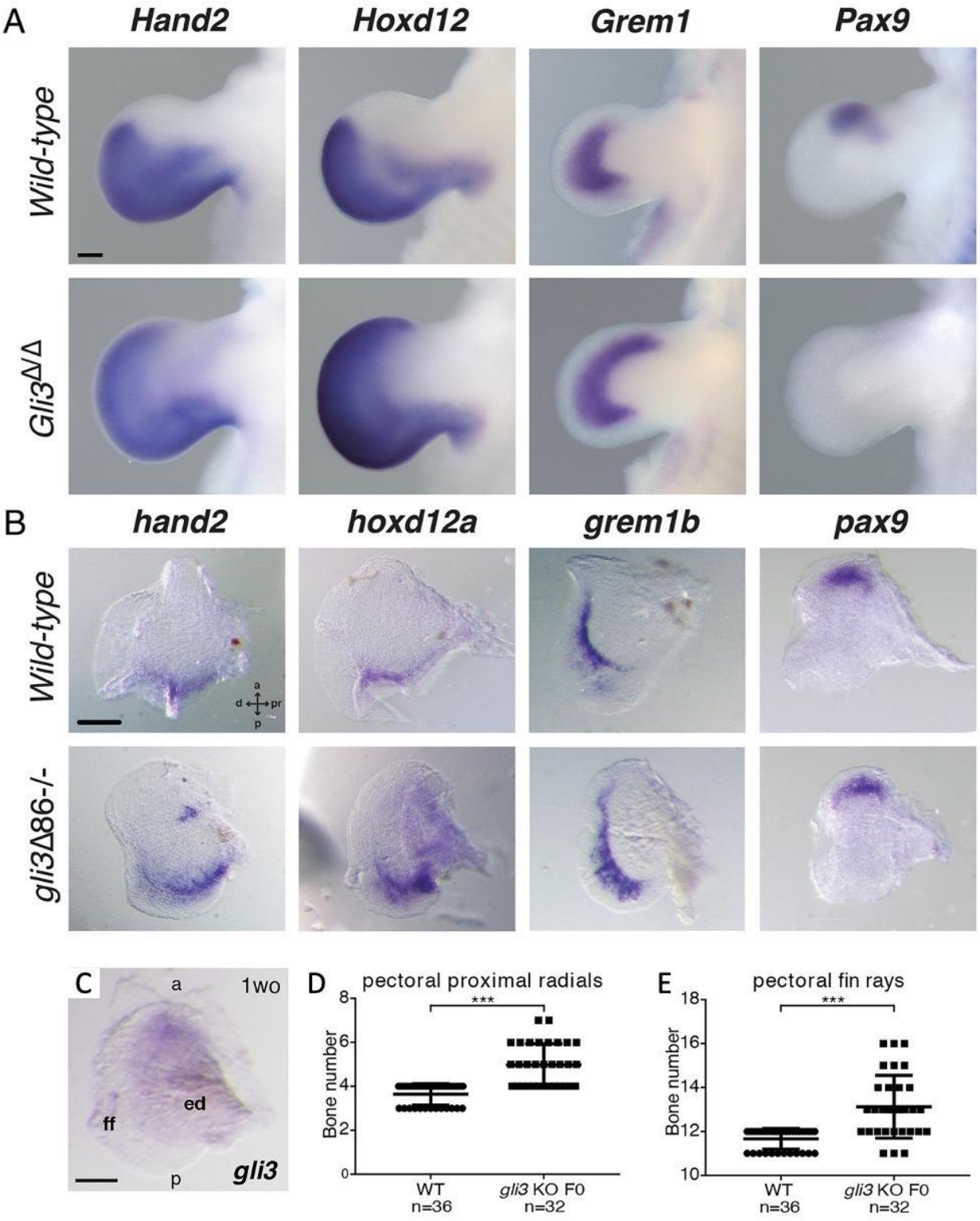

Figure 40. Effects of *gli3* mutations on the medaka pectoral fin fold. A: Wild-type and *Gli3-/-* mice at E11.5 stage of development. Expression of *Hand2*, *Hoxd12*, *Grem1*, and *Pax9* are shown

in both genotypes. Scale bar = 200µm B: 6dpf pectoral fin folds of wild-type and *gli3-/-* medaka, with expression of *hand2, hoxd12, grem1,* and *pax9* shown for each. Scale bar = 100µm C: Wild-type *gli3* expression at 7dpf in the medaka pectoral fin. Scale bar = 100µm. D/E: Number of proximal radials (D) and number of fin rays (E) in the pectoral fin of wild-type and *gli3-/-* medaka. Adapted from Letelier et al., (2021) with permissions from PNAS: Open Access Articles, April 22, 2023.

4.10 General conclusion

Overall, *hoxa13a, hoxa13b,* and *hoxd13a* have been shown to play an essential role in the development of normal zebrafish soft rays in this project. Overall, *hoxa13a* and *hoxa13b* appear to be more essential compared to *hoxd13a* in the proper formation of the adult fin rays. Although this difference is present, each of the *hox13* genes could have partially redundant function, where the differences observed can be attributed to the higher expression levels of the *hoxa13a/b* genes. The lack of *hox13* expression in the triple *hox13* mutant results in a transformed structure of the rays, that resembles the spiny rays of acanthomorphs. Thus, the reduction of *hox13* expression in the anterior part of acanthomorph fins may have contributed to the evolution of these spiny rays. What exactly caused this lower *hox13* expression in the anterior part of the fins remains to be elucidated, however this lower expression could have led to the loss of joint and bifurcations in these fins and resulted in the shorter length of the spines. Furthermore, the reduction of *hox13* expression in the spines may have caused a loss of actinotrichia in these structures, which resulted in altered osteoblast patterning and caused greater ossification in the spiny rays compared to soft rays. The exact downstream control mechanisms of *hox13* during ray development must still be

explored, although *hox13* expression appears to correlate with the specification of soft ray structures in the fins.

References:

Ahn, D., & Ho, R. K. (2008). Tri-phasic expression of posterior Hox genes during development of pectoral fins in zebrafish: Implications for the evolution of vertebrate paired appendages. *Developmental Biology*, *322*, 220–233. https://doi.org/10.1016/j.ydbio.2008.06.032

Akimenko, M.-A., Marí-Beffa, M., Becerra, J., & Géraudie, J. (2003). Old questions, new tools, and some answers to the mystery of fin regeneration. *Developmental Dynamics*, *226*, 190–201. https://doi.org/10.1002/dvdy.10248

Azevedo, A. S., Sousa, S., Jacinto, A., & Saúde, L. (2012). An amputation resets positional information to a proximal identity in the regenerating zebrafish caudal fin. *BMC Developmental Biology*, *12*, 24. https://doi.org/10.1186/1471-213X-12-24

Bastid, M. F., Pérez-Gómez, R., Trofka, A., Zhu, J., Rada-Iglesias, A., Sheth, R., Stadler, S. H., Mackem, S., & Ros, M. A. (2020). The formation of the thumb requires direct modulation of *Gli3* transcription by *Hoxa13*. *Proc Natl Acad Sci*, *117*, 1090–1096. https://doi.org/10.1073/pnas.19194701

Bird, N. C., & Mabee, P. M. (2003). Developmental morphology of the axial skeleton of the zebrafish, Danio rerio (Ostariophysi: Cyprinidae). *Developmental Dynamics*, *228*, 337–357. https://doi.org/10.1002/dvdy.10387

Borday, V., Thaëron, C., Avaron, F., Brulfert, A., Casane, D., Laurenti, P., & Géraudie, J. (2001). evx1 transcription in bony fin rays segment boundaries leads to a reiterated pattern during zebrafish fin development and regeneration. *Developmental Dynamics*, *220*(2), 91–98. https://doi.org/https://doi.org/10.1002/1097-

Briggs, J. P. (2002). The zebrafish: a new model organism for integrative physiology. *Am J Physiol Regulatory Integrative Comp Physiol*, *282*, 3–9. https://doi.org/10.1152/ajpregu.00589.2001

Bump, R. G., Goo, C. E. A., Horton, E. C., & Rasmussen, J. P. (2022). Osteoblasts pattern endothelium and somatosensory axons during zebrafish caudal fin organogenesis. *Development*, *149*(3). https://doi.org/10.1242/dev.200172

Chen, W.-J., Santini, F., Carnevale, G., Chen, J.-N., Liu, S.-H., Lavoué, S., Mayden, R. L., (2014). New insights on early evolution of spiny-rayed fishes (Teleostei: Acanthomorpha). *Frontiers in Marine Science*, *354*(1), 160–172. https://doi.org/10.3389/fmars.2014.00053

Chiang, C., Litingtung, Y., Harris, M. P., Simandl, K. B., Li, Y., Beachy, P. A., & Fallon, J. F. (2001). Manifestation of the limb prepattern: limb development in the absence of sonic hedgehog function. *Developmental Biology*, *236*, 421–435. https://doi.org/10.1006/dbio.2001.0346

Coates, M. I., Ruta, M., & Friedman, M. (2008). Ever since owen: changing perspectives on the early evolution of tetrapods. *Ecol. Evol. Syst*, *39*, 571–592. https://doi.org/10.1146/annurev.ecolsys.38.091206.095546

Davis, A. P., Witte, D. P., Hsieh-Li, H. M., Potter, S., & Capecchi, M. R. (1995). Absence of radius and ulna in mice lacking hoxa-11 and hoxd-11. *Nature*, *375*(3564), 791–795. https://doi.org/10.1038/375791a0

Dee, C. T., Szymoniuk, C. R., Mills, P. E. D., & Takahashi, T. (2013). Defective neural crest migration revealed by a zebrafish model of *Alx1*-related frontonasal dysplasia. *Hum Mol Genet*, 22(2), 239-5 https://doi.org/10.1093/hmg/dds423

Deschamps, J., & Wijgerde, M. (1993). Two Phases in the Establishment of HOX Expression Domains. *Developmental Biology*, *156*(2), 473–480. https://doi.org/10.1006/dbio.1993.1093

Duboule, D., & Dollé, P. (1989). The structural and functional organization of the murine HOX gene family resembles that of Drosophila homeotic genes. *EMBO Journal*, *8*(5), 1497–1505. https://doi.org/10.1002/j.1460-2075.1989.tb03534.x

Freitas, R., Zhang, G., & Cohn, M. J. (2006). Evidence that mechanisms of fin development evolved in the midline of early vertebrates. *Nature*, *442*, 1033–1037. https://doi.org/10.1038/nature04984

Fromental-Ramain, C., Warot, X., Messadecq, N., LeMeur, M., Dollé, P., & Chambon, P. (1996). *Hoxa-13* and *Hoxd-13* play a crucial role in the patterning of the limb autopod. *Development*, *122*, 2997–3011. https://doi.org/10.1242/dev.122.10.2997

Fu, C., Cao, Z. D., & Fu, S. J. (2013). The effects of caudal fin loss and regeneration on the swimming performance of three cyprinid fish species with different swimming capacities. *Journal of Experimental Biology*, *216*(16), 3164–3174. https://doi.org/10.1242/jeb.084244

Galli, A., Robay, D., Osterwalder, M., Bao, X., & Bénazet, J.-D. (2010). Distinct roles of Hand2 in initiating polarity and posterior Shh expression during the onset of mouse

limb bud development. *PLoS Genet*, *6*(4), 1000901 https://doi.org/10.1371/journal.pgen.1000901

Géraudie, J., & Landis, W. J. (1982). The fine structure of the developing pelvic fin dermal skeleton in the trout Salmo gairdneri. *The American Journal of Anatomy*, *163*, 141–156. https://doi.org/10.1002/aja.1001630204

Géraudie, J. (1984). Fine structural comparative peculiarities of the developing dipnoan dermal skeleton in the fins of Neoceratodus larvae. *The Anatomical Record*, *209*(1), 115–123. https://doi.org/10.1002/ar.1092090114

Géraudie, J., & Borday Birraux, V. (2003). Posterior hoxa genes expression during zebrafish bony fin ray development and regeneration suggests their involvement in scleroblast differentiation. *Dev Genes Evol*, *213*, 182–186. https://doi.org/10.1007/s00427-003-0307-y

Géraudie, J., & Meunier, F.-J. (1980). Elastoidin actinotrichia in coelacanth fins: a comparison with teleosts. *Tissue & Cell*, *12*(4), 637–645. https://doi.org/10.1016/0040-8166(80)90018-x

Grandel, H., & Schulte-Merker, S. (1998). The development of the paired fins in the Zebrafish (Danio rerio). *Mechanisms of Development*, *79*, 99–120. https://doi.org/10.1016/S0925-4773(98)00176-2

Höch, R., Schneider, R. F., Kickuth, A., Meyer, A., & Woltering, J. M. (2021). Spiny and soft-rayed fin domains in acanthomorph fish are established through a BMP-gremlin-shh signaling network. *Proc Natl Acad Sci*, *118*, 2101783118. https://doi.org/10.1073/pnas.2101783118/

Huang, C.-C., Lawson, N. D., Weinstein, B. M., & Johnson, S. L. (2003). *reg6* is required for branching morphogenesis during blood vessel regeneration in zebrafish caudal fins. *Developmental Biology*, *264*(1), 263–274. https://doi.org/10.1016/j.ydbio.2003.08.016

Kimmel, C. B., Ballard, W. W., Kimmel, S. R., Ullmann, B., & Schilling, T. F. (1995). Stages of embryonic development of the zebrafish. *Developmental Dynamics*, *203*, 253–310. https://doi.org/10.1002/aja.1002030302

Lalonde, R. L., & Akimenko, M.-A. (2018). Effects of fin fold mesenchyme ablation on fin development in zebrafish. *PLoS One*, *13*(2), 0192500. https://doi.org/10.1371/journal.pone.0192500

Lalonde, R. L., Moses, D., Zhang, J., Cornell, N., Ekker, M., & Akimenko, M. A. (2016). Differential actinodin1 regulation in zebrafish and mouse appendages. *Developmental Biology*, *417*(1), 91–103. https://doi.org/10.1016/j.ydbio.2016.05.019

Lawson, N. D., & Weinstein, B. M. (2002). In vivo imaging of embryonic vascular development using transgenic zebrafish. *Developmental Biology*, *248*(2), 307–318. https://doi.org/10.1006/dbio.2002.0711

Letelier, J., Naranjo, S., Sospedra-Arrufat, I., & Gómez-Skarmeta, J. L. (2021). The Shh/Gli3 gene regulatory network precedes the origin of paired fins and reveals the deep homology between distal fins and digits. *Proc Natl Acad Sci*, *118*(46), 2100575118. https://doi.org/10.1073/pnas.2100575118

Lettice, L. A., Heaney, S. J. H., Purdie, L. A., Li, L., De Beer, P., Oostra, B. A., Goode, D., Elgar, G., Hill, R. E., & De Graaff, E. (2003). A long-range Shh enhancer regulates

expression in the developing limb and fin and is associated with preaxial polydactyly. *Human Molecular Genetics*, *12*(14), 1725–1735. https://doi.org/10.1093/hmg/ddg180

Lewis, E. B. (1978). A gene complex controlling segmentation in Drosophila. *Nature*, *276*(5688), 565–570. https://doi.org/10.1038/276565a0

McMillan, S. C., Zhang, J., Phan, H. E., Jeradi, S., Probst, L., Hammerschmidt, M., & Akimenko, M. A. (2018). A regulatory pathway involving retinoic acid and calcineurin demarcates and maintains joint cells and osteoblasts in regenerating fin. *Development*, *145*(11), 161158 https://doi.org/10.1242/DEV.161158

Minghetti, P. P., & Norman, A. W. (1988). 1,25(OH) 2 -Vitamin D 3 receptors: gene regulation and genetic circuitry. *The FASEB Journal*, *2*(15), 3043–3053. https://doi.org/10.1096/fasebj.2.15.2847948

Nachtrab, G., Kikuchi, K., Tornini, V. A., & Poss, K. D. (2013). Transcriptional components of anteroposterior positional information during zebrafish fin regeneration. *Development*, *140*(18), 3754–3764. https://doi.org/10.1242/dev.098798

Naser, F., & Rashid, M. (2020). The influence of concave pectoral fin morphology in The performance of labriform swimming robot. *Iraqi Journal for Electrical and Electronic Engineering*, *16*(1), 1–8. https://doi.org/10.37917/ijeee.16.1.7

Nasiadka, A., & Clark, M. D. (2012). Zebrafish breeding in the laboratory environment. *ILAR J*, *53*(2), 161–168. https://doi.org/10.1093/ilar.53.2.161

Nelson, C. E., Morgan, B. A., Burke, A. C., Laufer, E., Dimambro, E., Murtaugh, L. C., Gonzales, E., Tessarollo, L., Parada, L. F., & Tabin, C. (1996). Analysis of Hox gene

expression in the chick limb bud. *Development*, 122 (5), 1449-1466. https://doi.org/10.1242/dev.122.5.1449

Paulissen, S. M., Castranova, D. M., Krispin, S. M., Burns, M. C., Menéndez, J., Torres-Vázquez, J., & Weinstein, B. M. (2022). Anatomy and development of the pectoral fin vascular network in the zebrafish. *Development 149*(5), 199676 https://doi.org/10.1242/dev.199676

Phan, H.-E., Northorp, M., Lalonde, R. L., Ngo, D. I., & Akimenko, M.-A. (2019). Differential actinodin1 regulation in embryonic development and adult fin regeneration in Danio rerio. *PLoS One, 14*(5), 0216370. https://doi.org/10.1371/journal.pone.0216370

Pinheiro, L. B., Coleman, V. A., Hindson, C. M., Herrmann, J., Hindson, B. J., Bhat, S., & Emslie, K. R. (2012). Evaluation of a droplet digital polymerase chain reaction format for DNA copy number quantification. *Analytical Chemistry*, *84*(2), 1003–1011. https://doi.org/10.1021/ac202578x

Price, S. A., Friedman, S. T., & Wainwright, P. C. (2015). How predation shaped fish: the impact of fin spines on body form evolution across teleosts. *Proc. R. Soc. B., 282,* 20151428. https://doi.org/10.1098/rspb.2015.1428

Qu, S., Niswender, K. D., Ji, Q., van der Meer, R., Keeney, D., Magnuson, M. A., & Wisdom, R. (1997). Polydactyly and ectopic ZPA formation in Alx-4 mutant mice. *Development*, *124*, 3999–4008.https://doi.org/10.1242/dev.124.20.3999

Quint, E., Smith, A., Avaron, F., Laforest, L., Miles, J., Gaffield, W., & Akimenko, M.-A. (2002). Bone patterning is altered in the regenerating zebrafish caudal fin after ectopic

expression of sonic hedgehog and bmp2b or exposure to cyclopamine. *Proc Natl Acad Sci.*, *25*(99), 8713–8718. https://doi.org/10.1073/pnas.122571799

Rabinowitz, J. S., Robitaille, A. M., Wang, Y., Ray, C. A., Thummel, R., Gu, H., Djukovic, D., Raftery, D., Berndt, J. D., & Moon, R. T. (2017). Transcriptomic, proteomic, and metabolomic landscape of positional memory in the caudal fin of zebrafish. *Proc Natl Acad Sci*, *114*(5), 717–726. https://doi.org/10.1073/pnas.1620755114

Rafferty, S. A., & Quinn, T. A. (2018). A beginner's guide to understanding and implementing the genetic modification of zebrafish. In *Progress in Biophysics and Molecular Biology*, 138, 3–19. https://doi.org/10.1016/j.pbiomolbio.2018.07.005

Ravi, V., & Venkatesh, B. (2008). Rapidly evolving fish genomes and teleost diversity. In *Current Opinion in Genetics and Development*, 18(6), 544–550. https://doi.org/10.1016/j.gde.2008.11.001

Riddle, R. D., Johnson, R. L., Laufer, E., & Tabin, C. (1993). Sonic hedgehog Mediates the Polarizing Activity of the ZPA. *Cell*, *75*, 1401–1416. https://doi.org/10.1016/0092-8674(93)90626-2.

Rockwell, D. M., O'Connor, A. K., Bentley-Ford, M. R., Haycraft, C. J., Croyle, M. J., Brewer, K. M., Berbari, N. F., Kesterson, R. A., & Yoder, B. K. (2022). A transgenic Alx4-CreER mouse to analyze anterior limb and nephric duct development. *Developmental Dynamics, 251*(9), 1524–1534. https://doi.org/10.1002/dvdy.328

Roselló-Díez, A., Ros, M. A., & Torres, M. (2011). Diffusible signals, not autonomous mechanisms, determine the main proximodistal limb subdivision. *Science*, *332*(6033), 1086–1088. https://doi.org/10.1126/science.ll99499

Sakata-Haga, H., Uchishiba, M., Shimada, H., Tsukada, T., Mitani, M., Arikawa, T., Shoji, H., & Hatta, T. (2018). A rapid and non-destructive protocol for whole-mount bone staining of small fish and Xenopus. *Sci Rep*, 8, 7453 https://doi.org/10.1038/s41598-018-25836-4

Santini, S., Boore, J. L., & Meyer, A. (2003). Evolutionary conservation of regulatory elements in vertebrate *Hox* gene clusters. *Genome Res.*, *6*, 1111–1122. https://doi.org/10.1101/gr.700503

Scherz, P. J., McGlinn, E., Nissim, S., & Tabin, C. J. (2007). Extended exposure to Sonic hedgehog is required for patterning the posterior digits of the vertebrate limb. *Developmental Biology*, *308*(2), 343–354. https://doi.org/10.1016/j.ydbio.2007.05.030

Schulte, C. J., Allen, C., England, S. J., Juárez-Morales, J. L., & Lewis, K. E. (2011). Evx1 is required for joint formation in zebrafish fin dermoskeleton. *Developmental Dynamics*, *240*(5), 1240–1248. https://doi.org/10.1002/dvdy.22534.

Shaut, C. A. E., Keene, D. R., Sorensen, L. K., Li, D. Y., & Stadler, H. S. (2008). HOXA13 Is Essential for Placental Vascular Patterning and Labyrinth Endothelial Specification. *PLoS Genet*, *4*(5), 1000073. https://doi.org/10.1371/journal.pgen.1000073

Sims, K., Eble, D. M., & Iovine, M. K. (2009). Connexin43 regulates joint location in zebrafish fins. *Developmental Biology*, *327*(2), 410–418. https://doi.org/10.1016/j.ydbio.2008.12.027

Singleman, C., & Holtzman, N. G. (2014). Growth and maturation in the zebrafish, danio rerio: a staging tool for teaching and research. *Zebrafish*, 11, 396–406 https://doi.org/10.1089/zeb.2014.0976

Siomava, N., Shkil, F., Voronezhskaya, E., & Diogo, R. (2018). Development of zebrafish paired and median fin musculature: basis for comparative, developmental, and macroevolutionary studies. *Sci Rep, 8,* 14187. https://doi.org/10.1038/s41598-018-32567-z

Smith, A., Zhang, J., Guay, D., Quint, E., Johnson, A., & Akimenko, M. A. (2008). Gene expression analysis on sections of zebrafish regenerating fins reveals limitations in the whole-mount in situ hybridization method. *Developmental Dynamics*, *237*(2), 417–425. https://doi.org/10.1002/dvdy.21417

Tao, W., Yang, L., Mayden, R. L., & He, S. (2019). Phylogenetic relationships of Cypriniformes and plasticity of pharyngeal teeth in the adaptive radiation of cyprinids. *Science China Life Sciences*, *62*(4), 553–565. https://doi.org/10.1007/s11427-019-9480-3

Tarchini, B., & Duboule, D. (2006). Control of *Hoxd* genes' collinearity during early limb development. *Developmental Cell*, *10*(1), 93–103. https://doi.org/10.1016/j.devcel.2005.11.014

Tayama, K., Fujita, H., Takahashi, H., Nagasawa, A., Yano, N., Yuzawa, K., & Ogata, A. (2006). Measuring mouse sperm parameters using a particle counter and sperm quality analyzer: A simple and inexpensive method. *Reproductive Toxicology*, *22*(1), 92–101. https://doi.org/10.1016/j.reprotox.2005.11.009

Te Welscher, P., Fernandez-Teran, M., Ros, M. A., & Zeller, R. (2002). Mutual genetic antagonism involving GLI3 and dHAND prepatterns the vertebrate limb bud

mesenchyme prior to SHH signaling. *Genes Dev. 16(4), 421–426.* https://doi.org/10.1101/gad.219202

Te Welscher, P., Zúeniga, A., Kuijper, S., Drenth, T., Goedemans, H. J., Meijlink, F., & Zeller, R. (2002). Progression of vertebrate limb development through SHH-mediated counteraction of GLI3. *Science*, *298*(5594), 827–830. https://doi.org/10.1126/science.1075620

Thisse, C., & Thisse, B. (2007). High-resolution in situ hybridization to whole-mount zebrafish embryos. *Nature Protocols*, *3*, 59–69. https://doi.org/10.1038/nprot.2007.514

Thummel, R., Ju, M., Sarras, M. P., & Godwin, A. R. (2007). Both Hoxc13 orthologs are functionally important for zebrafish tail fin regeneration. *Dev Genes Evol*, *217*, 413–420. https://doi.org/10.1007/s00427-007-0154-3

Uemoto, T., Abe, G., & Tamura, K. (2020). Regrowth of zebrafish caudal fin regeneration is determined by the amputated length. *Scientific Reports, 10* (649). https://doi.org/10.1038/s41598-020-57533-6

Warot, X., Fromental-Ramain, C., Fraulob, V., Chambon, P., & Dollé, P. (1997). Gene dosage-dependent effects of the Hoxa-13and Hoxd-13 mutations on morphogenesis of the terminal parts of the digestive and urogenital tracts. *Development*, *124*, 4781–4791. https://doi.org/10.1242/dev.124.23.4781.

Webb, P. W. (1973). Effects of partial caudal-fin amputation on the kinematics and metabolic rate of underyearling sockeye salmon (Oncorhynchus nerka) at steady swimming speeds. *J. Exp. Biol*, *59*, 565–581. https://doi.org/10.1242/jeb.59.3.565

Webb, P. W. (1977). Effects of median-fin amputation on fast-start performance of rainbow trout (Salmo gairdneri). *J. Exp. Biol*, *68*, 123–135. https://doi.org/10.1242/jeb.68.1.123

Weickhardt, A. F., Feilich, K. L., & Lauder, G. V. (2017). Structure of supporting elements in the dorsal fin of percid fishes. *Journal of Morphology*, *278*(12), 1716–1725. https://doi.org/10.1002/jmor.20744.

Wellik, D. M., & Capecchi, M. R. (2003). *Hox10* and H*ox11* genes are required to globally pattern the mammalian skeleton. *Science*, *301*, 363–367. https://doi.org/10.1126/science.1085672.

Woltering, J. M., & Durston, A. J. (2006). The zebrafish hoxDb cluster has been reduced to a single microRNA. *Nature*, *38*, 601–602. https://doi.org/10.1038/ng0606-601

Woltering, J. M., Holzem, M., Schneider, R. F., Nanos, V., & Meyer, A. (2018). The skeletal ontogeny of Astatotilapia burtoni-a direct-developing model system for the evolution and development of the teleost body plan. *BMC Developmental Biology*, *18*, 8. https://doi.org/10.1186/s12861-018-0166-4

Woltering, J. M., Noordermeer, D., Leleu, M., & Duboule, D. (2014). Conservation and divergence of regulatory strategies at Hox loci and the origin of tetrapod digits. *PLoS Biology*, *12*, 1001773. https://doi.org/10.1371/journal.pbio.1001773

Wood, A., & Thorogood, P. (1984). An analysis of in vivo cell migration during teleost fin morphogenesis. *J. Cell Set*, *66*, 205–222. https://doi.org/10.1242/jcs.66.1.205

Zákány, J., Kmita, M., & Duboule, D. (2004). A dual role for Hox genes in limb anterior-posterior asymmetry. *Science*, *301*, 363–367. https://doi.org/10.1126/science.1096049

Zardoya, R., & Meyer, A. (1997). Molecular phylogenetic information on the identity of the closest living relative(s) of land vertebrates. *Nature*, *84*, 389–397. https://doi.org/10.1007/s001140050415

Zempo, B., Tanaka, N., Daikoku, E., & Ono, F. (2021). High-speed camera recordings uncover previously unidentified elements of zebrafish mating behaviors integral to successful fertilization. *Scientific Reports*, *11*(1), 20228. https://doi.org/10.1038/s41598-021-99638-6

Zhang, J., Jeradi, S., Strähle, U., & Akimenko, M. A. (2012). Laser ablation of the sonic hedgehog-a-expressing cells during fin regeneration affects ray branching morphogenesis. *Developmental Biology*, *365*(2), 424–433. https://doi.org/10.1016/j.ydbio.2012.03.008

Zhang, J., Wagh, P., Guay, D., Sanchez-Pulido, L., Padhi, B. K., Korzh, V., Andrade-Navarro, M. A., & Akimenko, M.-A. (2010). Loss of fish actinotrichia proteins and the fin-to-limb transition. *Nature*, *466*, 234-237. https://doi.org/10.1038/nature09137

Zhang, X., Zhang, Z., Zhao, Q., & Lou, X. (2020). Rapid and efficient live zebrafish embryo genotyping *Zebrafish*, *17*, 56-58. https://doi.org/10.1089/zeb.2019.1796

Zúñiga, A., Haramis, A.-P. G., McMahonk, A. P., & Zeller, R. (1999). Signal relay by BMP antagonism controls the SHH/FGF4 feedback loop in vertebrate limb buds. *Nature*, *401*, 598–602. https://doi.org/10.1038/44157